Doctoral Thesis

Evaluation of the Photovoltaic System Installation Impact to an Electric Power Grid

太陽光発電システム導入による電力網への影響評価

2016

Environmental and Renewable Energy Systems Division

Graduate School of Engineering

Gifu University

Juan Ernesto Wyss Porras

Acknowledgements

Firstly, I would like to express my sincere gratitude to my advisor Prof. Tomonao Kobayashi for his support through my Doctoral degree study and related research, for his patience, motivation, and immense knowledge. His guidance helped me in all the time of research and writing of this thesis. Also, I would like to thank Prof. Jun Yoshino and Prof. Susumu Shimada, whose guidance also contributed to this research.

I would like to thank the Japanese Ministry of Education, Culture, Sports, Science and Technology for their financial support through the Monbukagakusho scholarship embassy recommended student program. Without their support I would not have been able to come to Japan and study at Gifu University.

I would also like to extend my gratitude all my friends from the Natural Energy Laboratory, who helped me both in studies and my daily life in Japan. Final Thanks are to my family and to Sakiko, thank you for waiting for me.

Abstract

The impact of the installation of a large-scale photovoltaic (PV) system to the electric power grid management is analyzed numerically in this work. First, the PV energy output potential is estimated. In order to estimate this PV output, the solar irradiance is required, for which a meteorological model was used. The computed data, i.e. global horizontal irradiance (GHI) and ambient temperature, is then processed in order to build a distribution map for the GHI and for the PV energy output. Using these distribution maps, the national data and a population distribution maps, the best area for a large-scale PV system is selected. The best area for a large-scale PV system is one that has high irradiance, high PV energy output and is close to the areas of consumption. In addition the optimal tilted angle of the PV panels is also evaluated and proposed. Having selected the best area for the PV system, the PV energy output time series is calculated for this particular area, using the optimal tilted angle, the global horizontal irradiance and the ambient temperature.

In order to evaluate the impact of the future electric grid management a non-linear model is proposed. This model was build using a system dynamics approach. The model includes all of the existing power plants in the target country Guatemala. The model includes the renewable energy power plants, i.e. hydroelectric, geothermal and biomass plant, as databases whose data is called in accordance to a timer and the thermal power plants are included as variables whose generation depends on a timer, and the generation priority that each one has. The generation priority of the thermal power plants is given by the laws of Guatemala and these laws are simulated in the system by use of logical functions and casual loops. In order to validate the model, a one year simulation with an hourly interval was conducted. The simulated data is then compared with the measured data of the simulated year. The accuracy of the model was validated by use of the coefficient of determination. The large-scale PV system was introduced with different installed capacities

from 0 to 200 MW with a 10 MW interval and a one year simulation was conducted for each installed capacity. The one year simulation showed that the thermal power plants' operation is reduced by installing the large-scale PV system. However, the effect of the PV system installation on each thermal power plant is different between each thermal power plant. The contribution of the PV installation to the reduction of operation of the largest generation thermal plants is very small or nothing, because of their high efficiency and low cost in operation. On the other hand, the middle-large generation thermal power plants reduce their operation after installing PV system in this simulation. The reduction of thermal plants' operation becomes large as the PV installing capacity becomes large, but its reduction gradient becomes small as the PV installing capacity increases.

Keywords: Meteorological model, WRF, solar irradiance, PV map, tilted plane, System Dynamics, sensitivity analysis, priority, efficiency, energy cost

Table of Contents

List of Figures

List of Tables

1. Introduction

Photovoltaic (PV) energy has been expanding rapidly throughout the developed nations around the world. According to the "PV status report 2012" (Jäger-Waldau 2012), from the European Commission, the increasing usage of PV energy is due to the creation of new laws promoting its use. Emerging markets in The Americas have also created similar laws, however PV development has not reached such levels. Guatemala, which is located in the lower latitudes of Central America, is selected as the target for the analysis of photovoltaic (PV) installation.

There are two main reasons for choosing Guatemala as a target country for the present work: There were no PV power plants connected to the electric power grid in December 2013. Therefore we can compare the simulated power grid management after installing a PV system with the current status, and can discuss the effect of the PV installation. Next, Guatemala's electric power grid consists in only one grid which connects all the urban areas and most of the rural areas, this makes an impact analysis of the PV installation easy.

The variation of the PV output might cause instability of the electricity supply to the electric power grid. The objective of this research is to analyze the introduction of a large scale PV system in to Guatemala's electric power grid. First, the potential PV electric energy potential is required; in order to achieve this, the solar irradiance was computed by the use of a meteorological model. These results were the irradiance time series and irradiance distribution maps. Next the PV output was estimated using the results from the meteorological model in an empirical equation developed for crystalline silicon PV panels. The results were the time series of PV output and PV output distribution maps.

With the irradiance distribution maps and the PV output distribution maps the best area for the large scale PV system was selected. Last the

future grid management was evaluated using a non-linear dynamics model of the power grid where the PV output time series is introduced and the changes in the grid management were evaluated and discussed.

Extensive research has been done in the political, sociological and economic impact of PV energy development. However, few studies exist on the impact that such source of energy has on the electric power grid.

Dincer (2011) reported about the use of PV in developed nations and the trend in its use. De la Hoz et. al (2010) went deeper in detail with his industry report about the PV development in Spain, where the development trend changed dramatically in 2008 (Movilla, Miguel, and Blázquez 2013) after the economic crisis.

In addition to industry reports and reviews, papers such as Bazilian et al. (2013) and Cucciella and D'Adamo (2012) focus on analyzing the economic implications of the use and development of PV energy. They also briefly discuss the policies promoted in their respective cases. De Martino and de Melo (2013) try to incorporate both a political and an economical long term analysis to grid-connected PV energy systems.

When talking about grid-connected PV energy, it is important to analyze the technical implications as well. Negrao Macedo and Zilles (2009) conducted a case study on a 11.07 kW grid connected PV system, by analyzing the technical requirements and the economic performance of the system.

System dynamics has also been applied to renewable energy and electric power grid research. However, the research focuses on economic, political, sociological and managerial analysis. Movilla et al. (2013) focused on the future profitability of PV energy in Spain. In contrast, Hsu (2012), Ahmad, Mat Tahar, Muhammad-Sukki, Munir and Abdul Rahim (2015) and Silveira, Tuna and Lamas (2013) used the System Dynamics in order to conduct a policy analysis in their respective countries.

2. Guatemala as a Target Area

2.1. Location

The target country, Guatemala, is located at the low latitude between 14°N to 18°N in Central America as shown in Figures 1, 2 and 3. This area is known as the tropics. Guatemala is bordered by Mexico to the north and west, Belize to the northeast, Honduras to the east and El Salvador to the southeast. Finally it has the Pacific Ocean coastline to the south-southwest and Atlantic coastline to the Northeast.

Fig. 1: Map of the Americas (Instituto Geográfico Nacional, Guatemala C.A. 2014)

Fig. 2: Map of Central America (Instituto Geográfico Nacional, Guatemala C.A. 2014)

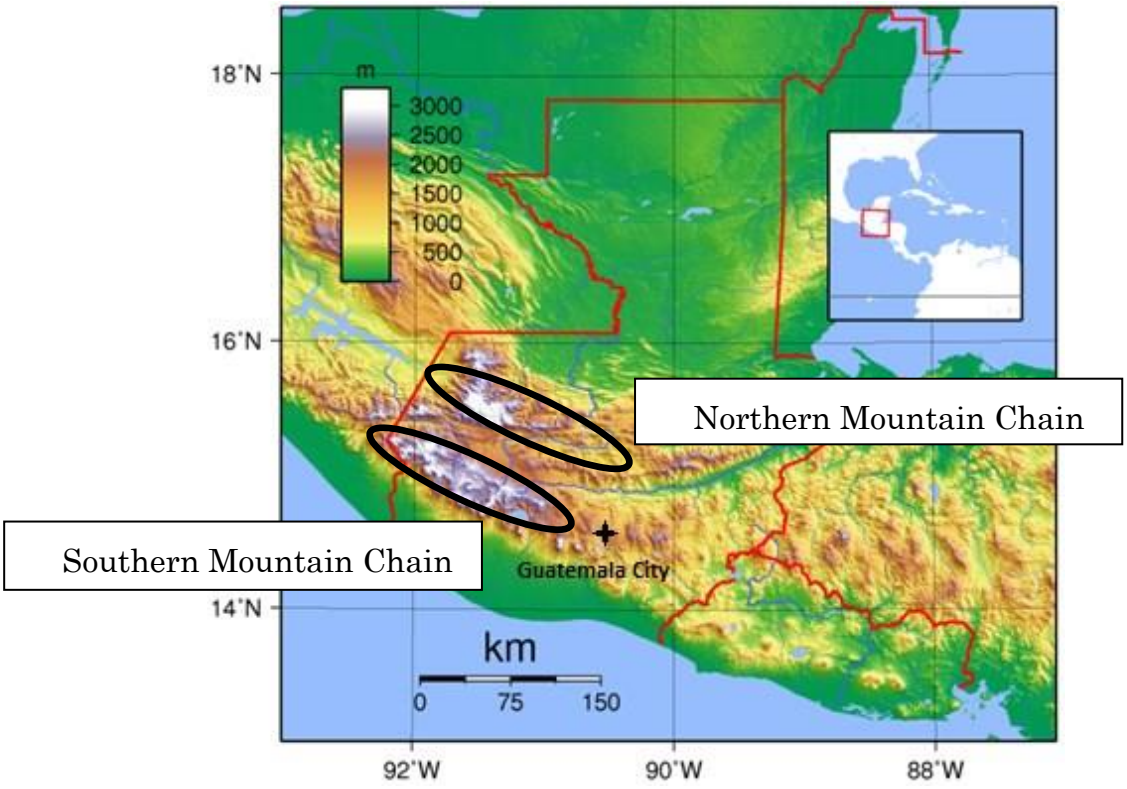

Fig. 3: Guatemala's topography (Instituto Geográfico Nacional, Guatemala C.A. 2014)

The capital city is Guatemala City (the proper name in Spanish is La Nueva Guatemala de la Asunción) and it can be seen in Fig. 3. The country's population is estimated to be 14,636,487 according to 2014 estimations by the National Institute for Statistics Guatemala (INE, for its initials in Spanish).

2.2. Topography

Guatemala is a mountainous country, with flatlands in the south coast and the northern lowlands of the department of Petén. Two mountain chains enter Guatemalan territory from west to east, as it can be seen in Fig. 3. These mountain chains divide the country in to three major regions: the highlands, where the mountains are located; the Pacific coast, south of the mountains; and the Petén region, north of the mountains. These areas vary in climate, elevation, and landscape, and provide dramatic contrast between hot and humid tropical lowlands and highland peaks and valleys.

The Southern mountain chain is called Sierra Madre. It enters throw Guatemala`s south west, stretching from the Mexican border south and east, and continues at lower elevations towards El Salvador. The mountain chain is characterized by steep volcanic cones, including Tajumulco Volcano, which is the tallest peak in Guatemala and in Central America (4,220 m). Guatemala has inside its territory a total of 37 volcanoes (4 of them active; Pacaya, Santiaguito, Fuego and Tacaná), all of them are located inside this mountain chain.

The northern mountain chain begins near the Mexican border with the Cuchumatanes range, then stretches east through the Chuacús and Chamá sierras, down to the Santa Cruz and Minas sierras, near the Caribbean Sea. The northern and southern mountains are separated by the Motagua valley, where the Motagua river and its tributaries drains from the highlands into the Caribbean being navigable in its lower end, where it forms the boundary with Honduras.

2.3. Weather

Guatemala's weather acquires particular characteristics due to its geographical position and its topographic conditions. The country has been divided in to 6 climatic regions according to Thorntwaite's system for climate classification (Thornthwaite 1931) shown in Fig. 4. Its climate is hot and humid in the Pacific and Northern Lowlands, more temperate in the highlands, and hot and drier in the easternmost departments. Guatemala has the wet season from June to November and the dry season from December to the next May.

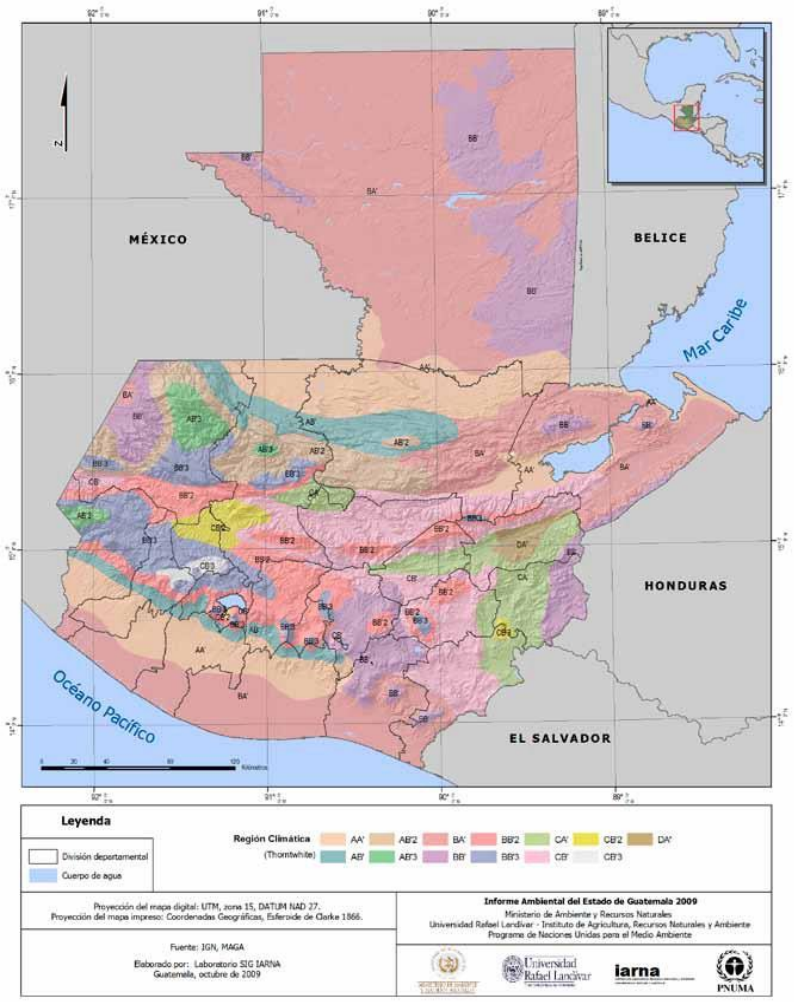

Fig. 4: Map of the climatic regions of Guatemala according to Thornthwaite classification system (Thornthwaite 1931)

Guatemala's location between the Caribbean Sea and Pacific Ocean put the country at high risk of Hurricanes such as Mitch in 1998 and Stan in October 2005, which killed more than 1,500 people. The damages caused by these hurricanes were mainly due to flooding and landslides.

2.4. Guatemala's Economy

Guatemala is mainly an agricultural country; its main exports are Coffee, sugar and bananas. Its main export partner is the United States of America, to whom 39% of the exports go to. The other main export partners are El Salvador, Honduras, Mexico and Nicaragua (The World Bank 2014).

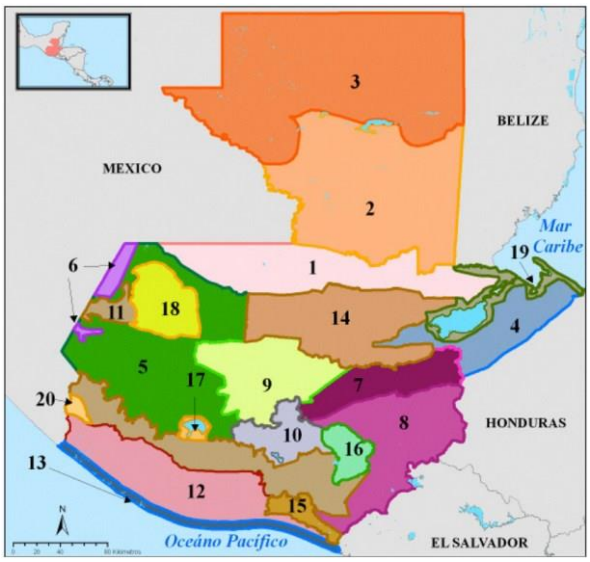

1 Misc Agriculture
2 Logging, Misc agriculture
3 Logging, Misc agriculture
4 Agribusiness export, Livestock
5 Agribusiness local consumption
6 Agribusiness local consumption
7 Agribusiness, logging, mining
8 Basic grains, corn and beans
9 Basic grains, corn and beans
10 Agribusiness and clothes factories
11 Coffee plantations
12 Agribusiness and basic grains
13 Fishery, agribusiness
14 Cardamom and coffee
15 Livestock
16 Fruits and Vegetables
17 Tourism
18 Forest Natural reserves
19 Fishery
20 Agribusiness, Misc commerce

Fig. 5: Economic activities per region (Nicoló et al. 2010).

As it can be seen in Fig. 5, most of the country is involved in agribusiness. The sugar industry is mainly located in areas 12 and 13, and they are also involved in the electric system, and its participation is discussed in section 2.5.

2.5. Current Energy Conditions

At present, Guatemala's energy demand is supplied by a combination of hydro, geothermal, biomass and thermal power plants. Figures 6 and 7 show the installed capacity and energy produced in Guatemala for the year 2013, respectively. It can be seen from them that the country relies heavily on hydro and thermal power plants. They are about one third and 40% of the installed capacity, and supply about half and one third of the demanded energy, respectively. As of December 2013, large-scale PV systems have not been installed into the electric grid, as shown in Fig. 6. Figure 8 shows the energy use ratio of the power plants in each month.

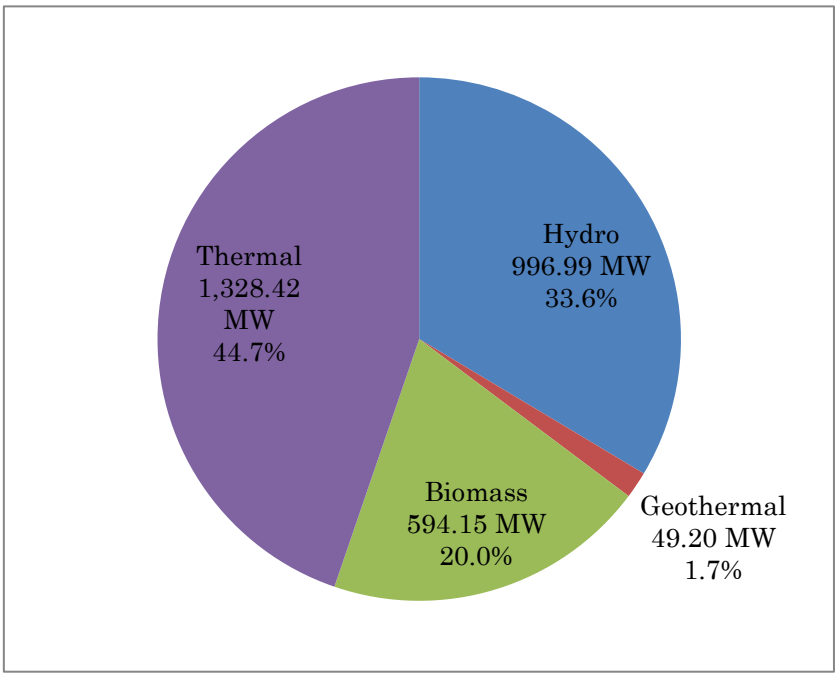

Fig. 6: Guatemala's installed capacity of electric power plants, in January 2013 (Administrador del Mercado Mayorista 2014)

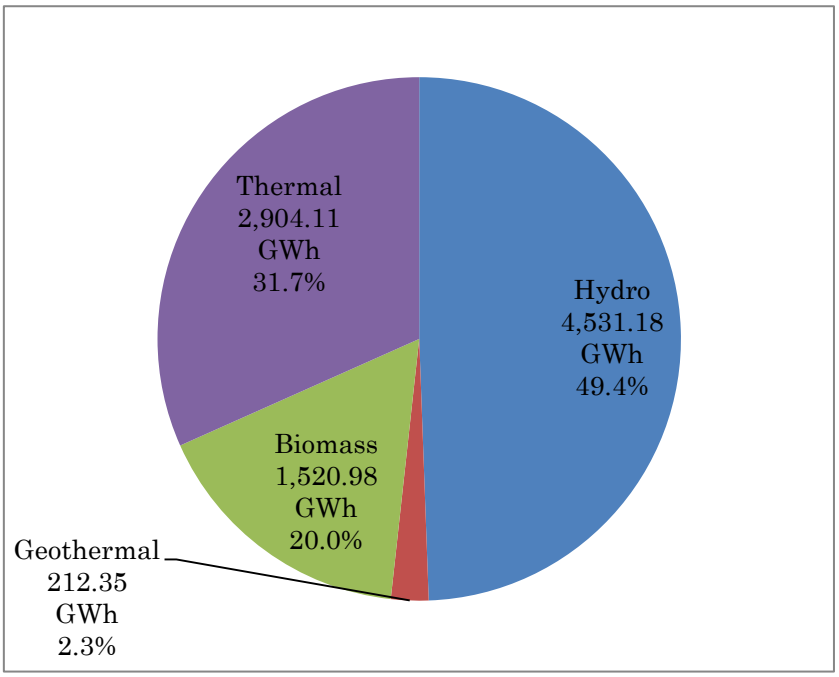

Fig. 7: Guatemala's energy production of electric power plants in 2013 (Administrador del Mercado Mayorista 2014)

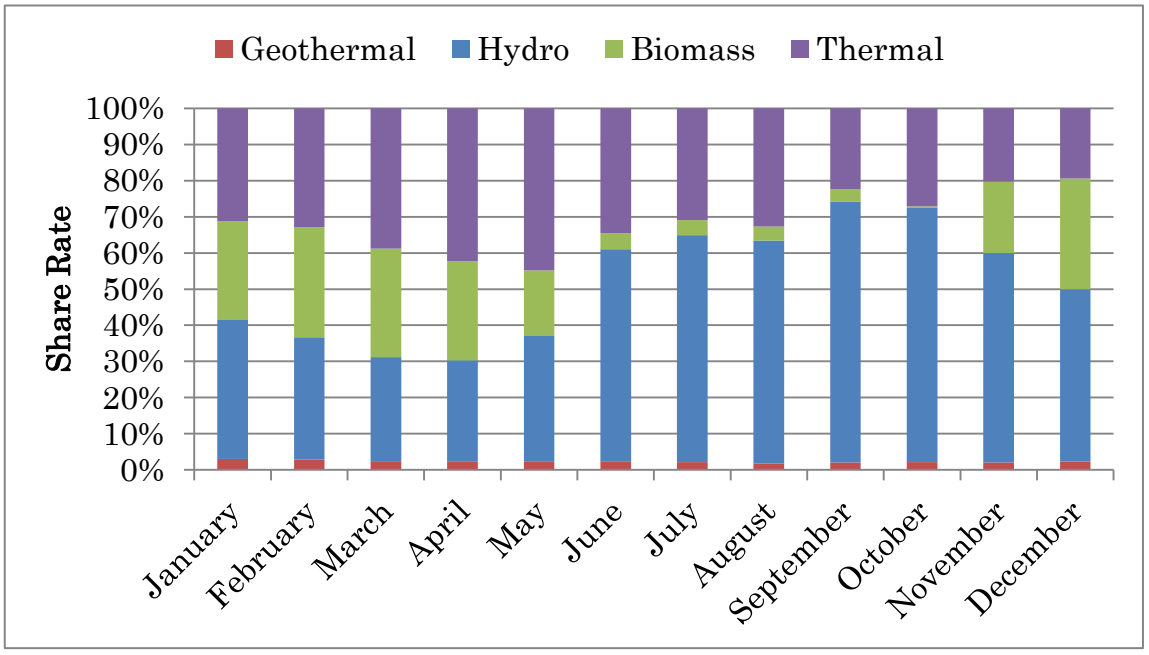

Fig. 8: Monthly energy supply share in Guatemala in 2011 (Administrador del Mercado Mayorista 2014).

2.5.1. Electric Power Plants

As of January 2012, there are 85 power plants in Guatemala, and their total capacity is 2,795 MW. Table 1 indicates the number of the plants.

Table 1: Summary of Guatemala's energy supply as of January 2012, (Administrador del Mercado Mayorista 2014)

Energy Source	Number of power plants	Total Installed Capacity (MW)	Fuel Type
Hydro Power	27	880.0	NA
Geothermal Power	2	49.2	NA
Biomass Power	25	538.0	Sugarcane bagase
Thermal Power	31	1,328.0	Diesel, Heavy Oil and Coal

2.5.1.1. Hydropower plants

There are different types of hydropower plants, the types used in Guatemala are:

Conventional: the concept is to store water behind large dams, and transform the potential energy in to kinetic energy by the use of the difference in height between the intake of the water and the outtake of the flow.

Run-of-the-river: these are hydropower plants with small or no reservoir, therefore the water coming from upstream is available for generation at that moment. Because of their inability to store water in a reservoir, these power plants do not have the capacity to choose when they can or cannot generate electricity and their generation is linked to seasonal river flows. These power plants may have a small pond that allows them to store water during the periods of low energy demand and then generate in high demand hours.

In Guatemala, most hydropower plants are run-of-the-river, this means that their electric generation changes due to the precipitation. It becomes large after the rainy season from June to November. Only a few power plants in the country have yearly-regulated reservoirs which allow them to store water during the rainy season and to generate electric power during the whole dry season.

2.5.1.2. Biomass power plants

The term biomass refers to diverse fuels derived from timber, agriculture and food processing wastes or from fuel crops that are specifically grown or reserved for electricity generation. A biomass power station uses these fuels in order to warm boilers and use the resulting steam in order to move a turbine and produce electricity.

In Guatemala's case, the biomass power plants use the waste material from the production of sugar from sugar cane as fuel. Their generation also changes evidently in a year due to the agricultural cycle of sugar cane as shown in Fig. 8.

The waste material from the sugar production from sugarcane is called bagasse. Originally, sugar mills would use the bagasse to produce heat energy and electricity used to power the production of sugar. However, the produced electricity exceeds the needs of the mill and therefore the excess is inputted in to the electric power grid.

2.5.1.3. Geothermal power plants

Similar to the biomass and thermal power plants, geothermal power plants use heat to generate electricity. In their case, the heat from the Earth is used. In order to access this type of energy, a well must be drilled into a geothermal reservoir, and then the geothermal fluids flow through pipes to a power plant where the pressurized fluid is allowed to expand rapidly and provide rotational energy to turn a turbine. The rotational energy from the

turbine is then used to spin the generator and generate electricity which is then connected to an electric power grid and transmitted to the areas of consumption.

2.5.1.4. Thermal power plants

The thermal power plants are categorized into three types from the different fuels; coal, heavy oil and gas. The energy price, efficiency and the reaction time are different between them. The specifications of major thermal power plants are listed in Table 2. In this table the actual electric generations in the year 2011 are also indicated, and it's sorted with the parameter for the latter discussion.

Table 2: Thermal power plants in Guatemala, sorted with the actual power generation in the year 2011.

Thermal Power Plants	Installed Capacity (MW)	Fuel Type	Actual Generation in 2011 (MWh/year)
San José	139.00	Coal	822,155.12
Arizona	160.00	Heavy Oil	621,056.47
Poliwatt	129.36	Heavy Oil	558,486.51
Las Palmas 2	83.00	Coal	437,521.09
Genor	46.24	Heavy Oil	203,001.98
La Libertad	20.00	Coal	100,874.54
Puerto Quetzal Power	118.00	Heavy Oil	94,380.42
Las Palmas	66.80	Heavy Oil	91,428.92
Sidegua	44.00	Heavy Oil	26,000.00
Electro Generación	15.75	Heavy Oil	21,287.98
Industria Textiles del Lago (ITDL10)	30.00	Heavy Oil	19,488.70
Generadora CS	30.20	Coal	14,765.10

Arizona Vapor	12.50	Heavy Oil	10,275.20
Genosa	12.40	Heavy Oil	4,332.00
Industria Textiles del Lago (ITDL3)	30.00	Heavy Oil	2,487.00
Tampa	80.00	Diesel	2,150.00
Industria Textiles del Lago (ITDL6)	30.00	Heavy Oil	1,695.00
Generadora Progreso	22.00	Heavy Oil	1,358.20
Stewart & Stevenson	51.00	Diesel	215.54
Escuintla Gas 5	41.85	Diesel	178.45
Inteccsa Bunker	3.00	Heavy Oil	158.50
Coenesa	10.00	Diesel	73.45
Escuintla Gas 3	35.00	Diesel	15.64
Inteccsa Diesel	6.40	Diesel	13.60
Laguna Gas	26.00	Diesel	0.00

Figure 9 indicates the typical energy supply in the dry season in 2011. In short term, the output of the geothermal and biomass power plants is constant, and the hydro power plants are operated under a schedule planed in advance. The output of the thermal power plants, especially the gas-turbine plants, is controlled to respond to the short-term fluctuation of the demand.

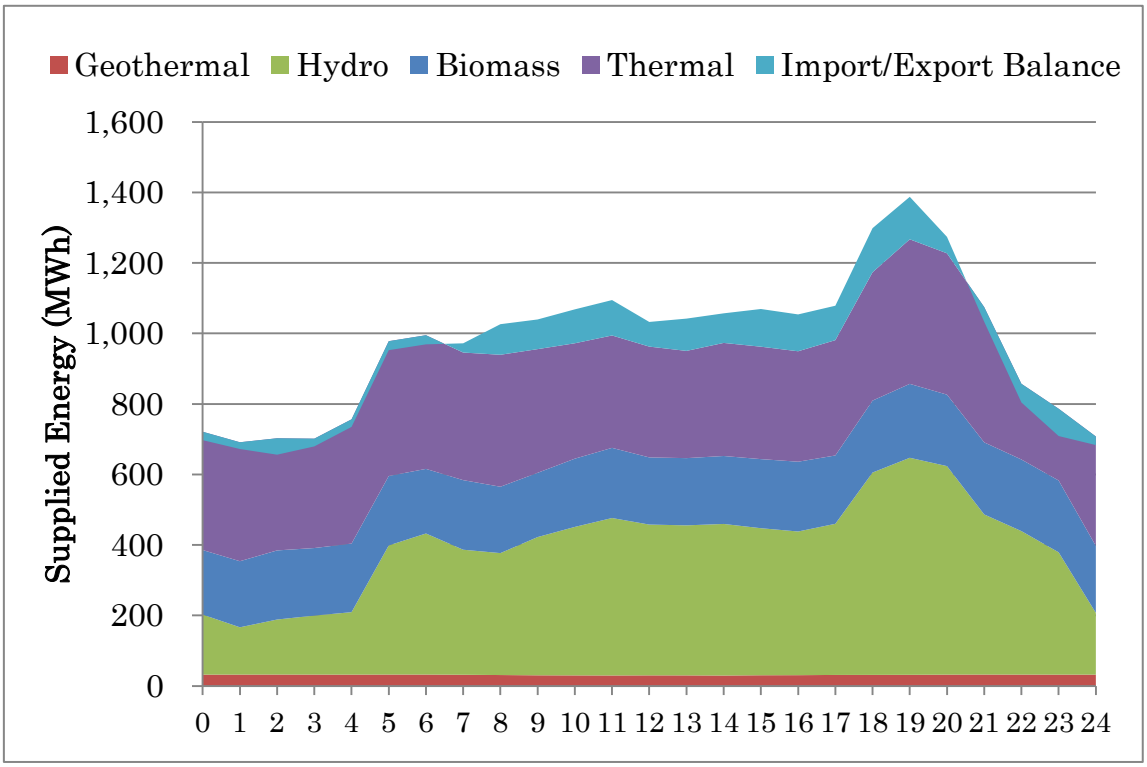

Fig. 9: Guatemala's typical energy supply in dry season in 2011 (Administrador del Mercado Mayorista 2014)

2.5.2. Electric Grids

Guatemala's electric system consists in one grid, and it connects all the power plants and all urban and most rural areas. It makes the analysis of the grid management simple, and is the advantage of this study. A map of Guatemala's electric system is indicated in Fig. 10.

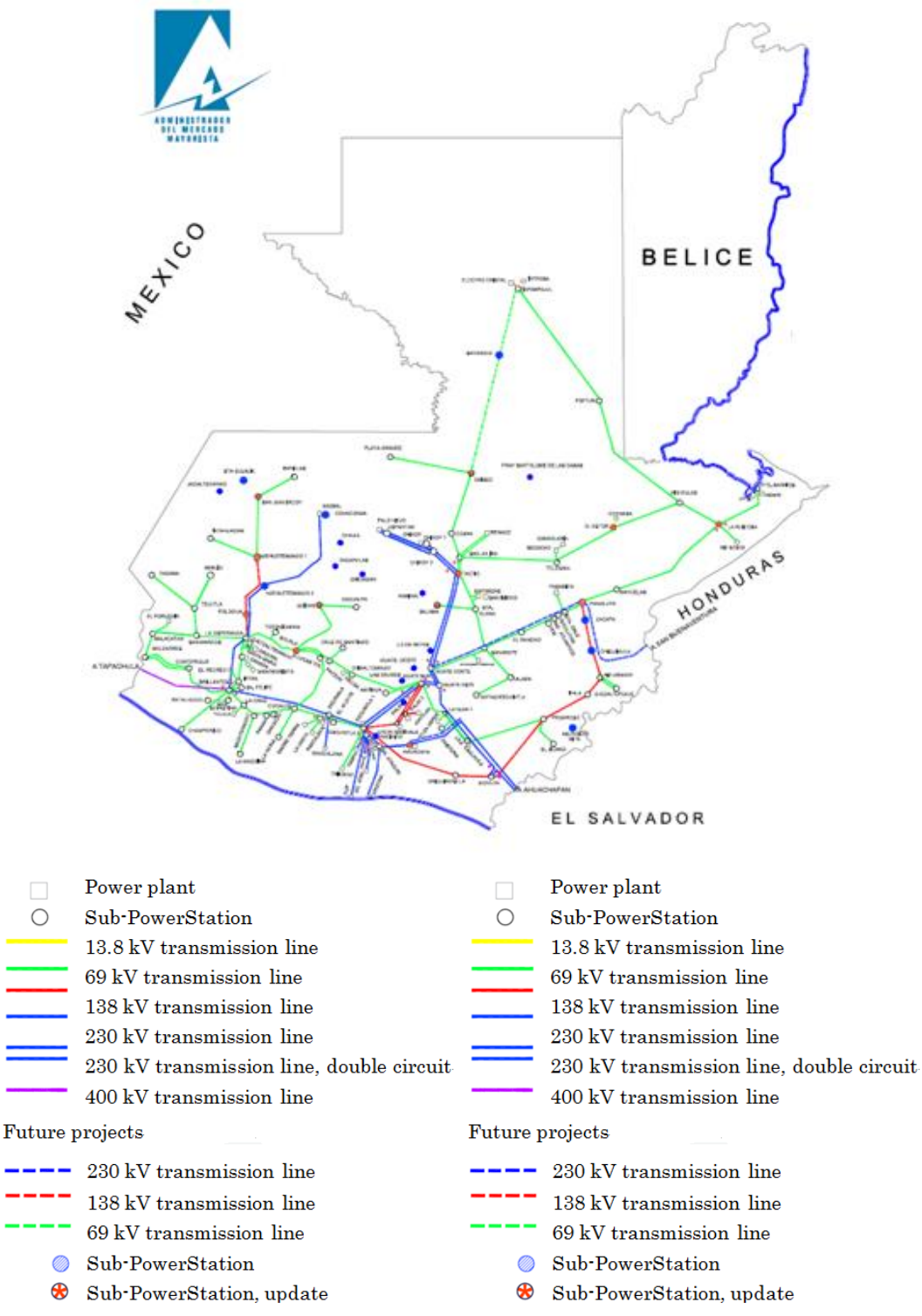

Fig. 10: Guatemala's electric grid as of December 2011 (Administrador del Mercado Mayorista 2014)

This system is managed by the Wholesale Market Administrator (Administrador del Mercado Mayorista, AMM) who is responsible for estimating the daily energy demand and preparing an electric generation schedule for the available power plants.

2.5.3. Electricity Demand

The typical energy demand curve for the year 2011 is indicated in Fig. 11. The demand increases during the day and reaches its peak in the early evening. The demand in the midnight is about half of the peak demand.

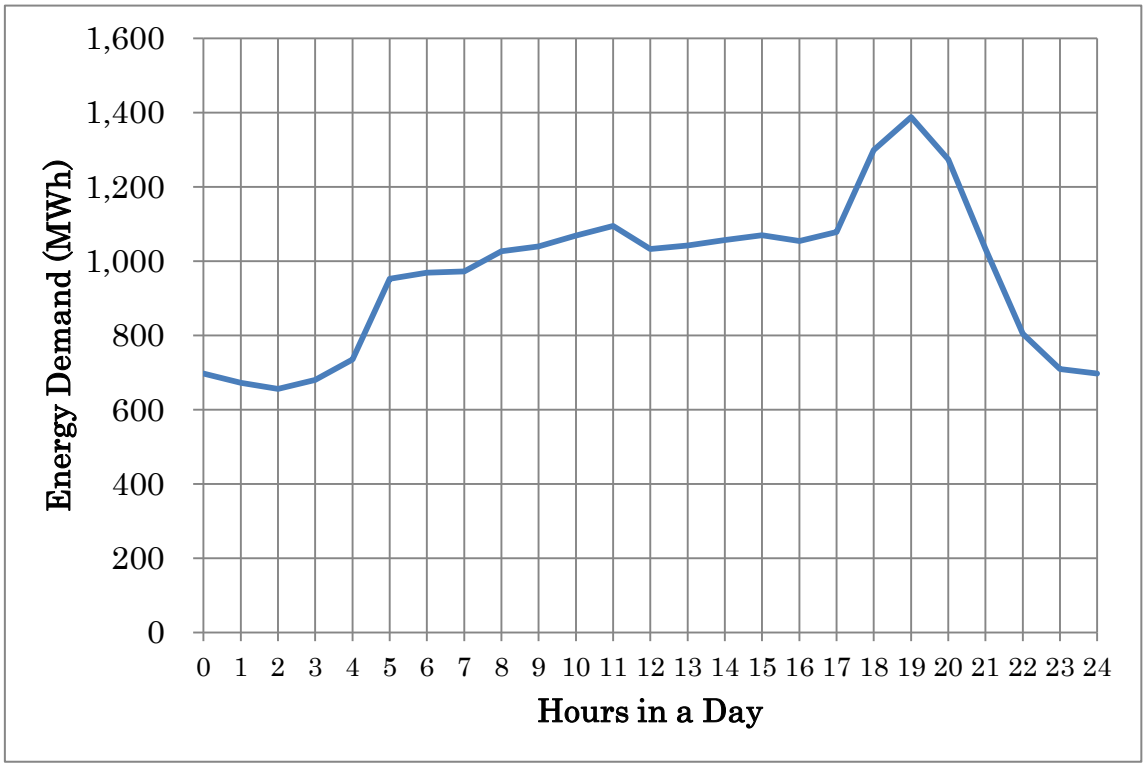

Fig. 11: Guatemala's typical daily energy demand curve in 2011 (Administrador del Mercado Mayorista 2014).

2.5.4. Electric Power Trading

Guatemala imports or exports the electric power between the neighbor countries; Mexico and El Salvador. Figure 12 indicates the typical daily import-export trend of the traded power. The power trading supports the

electricity demand usually in daytime, as shown in Fig. 9. However, most of the trading electric power, about 150 MWh in daytime is passing through Guatemala, and the consumed power in Guatemala is about 50 MWh during the daytime as shown in Figures 11 and 12. The consumed power is small compared with the total capacity 2,795 MW of the electric power plants in Guatemala.

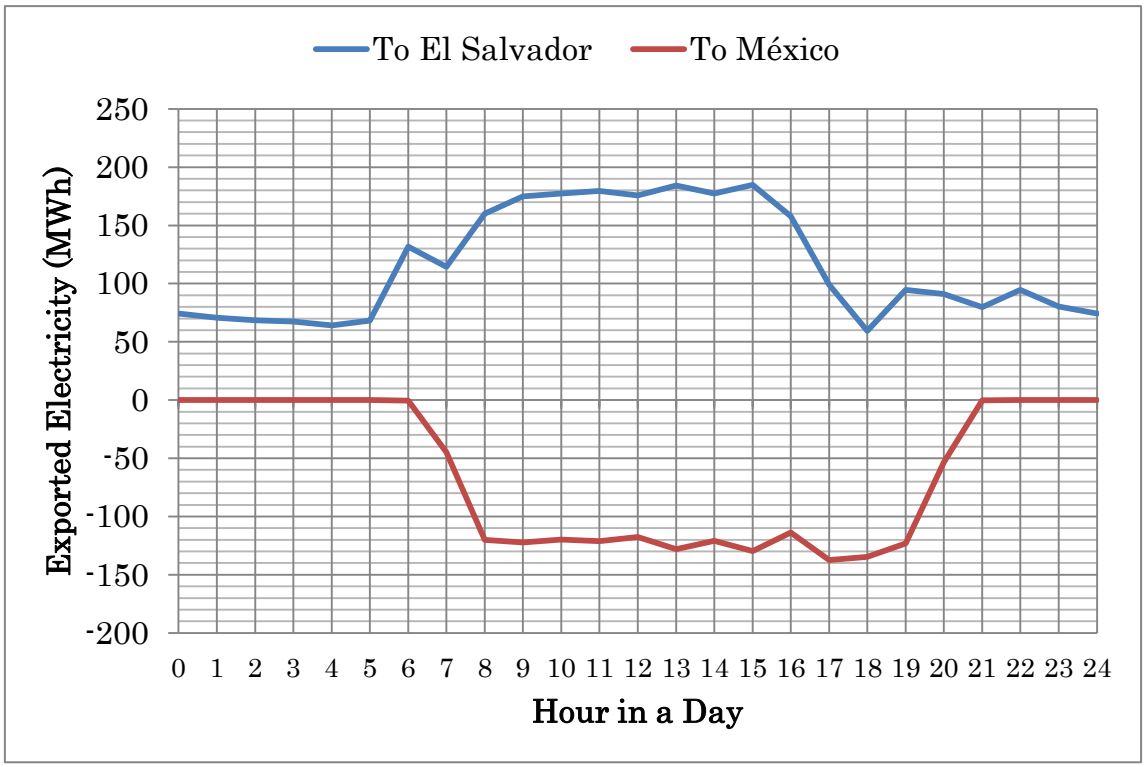

Fig. 12: Typical daily exported electricity in Guatemala in 2011; negative values indicate import (Administrador del Mercado Mayorista 2014).

2.5.5. Background of Energy systems in Guatemala

Guatemala's electric energy system is mainly composed by suppliers and consumers. The suppliers in this system are the owners of the power plants and the consumers are domestic, offices and industries. In addition, since the energy systems require large infrastructure for transportation and distribution, separate entities exist to manage and operate them.

In the past, the electric system was controlled by the state owned National Electrification Institute (Instituto Nacional de Electrificación, INDE). This state run company controlled everything including generation, transportation and distribution. Some private companies were allowed to build their own power plants and sell directly to INDE. This changed in December 7th 1994 when it was declared as an autonomous entity by the national decree 64-94. Afterwards in 1996 the Wholesale Market Administrator (Administrador del Mercado Mayorista, AMM) was created was created). This new entity is an energy trader, whose function are:

- Operational coordination of the power plants, international interconnection and transportation at minimum cost.
- Establish market prices for energy and power transfer between suppliers, consumers, distributors and transporters.
- Guarantee the safety and supply of energy for Guatemala.

Along with this new entity, the General Law for Electricity was created by the Decree No. 93-96 and regulated by a governmental agreement No. 256-97. This new law transforms Guatemala's electric system in to an open market, in which private parties may invest.

3. Solar Irradiance

There are several studies on solar energy potential for Guatemala; Bracamonte Orozco (1986) prepared a Guatemala solar map from the field observation data. National Renewable Energy Laboratory (2014) evaluated yearly and monthly averaged Global Horizontal Irradiance (GHI) and Direct Normal Irradiance (DNI), and Perez (2004) also evaluated yearly and monthly GHI. They applied Perez et al. (2002) model which evaluates irradiance from satellite visible images. These prior studies showed the high potential of PV production in Guatemala, and also indicated the regional difference of the potential in this country. However, the PV potential analyses for this country are limited.

3.1. Previous studies

Solar and Wind Energy Assessment (SWERA) is a programme by the United Nations Environmental Programme (UNEP) that started in 2006 with a mission to provide high quality information on renewable energy resources around the world, along with the tools needed to apply these data in ways that facilitate renewable energy policies and investments.

The programme uses a range of established data gathering techniques such as Satellite derived data. This data can be used to prepare rough assessment of solar and wind energy potentials, relying on sophisticated computer models of atmospheric dynamics. High resolution modeling results are available for several world regions.

The data from the SWERA project can be found in the website titled “Open Energy Info”, sponsored by the U.S. Department of Energy and developed by the National Renewable Energy Laboratory. The data includes Geographic Information Systems (GIS), time data series and maps (OpenEI, Open Energy Info 2012). Included in this database are datasets, time series, maps and geographic information system (GIS) for Guatemala and Central

America.

3.1.1. National Renewable Energy Laboratory (NREL)

This research institutes is part of the Department of Energy, Office of Energy Efficiency and Renewable Energy, and operated by the Alliance for Sustainable Energy, LLC.

For the SWERA programme, they generated the following data for Guatemala and Central America Monthly and annual average direct normal irradiance (DNI), global horizontal irradiance (GHI), and diffuse irradiance data and GIS data at 40km resolution for Central America and the Caribbean.

These data provide monthly average and annual average daily total solar resource over a surface grid of approximately 40 km by 40 km in size. The solar resource value is represented in watt-hours per square meter per day for each month. The data was developed from NREL's Climatological Solar irradiance (CSR) Mode (OpenEI, Open Energy Info 2012).

Figures 13 and 14 are maps available in the Open Energy Info webpage. They are generated using the data described previously.

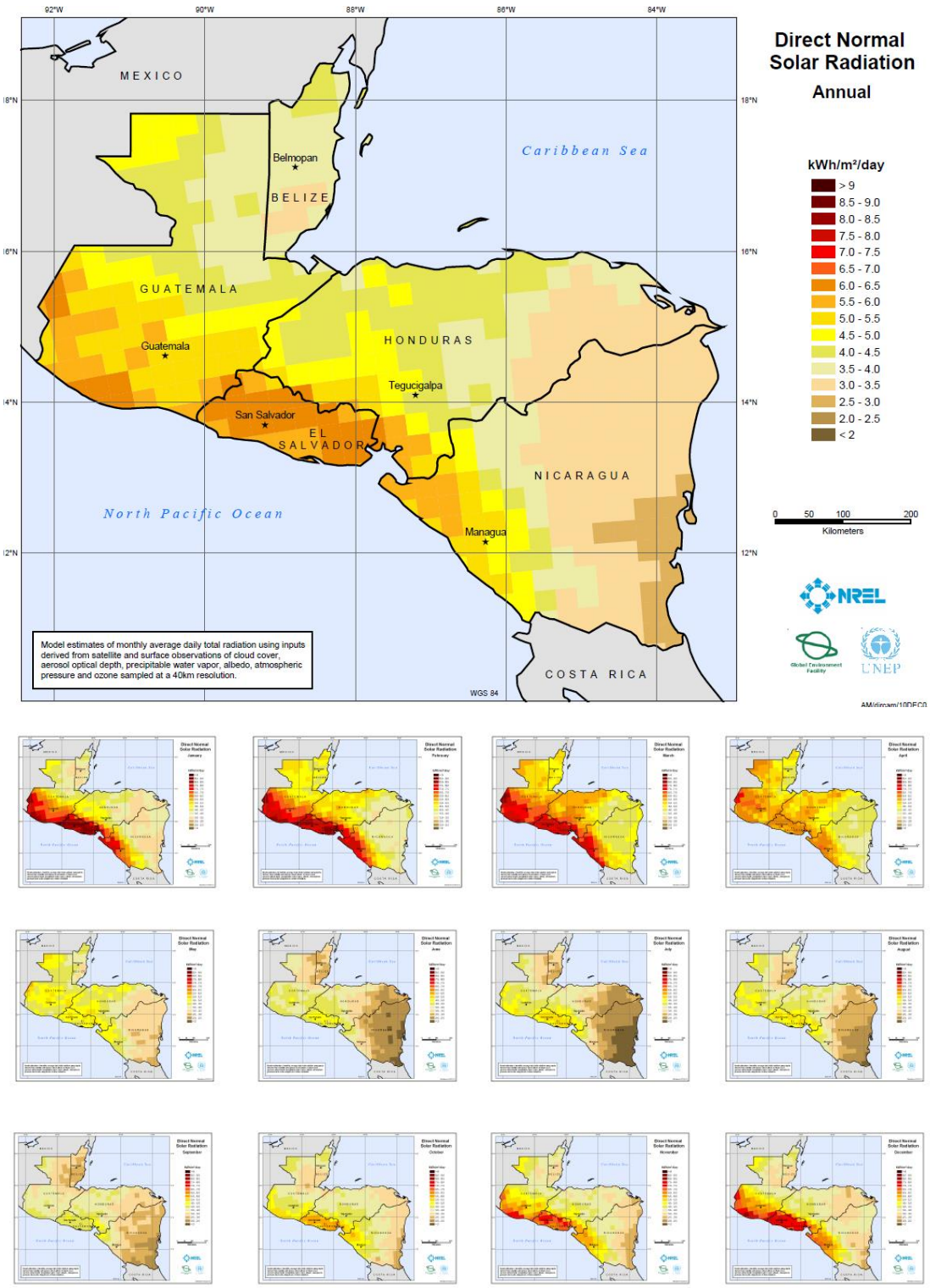

Fig. 13: Direct normal irradiance for Central America, year average and month average (National Renewable Energy Laboratory 2014)

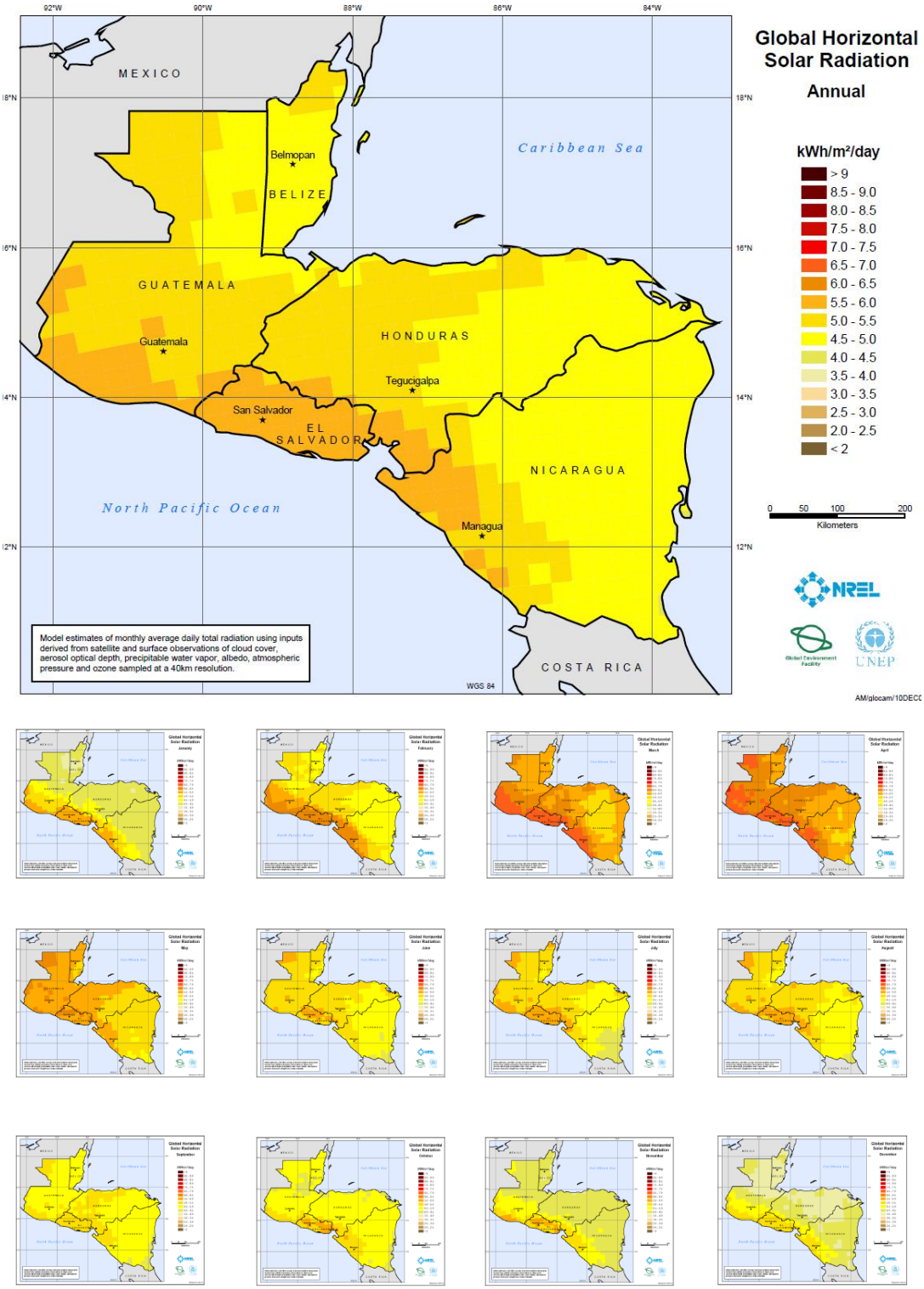

Fig. 14: Global horizontal irradiance for Central America, year average and month average (National Renewable Energy Laboratory 2014).

3.1.1. State University of New York (SUNY)

SUNY is a system of public institutions of higher education in New York, United States. It is composed by 64 campuses across New York State, which includes four University Centers: Albany, Buffalo, Binghamton and Stony Brook. The main contributor for the Solar and Wind Energy Resource Assessment (SWERA) project is the campus at Albany, New York. By whom the following data for Guatemala and Central America was generated:

3.1.1.1. State University of New York (SUNY), estimated data

The State University of New York developed a data set for Central America that includes monthly average direct normal and global horizontal irradiance with a 10km by 10km resolution. These data provide monthly average and annual average daily total solar resource averaged over surface cell of approximately 10 km by 10 km in size. The solar value is represented as kilowatt-hours per square meter per day for each month. The data sets were developed from the State University of New York's GOES satellite solar model (Perez, et al. 2002) for the SWERA programme. Figure 15 displays the daily average global horizontal irradiance distribution for Guatemala.

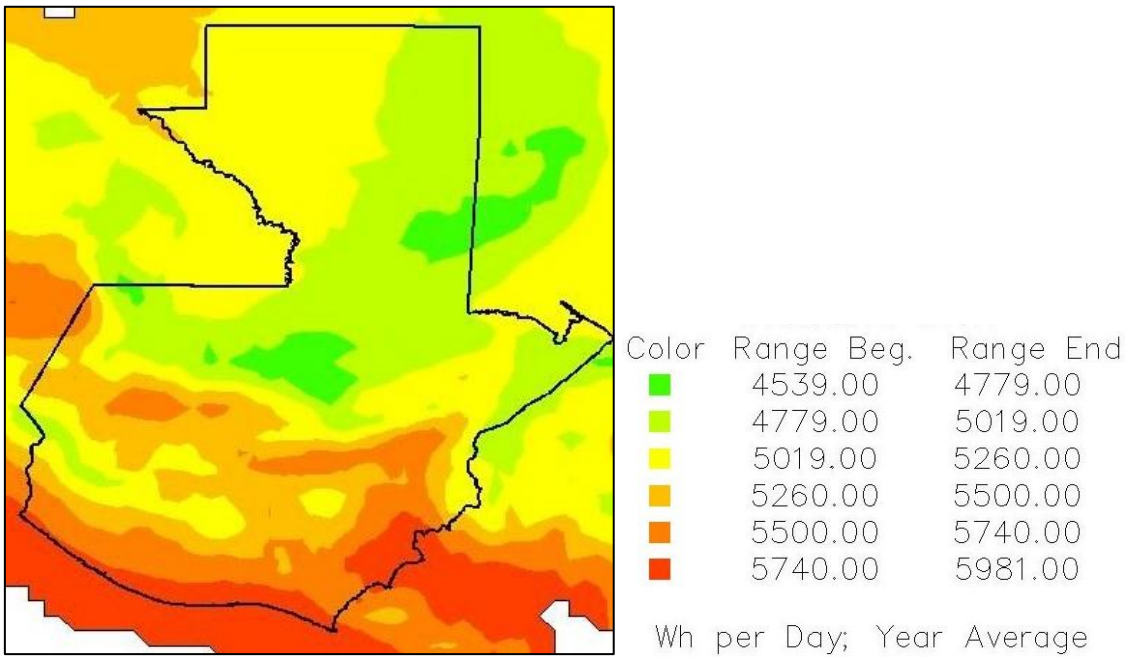

Fig. 15: Global horizontal irradiance, year daily average kWh per day. State University of New York (Perez, et al. 2002).

3.1.1.2. SUNY observed data

From 1998 to 2002 the State University of New York collected hourly direct normal irradiance (DNI), global horizontal irradiance (GHI) and diffuse irradiance from 1998 to 2002 for the following stations in Guatemala:

Table 3: Meteorological stations location.

Meteorological Station	Department	Longitude	Latitude
Chiquimula	Chiquimula	14.85°	-89.55°
Cobán	Alta Verapaz	15.45°	-90.45°
Guatemala City	Guatemala	14.65°	-90.55°
Huehuetenango	Huehuetenango	15.35°	-91.45°
Highest Guatemala	Huehuetenango	15.45°	-91.65°
Jalapa	Jalapa	14.65°	-89.95°
Motagua Valley	Izabal	15.35°	-88.85°

Pacific Coast 1	Retalhuleu	15.75°	-91.75°
Pacific Coast 2	Escuintla	13.95°	-90.65°
Lowest Guatemala	Escuintla	14.45°	-90.25°
Puerto Barrios	Izabal	15.75°	-88.65°
Quetzaltenango	Quetzaltenango	14.85°	-91.55°
Retalhuleu	Retalhuleu	14.55°	-91.65°
North Lake	Petén	16.95°	-89.95°

Figure 16 shows the location of the meteorological stations described in Table 3.

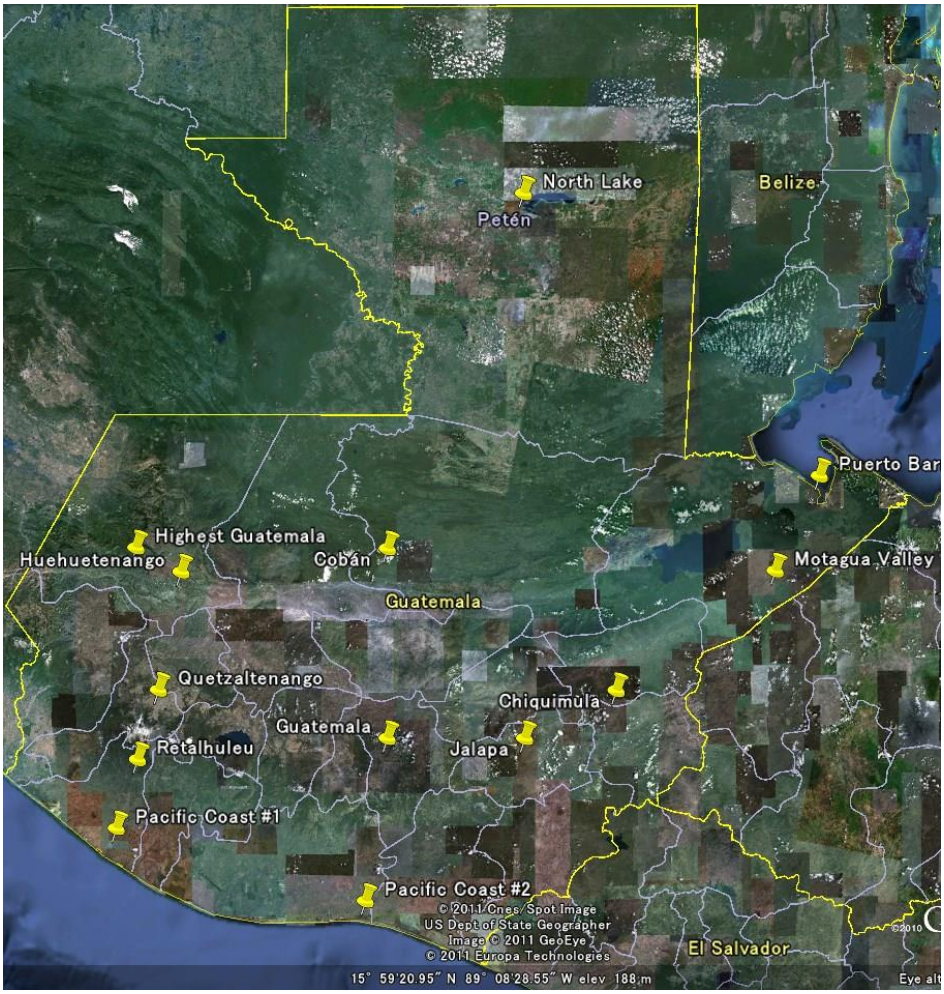

Fig. 16: Meteorological stations location (Google Earth 2015).

Al of the meteorological stations are still in operation, however the equipment for the observation of DNI and GHI was removed after the study reached its end. In December 2014, the only meteorological station that measures GHI is located in Guatemala City in the head offices of the National Institute of Seismology, Volcanology, Meteorology and Hydrology (INSIVUMEH).

3.2. Estimation of Solar Irradiance

PV panel output can be described as a function of power rating, solar irradiance, conversion efficiency, etc. Therefore, in order to estimate the PV output the estimation of the meteorological data, e.g. solar irradiance and ambient temperature which is related to the panel efficiency, are required.

Observed irradiance data for Guatemala is limited and is from only a meteorological station in Guatemala City (14°35'14" N, 90°31'59"W) as indicated its location in Fig. 3. Furthermore the data sets only include daily and monthly average irradiance. For the temperature, the data sets only include its daily maximum, minimum and average. The present study requires hourly irradiance and ambient temperature for one year in the whole country.

3.3. Meteorological Model, Weather Research and Forecasting

In order to obtain the time series meteorological data, the numerical model Weather Research and Forecasting (WRF) is employed as a meteorological model. This model simulates the weather over the target area including rain, clouds, irradiance and temperature. The WRF is developed by the National Oceanic and Atmospheric Administration (NOAA) and the National Center for Atmospheric Research (NCAR) (Skamarock et al. 2008). The WRF is a fully compressible, non-hydrostatic mesoscale meteorological model.

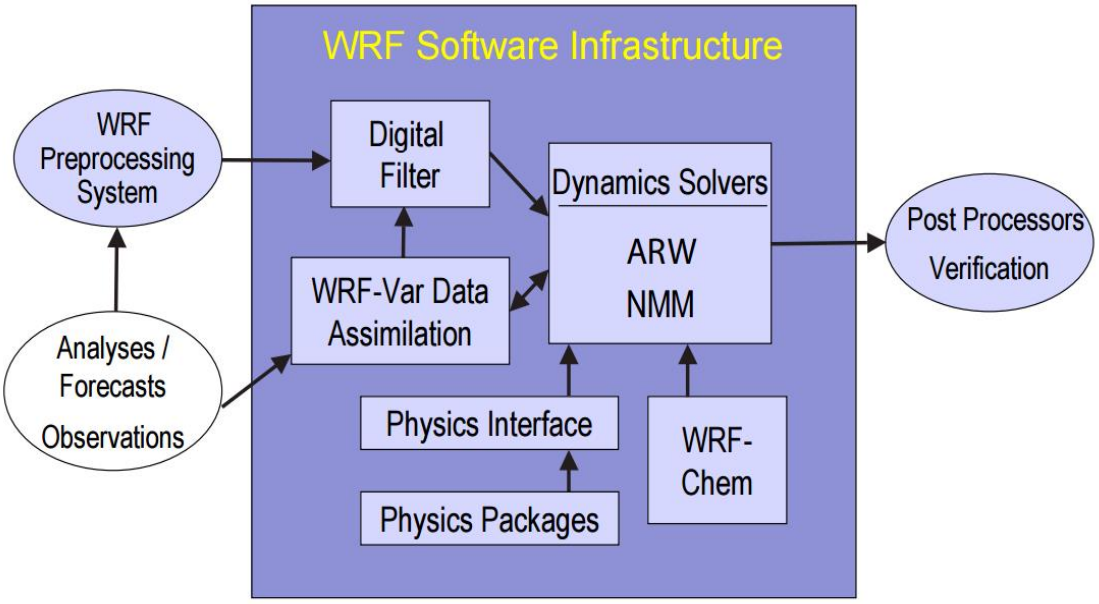

Fig. 17: WRF system components (Skamarock et al. 2008)

Figure 17 shows the principal components of the WRF system, the WRF software framework (WSF) provides the infrastructure that accommodates the dynamics solvers, physics packages that interface with the solvers, programs for initialization, WRF-Var, and WRF-Chem. There are two dynamics solvers in the WSF' the Advanced Research WRF (ARW) solver and the Nonhydrostatic Mesoscale Model (NMM) solver (Skamarock et al. 2008).

3.3.1. Governing Equations

The ARW dynamics solver integrates the compressible, non-hydrostatic Euler equations. The equations are formulated using a terrain-following hydrostatic-pressure vertical coordinate denoted by η and defined as:

$$\eta = (p_h - p_{ht})/\mu \qquad \text{where} \quad \mu = p_{hs} - p_{ht}. \tag{1}$$

p_h is the hydrostatis component of the pressure and p_{hs} and p_{ht} refer to values along the surface and top boundaries respectively. η varies from a value of 1 at the surface to 0 at the upper boundary of the model domain, refer to Fig. 18. This vertical coordinate is also called a mass vertical

coordinate.

$\mu(x,y)$ represents the mass per unit area within the column in the model domain at (x,y), the appropriate flux form variables are

$$\mathbf{V} = \mu\mathbf{v} = (U,V,W), \quad \Omega = \mu\dot{\eta}, \quad \Theta = \mu\theta. \tag{2}$$

$V = (U,V,W)$ are the covariant velocities in the two horizontal and vertical directions, respectively, while $\omega = \eta$ is the contravariant "vertical" velocity. θ is the potential temperature. Also apperating in the governing equations of the ARW are the non-conserved variables $\phi = gz$ (the geopotential), p (pressure), and $\alpha = 1/\rho$ (the inverse density).

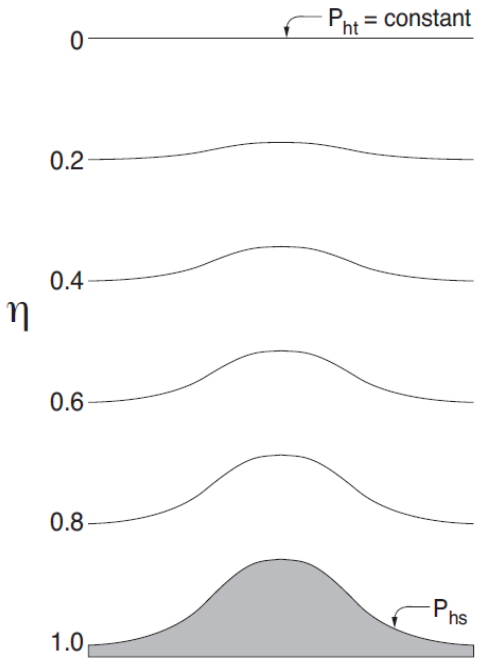

Fig. 18: ARW η coordinate.

Using these variables definitions, the flux-form Euler equations can be written as:

$$\partial_t U + (\nabla \cdot \mathbf{V}u) - \partial_x(p\phi_\eta) + \partial_\eta(p\phi_x) = F_U \tag{3}$$

$$\partial_t V + (\nabla \cdot \mathbf{V}v) - \partial_y(p\phi_\eta) + \partial_\eta(p\phi_y) = F_V \tag{4}$$

$$\partial_t W + (\nabla \cdot \mathbf{V}w) - g(\partial_\eta p - \mu) = F_W \quad (5)$$

$$\partial_t \Theta + (\nabla \cdot \mathbf{V}\theta) = F_\Theta \quad (6)$$

$$\partial_t \mu + (\nabla \cdot \mathbf{V}) = 0 \quad (7)$$

$$\partial_t \phi + \mu^{-1}[(\mathbf{V} \cdot \nabla\phi) - gW] = 0 \quad (8)$$

Along with the diagnostic relation for the inverse density

$$\partial_\eta \phi = -\alpha\mu \quad (9)$$

And the equation of state

$$p = p_0(R_d\theta/p_0\alpha)^\gamma \quad (10)$$

In equations 3 and 10, the subscripts x, y and h denote differentiation

$$\nabla \cdot \mathbf{V}a = \partial_x(Ua) + \partial_y(Va) + \partial_\eta(\Omega a) \quad (11)$$

and

$$\mathbf{V} \cdot \nabla a = U\partial_x a + V\partial_y a + \Omega\partial_\eta a \quad (12)$$

Where a represents a generic variable $\gamma = c_p/c_v$=1.4 is the ratio of the heat capacities for dry air, R_d is the gas constant for dry air, and p_0 is a reference pressure (typically 10^5). The right hand side terms F_U, F_V, F_W, and F_Θ represent forcing terms arising from model physics, turbulent mixing, spherical projections, and the earth's rotation

The prognostic equations 3 to 8 are cast in conservative form except for 8 which is the material derivative of the determination of the geopotential.

Moisture is included by formulating the moist Euler equations, which retain the coupling of dry air mass to the prognostic variables and also retain the conversion equation for dry air (equation 7), In addition the coordinate is defined with respect to the dry air mass, the vertical coordinate can be written as:

$$\eta = (p_{dh} - p_{dht})/\mu_d \tag{13}$$

Where μ_d represents the mass of the dry air in the column and p_{dh} and p_{dht} represent the hydrostatic pressure of the dry atmosphere and the hydrostatic pressure at the top of the dry atmosphere. The coumpled variables are defined as:

$$\mathbf{V} = \mu_d \mathbf{v}, \quad \Omega = \mu_d \dot{\eta}, \quad \Theta = \mu_d \theta. \tag{14}$$

With these definitions, the moist Euler equations can be written as:

$$\partial_t U + (\nabla \cdot \mathbf{V}u) + \mu_d \alpha \partial_x p + (\alpha/\alpha_d)\partial_\eta p \partial_x \phi = F_U \tag{15}$$
$$\partial_t V + (\nabla \cdot \mathbf{V}v) + \mu_d \alpha \partial_y p + (\alpha/\alpha_d)\partial_\eta p \partial_y \phi = F_V \tag{16}$$
$$\partial_t W + (\nabla \cdot \mathbf{V}w) - g[(\alpha/\alpha_d)\partial_\eta p - \mu_d] = F_W \tag{17}$$
$$\partial_t \Theta + (\nabla \cdot \mathbf{V}\theta) = F_\Theta \tag{18}$$
$$\partial_t \mu_d + (\nabla \cdot \mathbf{V}) = 0 \tag{19}$$
$$\partial_t \phi + \mu_d^{-1}[(\mathbf{V} \cdot \nabla \phi) - gW] = 0 \tag{20}$$
$$\partial_t Q_m + (\nabla \cdot \mathbf{V}q_m) = F_{Q_m} \tag{21}$$

With the diagnostic equation for dry inverse density

$$\partial_\eta \phi = -\alpha_d \mu_d \tag{22}$$

And the diagnostic relation for the full pressure

$$p = p_0 (R_d \theta_m / p_0 \alpha_d)^\gamma \tag{23}$$

Where α_d is the inverse density of the dry air and α is the inverse density taking into account the full parcel density $\alpha = (1 + q_v + q_c + q_v + \cdots)$ where q_* are the mixing rations for water vapor, cloud, rain, ice, etc.

3.3.2. Initial Conditions

The ARW may be run with user-defined initial conditions for idealized

simulations, or it may be run using interpolated data from either an external analysis or forecast for real-data cases.

The initial conditions for the real-data cases are pre-processed through a separate package called the WRF Preprocessing System. The output from WPS is passed to the real-data pre-processor in the ARW which generates initial and lateral boundary conditions.

3.3.2.1. Reference State

In order to conduct the simulation for real-data conditions the flow in Fig. 19 is required. The flow chart shows the data flow and program components and how it feeds the initial conditions to ARW. The names inside the rectangular boxes are the program's names, GEOGRID defines the model domain and create static files of terrestrial data, UNGRIB decodes GriB data and METGRID interpolates meteorological data to the model domain.

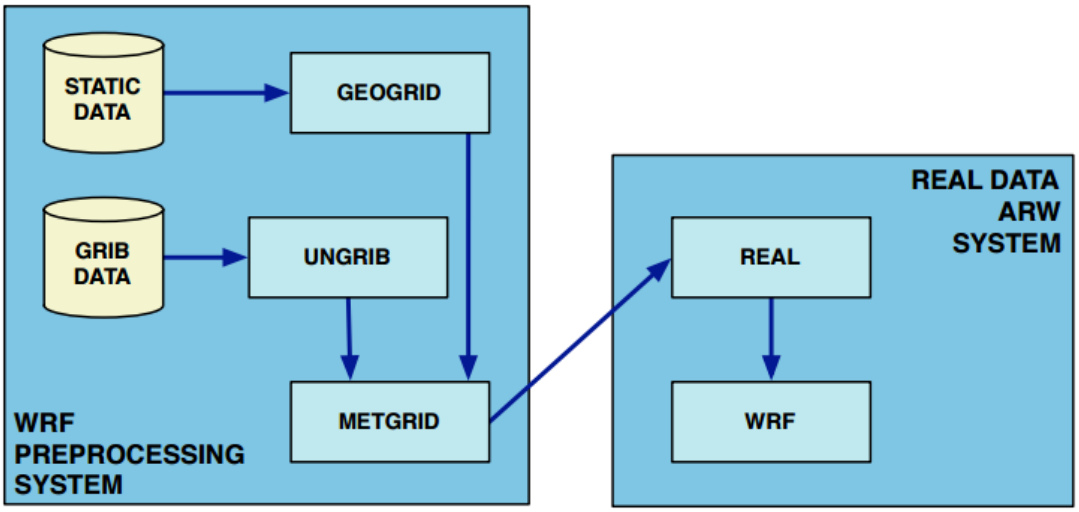

Fig. 19: Flow chart displaying the data flow and program components for the use of a Reference State for a simulation (Skamarock et al. 2008).

The reference state is defined by terrain elevation and three constants: p_o (10^5Pa) reference sea level pressure, T_o (270 °K – 300 °K) reference sea level temperature, and A (50 °K) temperature difference between the pressure levels of p_o and p_o/e.

With these parameters, the dry reference state surface pressure is given by

$$p_{dhs} = p_0 \; exp\left(\frac{-T_0}{A} + \sqrt{\left(\frac{T_0}{A}\right)^2 - \frac{2\phi_{sfc}}{A\; R_d}}\right) \tag{24}$$

From equation 24, the three dimensional reference pressure (dry hydrostatic pressure p_{dh}) is computed as a function of the vertical coordinate η levels and the model top p_{dht}:

$$p_{dh} = \overline{p}_d = \eta\; (p_{dhs} - p_{dht}) + p_{dht} \tag{25}$$

With equation 25, the reference temperature is defined as

$$T = T_0 + A\; ln\frac{\overline{p}_d}{p_0} \tag{26}$$

From the reference temperature and pressure, the reference potential temperature is defined as

$$\overline{\theta}_d = \left(T_0 + A\; ln\frac{\overline{p}_d}{p_0}\right)\left(\frac{p_0}{\overline{p}_d}\right)^{\frac{R_d}{C_p}} \tag{27}$$

Then the reciprocal of the reference density using equations 25 and 27 is given by

$$\overline{\alpha}_d = \frac{1}{\overline{\rho}_d} = \frac{R_d\; \overline{\theta}_d}{p_0}\left(\frac{\overline{p}_d}{p_0}\right)^{-\frac{C_v}{C_p}} \tag{28}$$

The base state difference of the dry surface pressure from equation 24 and the model top is given by

$$\overline{\mu}_d = p_{dhs} - p_{dht} \tag{29}$$

From equations 28 and 29, the reference state geopotential defined from the hydrostatic relation is given by

$$\delta_\eta \overline{\phi} = -\overline{\alpha}_d\; \overline{\mu}_d \tag{30}$$

3.3.3. Nesting

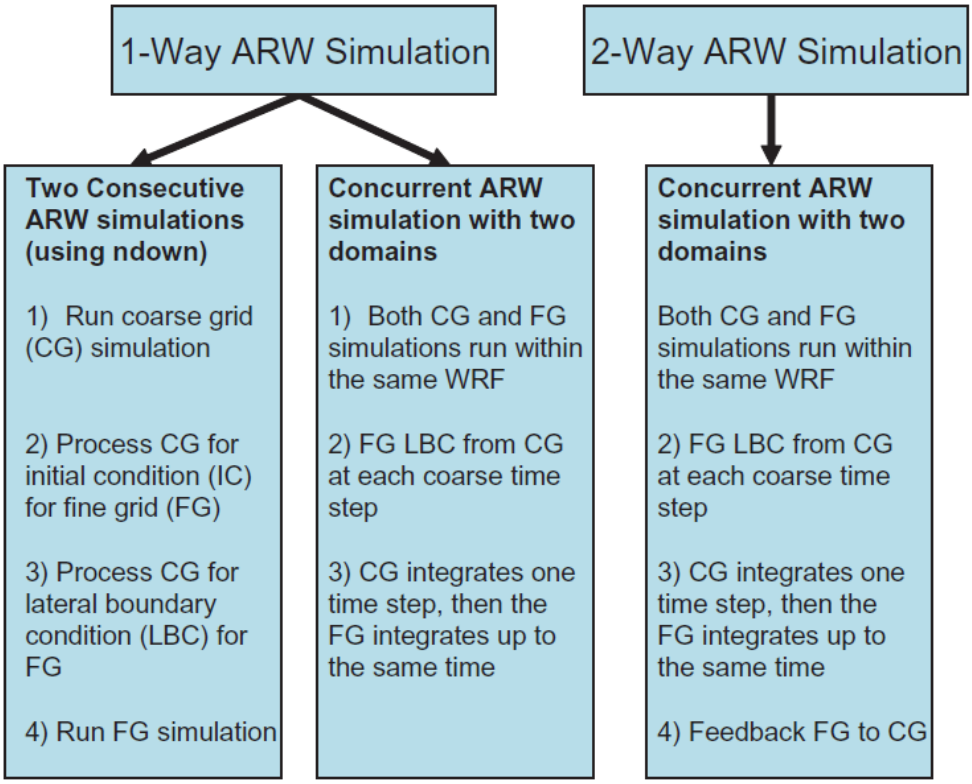

Fig. 20: 1-way and 2-way nesting options (Skamarock et al. 2008).

Nested grid simulations can be produced using either 1-way nesting or 2-way nesting as outlined in Fig. 20. The 1-way and 2-way nesting options refer to how a coarse grid and the fine grid interact. In both the 1-way and 2-way simulation modes, the fine grid boundary conditions are interpolated from the coarse grid forecast. In a 1-way nest, this is the only information exchange between the grids. In the 2-way nest integration, the fine grid solution replaces the coarse grid solution for coarse grid points that lie inside the fine grid. This information exchange between the grids is now in both directions.

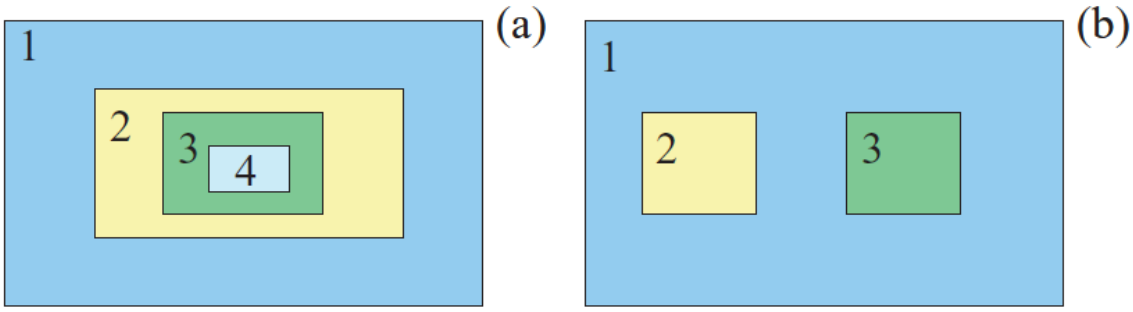

Fig. 21: Various nest configurations for multiple grids (Skamarock et al. 2008).

Figure 21 displays different nest configurations available. (a) simulation involves one outer grid and may contain multiple inner nested grids.

3.4. Computational Conditions

In order to simulate the weather over the Guatemalan territory the computational domains are set as Fig. 22. The domains are nested as indicated in the figure. Table 5 shows the computational conditions. The horizontal resolution of the inner domain, Domain 2 is 10 km. The computation period is the whole one year in 2011. As the initial and boundary conditions for the weather computations, the Final Analysis Data released from the National Center for Environmental Prediction (NCEP) (NCAR Data Support Section, Data for Atmospheric and Geosciences Research 2014) is applied.

The NCEP Final Operational Global Analysis data are on 1-degree by 1-degree grids prepared operationally every six hours. The data comes from the Global Data Assimilation System (GDAS), which continuously collects observational data from the Global Telecommunications System (GTS), and other sources. The analyses are available on the surface, at 26 mandatory levels from 1000 millibars to 10 millibars, in the surface boundary layer and at some sigma layers, the tropopause and a few others. Parameters include surface pressure, sea level pressure, geopotential height, temperature, sea surface temperature, soil values, ice cover, relative humidity, u- and v- winds,

vertical motion, vorticity and ozone (NCAR Data Support Section, Data for Atmospheric and Geosciences Research 2014). The variables included in the NCEP Final Analysis are displayed in Table 4.

Table 4: Variables included in NCEP Final Analysis (NCAR Data Support Section, Data for Atmospheric and Geosciences Research 2014)

Air Temperature	Clud Liquid Water/Ice	Convection	Evaporation
Geoptential Height	Humidity	Hydrostatic Pressure	Ice Extent
Land Cover	Planetary Boundary Layer Height	Potential Temperature	Precipitable Water
Sea Level Pressure	Sea Surface Temperature	Skin Temperature	Snow Water Equivalent
Soild Moisture/Water Content	Soil Temperature	Surface Air Temperature	Surface Pressure
Surface winds	Terrain Elevation	Tropopause	Tropospheric Ozone
Upper Level Winds	Vertical Wind Motion	Vorticity	

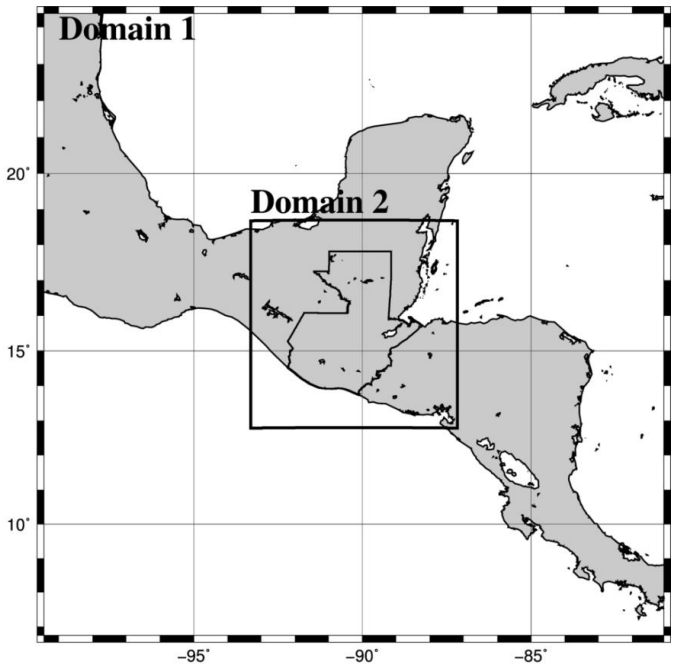

Fig. 22: Computational domains for the meteorological model, WRF

Table 5: WRF model settings for the evaluation of the weather and irradiance in Guatemala.

Period	Start: 2011/01/01 00:00:00 UTC
	End: 2012/01/01 00:00:00 UTC
Input Data	NCEP final analysis (6-hourly, 1 degree x 1 degree)
Output Data	1-hour interval
Nesting	2-way nesting
Domain	Domain 01, D01 (30 km, 61 x 61 grids)
	Domain 02, D02 (10 km, 61 x 61 grids)
Vertical layer	50 levels (surface to 100 hPa)
FDDA option	Disable

3.5. Computed Solar Irradiance

3.5.1. Irradiance Maps

Figure 23 shows the global horizontal irradiance (GHI) calculated with WRF. The GHI in this figure is the daily irradiance averaged in the year

2011. The irradiance distribution is discussed here with the geography of the country shown in Fig. 3. As it can be seen in Fig. 3, There are two mountain chains south of the 16°N grid line that cross the country from west to east. These areas have low GHI in the mountains (3.5 - 4.5 kWh/m^2), and high (5.5 – 7.0 kWh/m^2) GHI in the plateaus in the middle of the mountain ranges. North of the 16°N grid line is a flat area with rain forests and high humidity, where GHI is low (4.0 - 5.0 kWh/m^2). The southern coast facing the Pacific Ocean has high GHI (6.0 - 7.0 kWh/m^2) and is a relatively flat area. Figure 24 shows the yearly GHI in 2011. The irradiance in the high GHI area located in the southern coast reaches almost 2.5 MWh in the year.

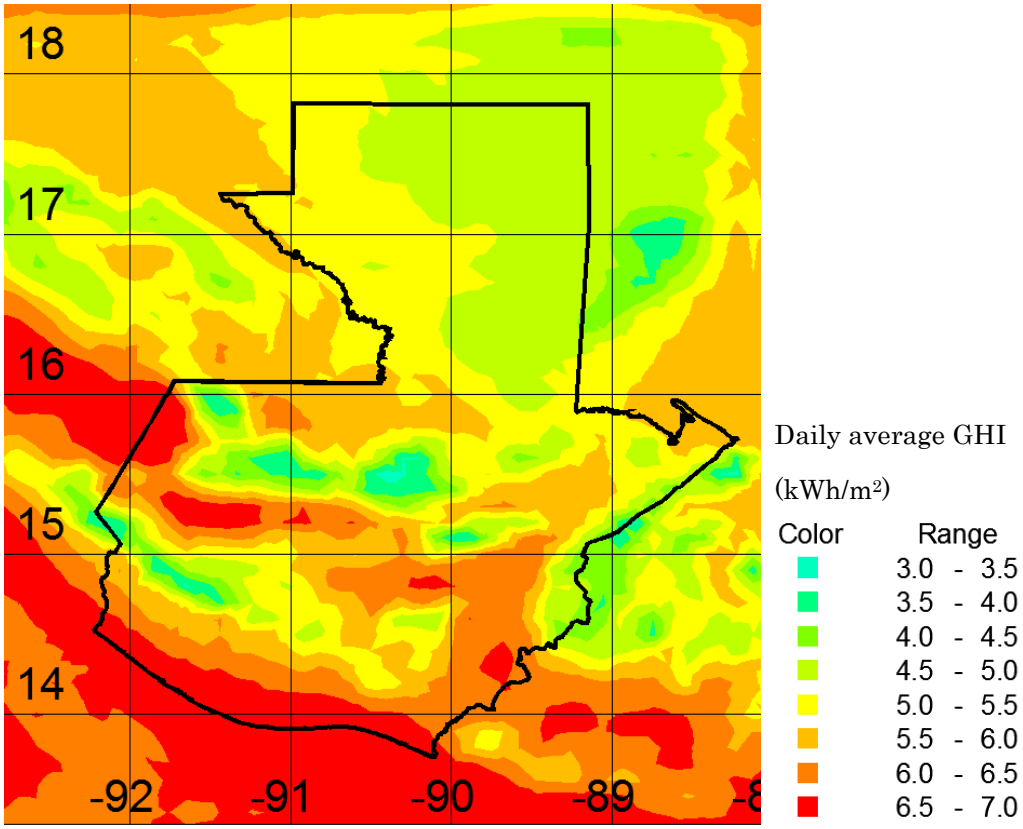

Fig. 23: Global horizontal irradiance in Guatemala. Daily irradiance averaged in the year 2011.

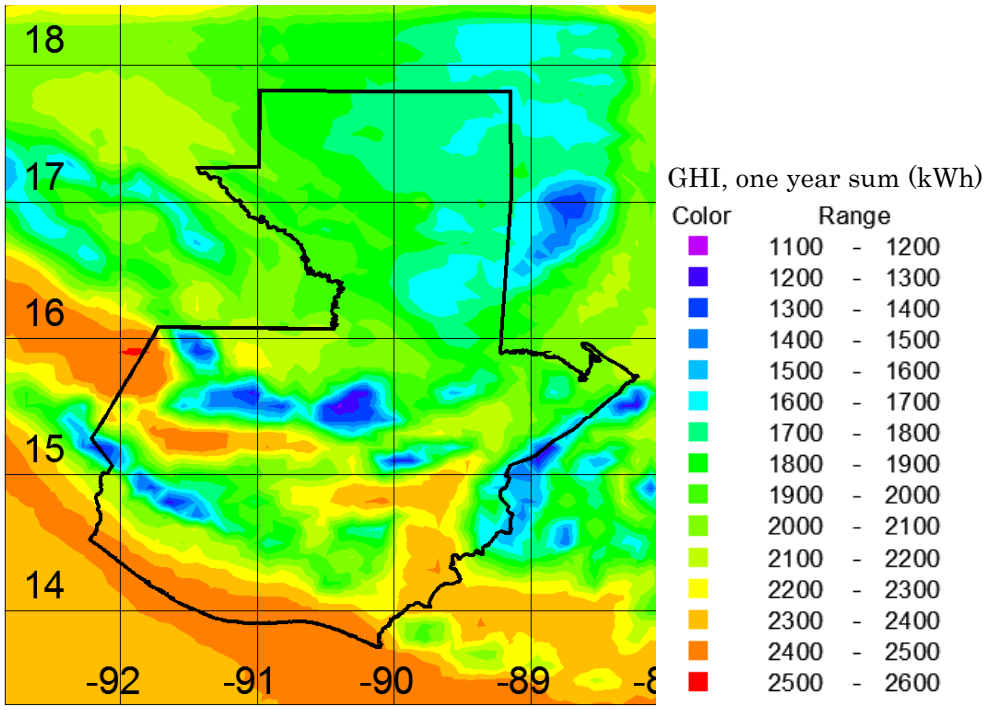

Fig. 24: Global horizontal irradiance in Guatemala. Yearly in 2011.

3.5.2. Time Series Solar Irradiance

Figure 25 shows the daily GHI averaged in a week at the meteorological station in Guatemala City in 2011 (Instituto Nacional de Sismología, Vulcanología, Meteorología e Hidrología 2014). The station is located in low latitude, the sun passes the zenith at the end of April and the middle of August there. Therefore, if there aren't are any effects of the weather to the irradiance the GHI should be the largest in these months, the figure shows that the higher irradiance is relatively high in the dry season (from December to the next May), particularly from February to April, and low due to the cloudy and rainy weather of the wet season (from June to November) in particular from August to October. Due to the variations in GHI throughout the year, the daily solar irradiance and also the PV generation is required for the analysis of the grid management in the following section 6. The observed daily GHI averaged in each month is compared between the simulated data with the WRF in Fig. 26. The WRF estimates the GHI is a

little larger than the observations. The difference is 8% in average for the daily irradiance. The WRF traces the observed monthly irradiance as shown in Fig. 26.

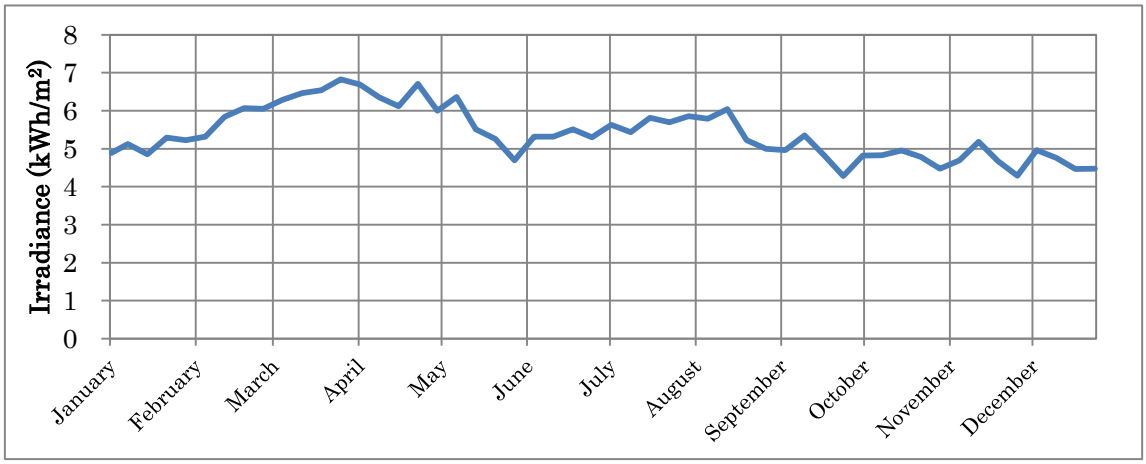

Fig. 25: Observed daily Global Horizontal Irradiance at the meteorological station in Guatemala City, averaged in a week (Instituto Nacional de Sismología, Vulcanología, Meteorología e Hidrología 2014)

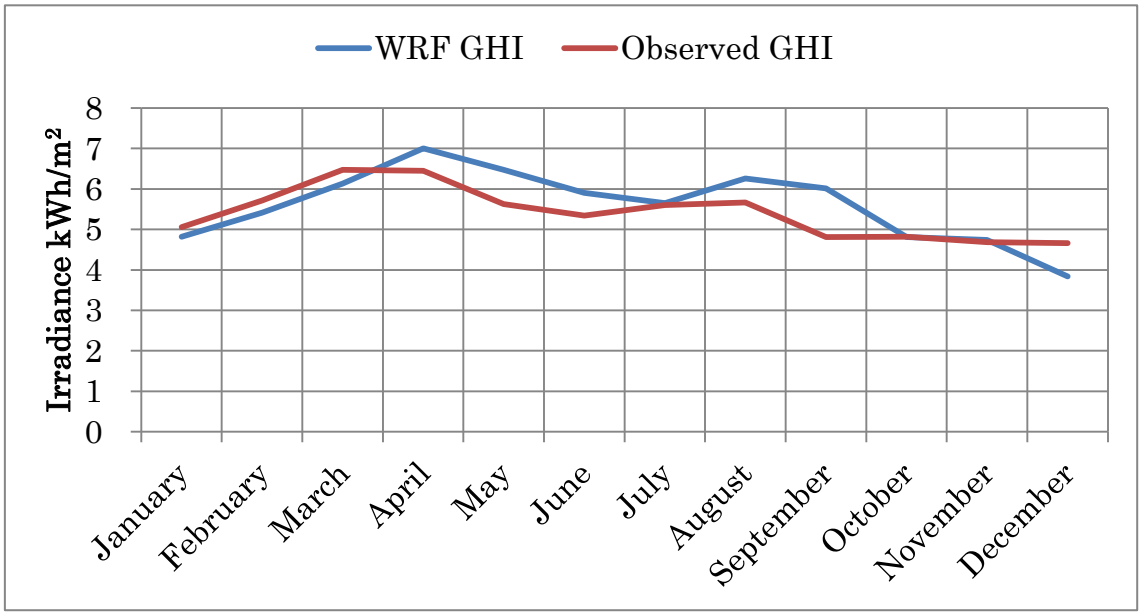

Fig. 26: Daily GHI averaged in each month, evaluated with WRF and observed. (Instituto Nacional de Sismología, Vulcanología, Meteorología e Hidrología 2014)

3.5.2.1. WRF Irradiance validation

In addition the measurements from selected stations in Guatemala, collected by SUNY, are compared to the WRF. The following graphs (Fig. 27(a) – 27 (n)) compare the 5 years of observed data from the 14 meteorological stations. The meteorological stations used in the study conducted by SUNY are still in operation, however, the instruments for measuring DNI and GHI belonged to SUNY and were removed after they study was finished. The only station that still measures GHI is in Guatemala City and the measurements are compared with the results from WRF in Fig. 26.

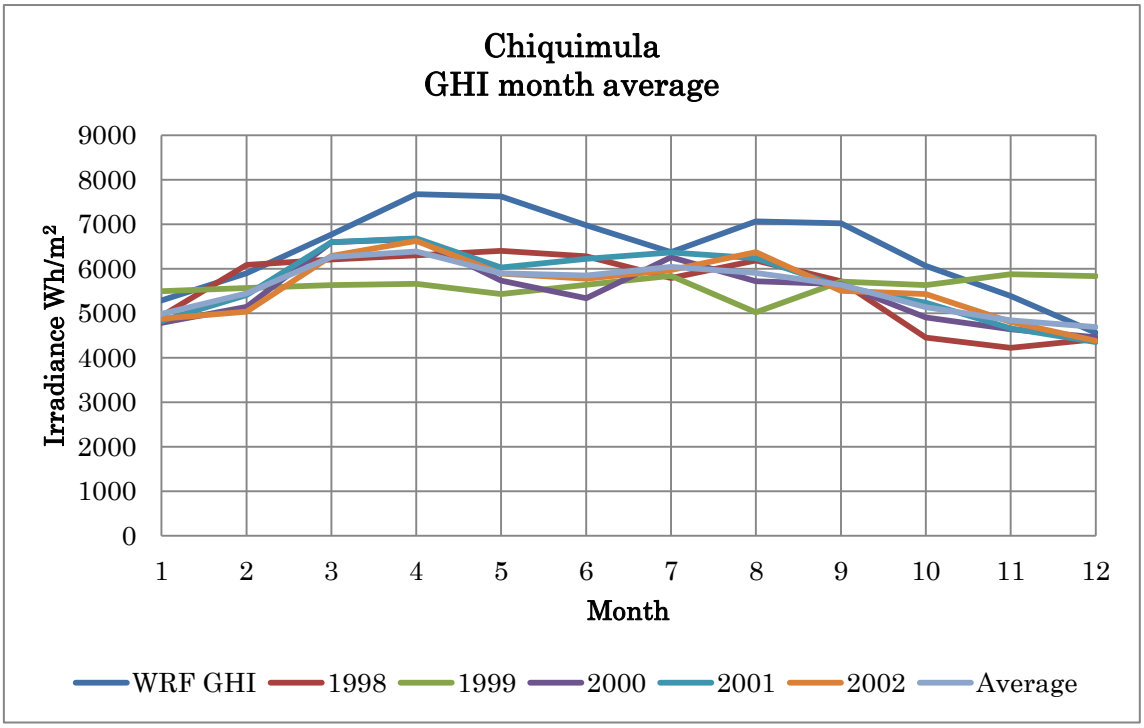

Fig. 27 (a): Chiquimula meteorological station, daily global horizontal irradiance Wh/m²

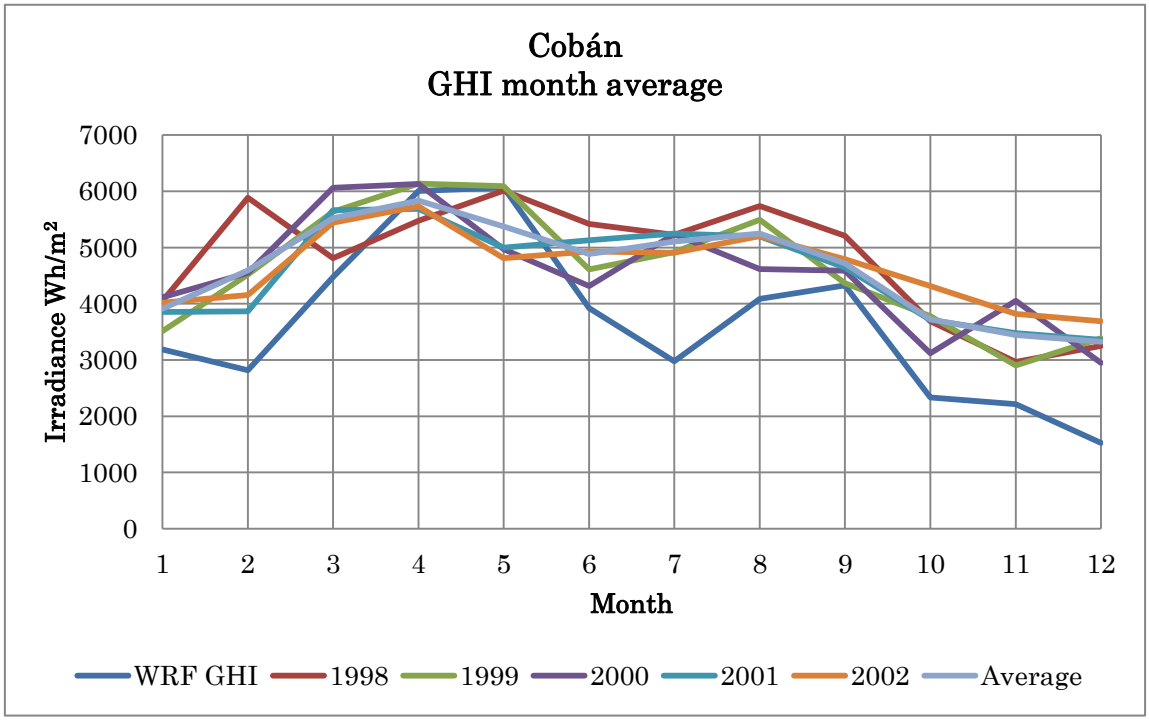

Fig. 27 (b): Cobán meteorological station, daily global horizontal irradiance Wh/m²

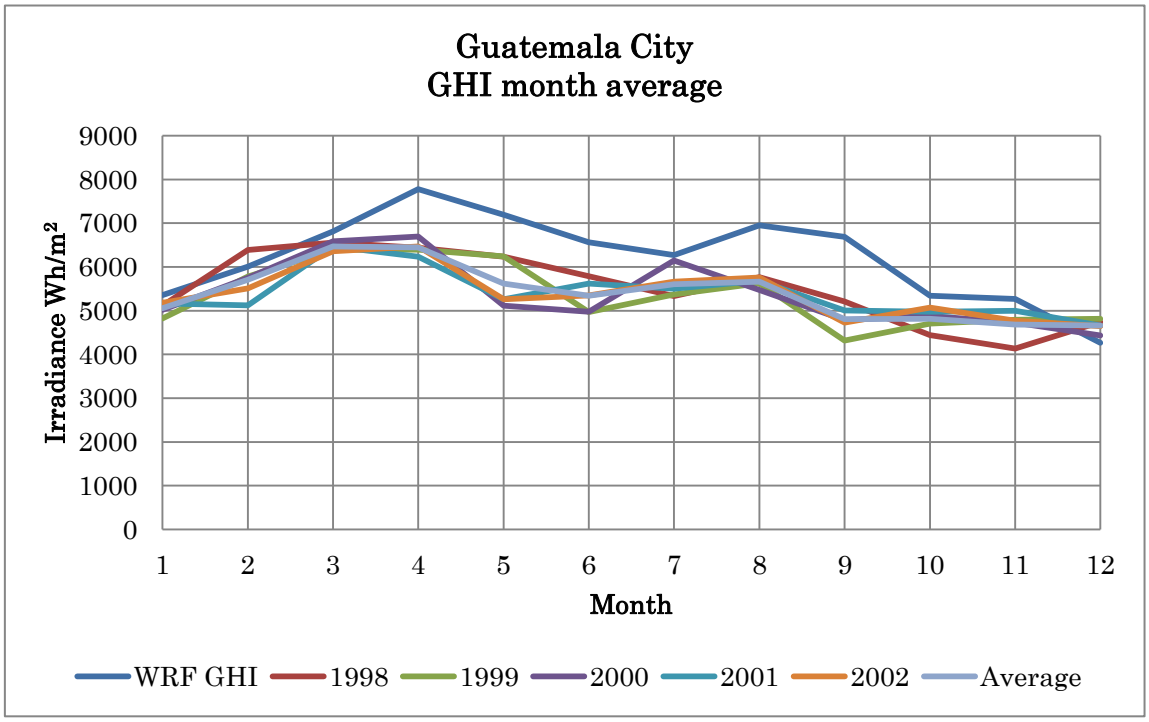

Fig. 27 (c): Guatemala City meteorological station, daily global horizontal irradiance Wh/m²

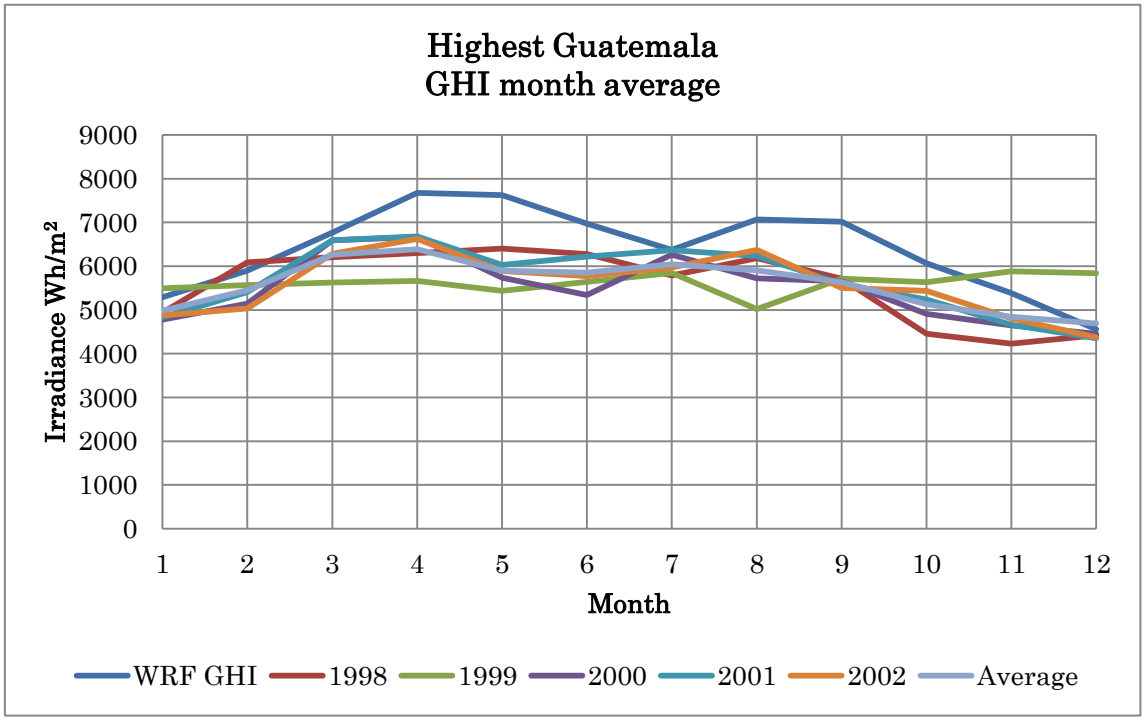

Fig. 27 (d): Highest Guatemala meteorological station, daily global horizontal irradiance Wh/m²

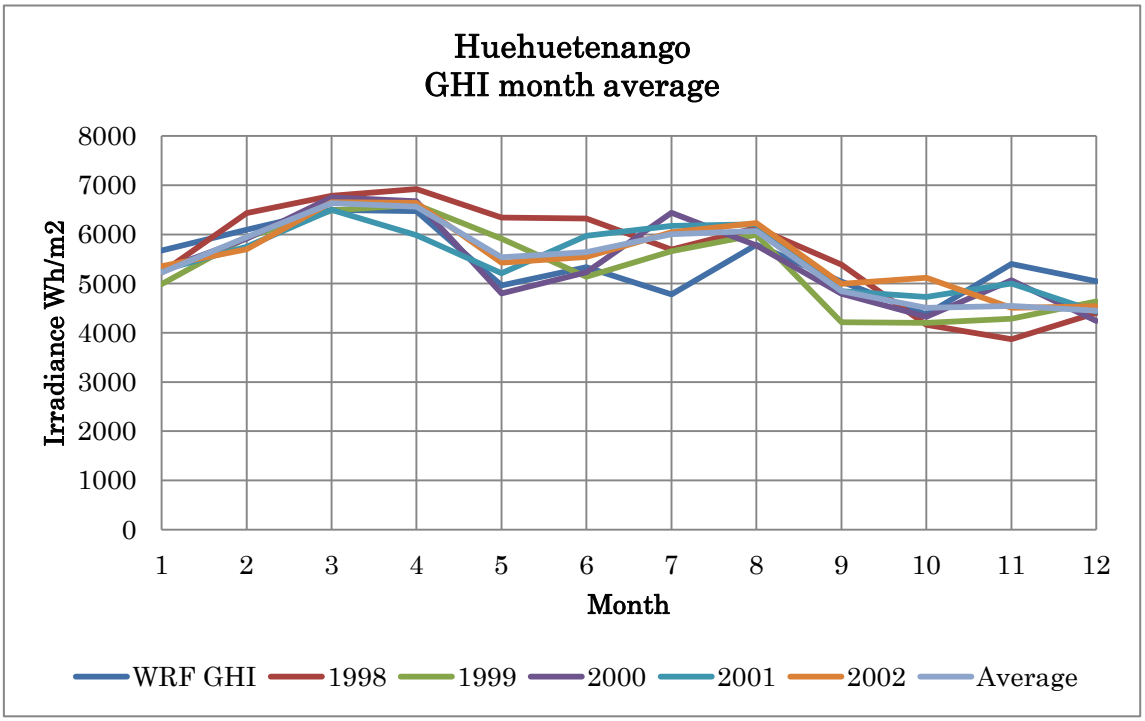

Fig. 27 (e): Huehuetenango meteorological station, daily global horizontal irradiance Wh/m²

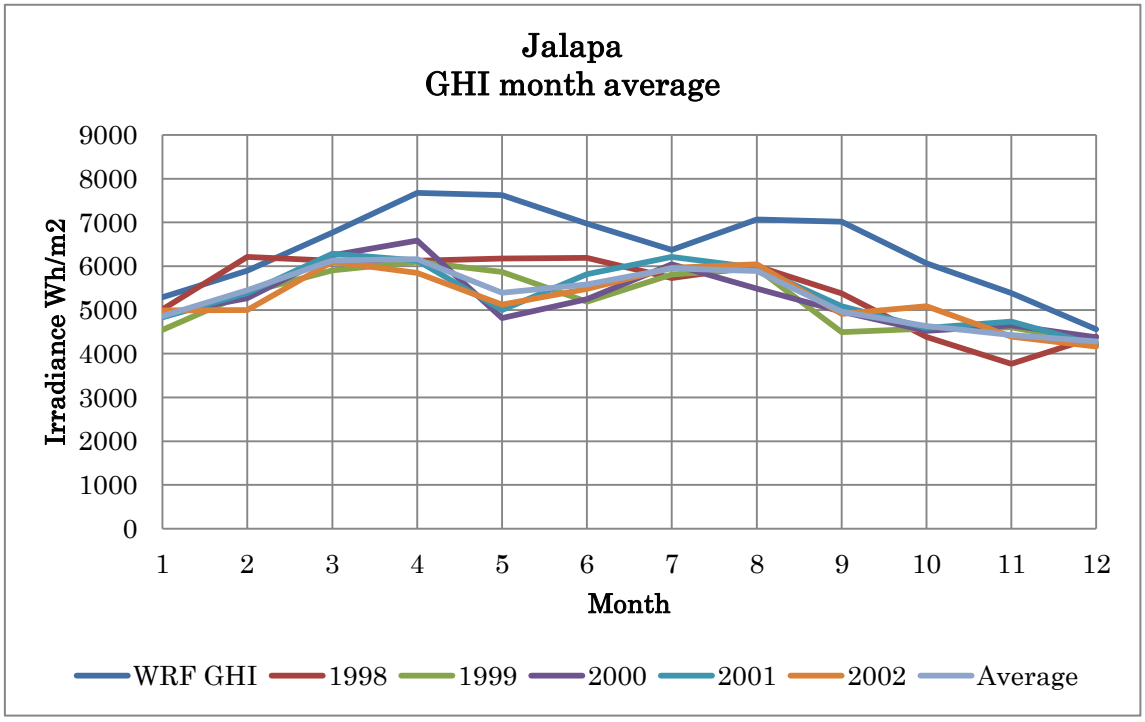

Fig. 27 (f): Jalapa meteorological station, daily global horizontal irradiance Wh/m^2

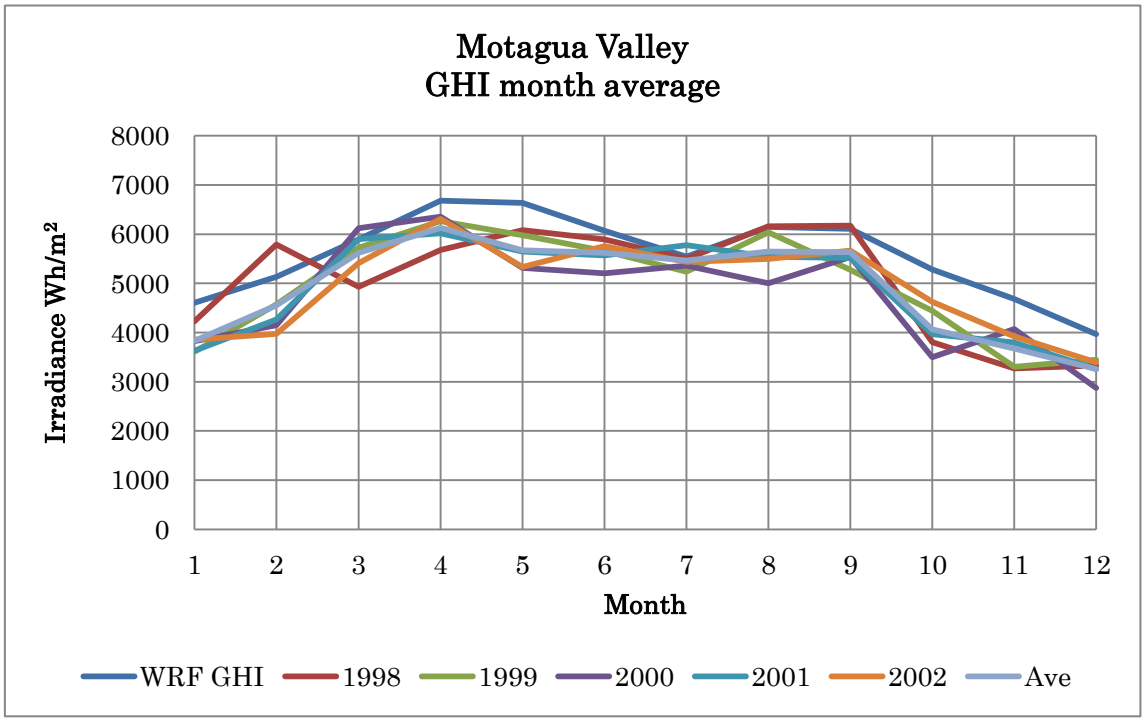

Fig. 27 (g): Motagua Valley meteorological station, daily global horizontal irradiance Wh/m^2

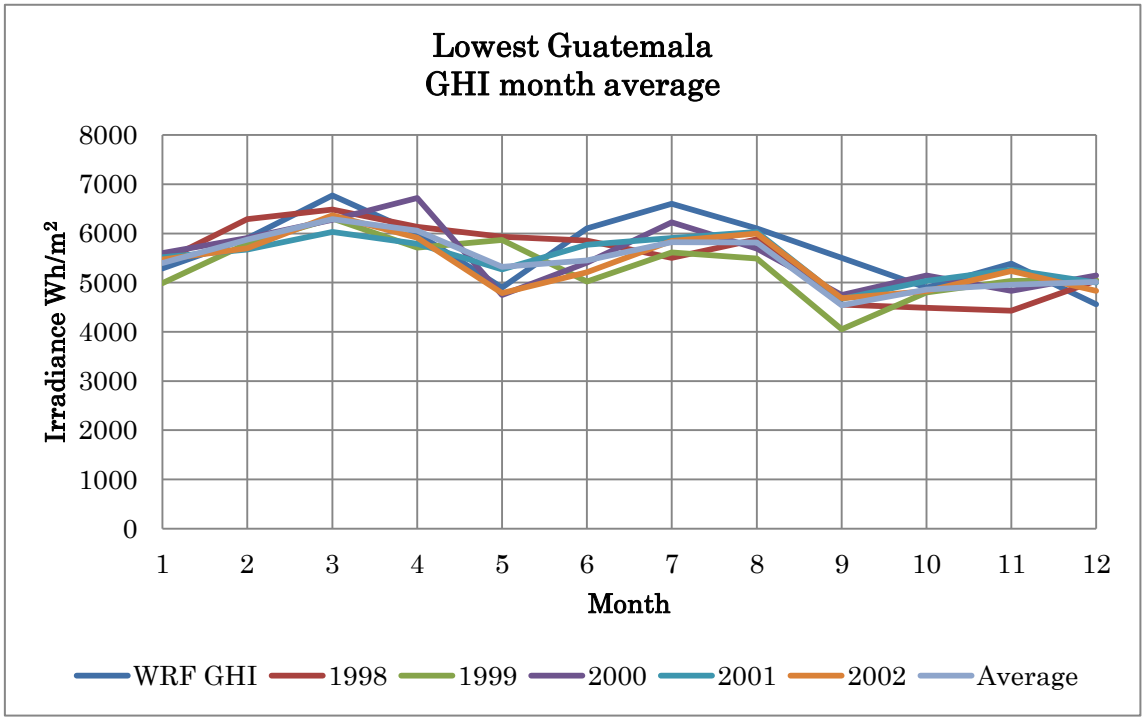

Fig. 27 (h): Lowest Guatemala meteorological station, daily global horizontal irradiance Wh/m²

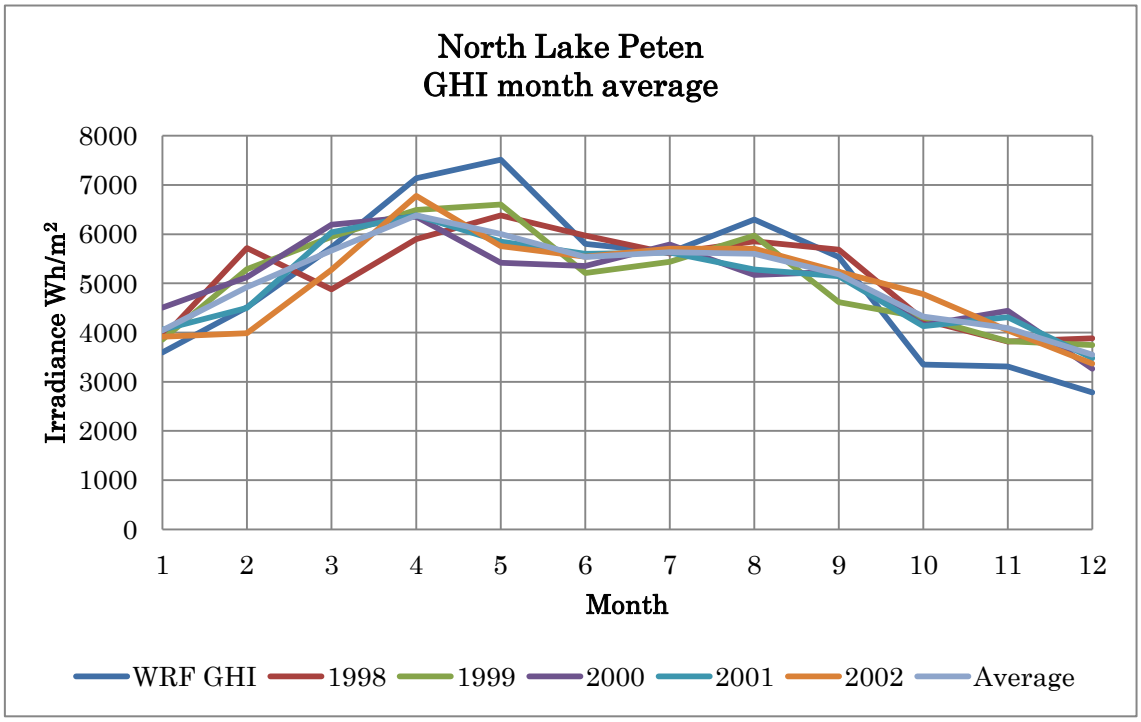

Fig. 27 (i): North Lake Petén meteorological station, daily global horizontal irradiance Wh/m²

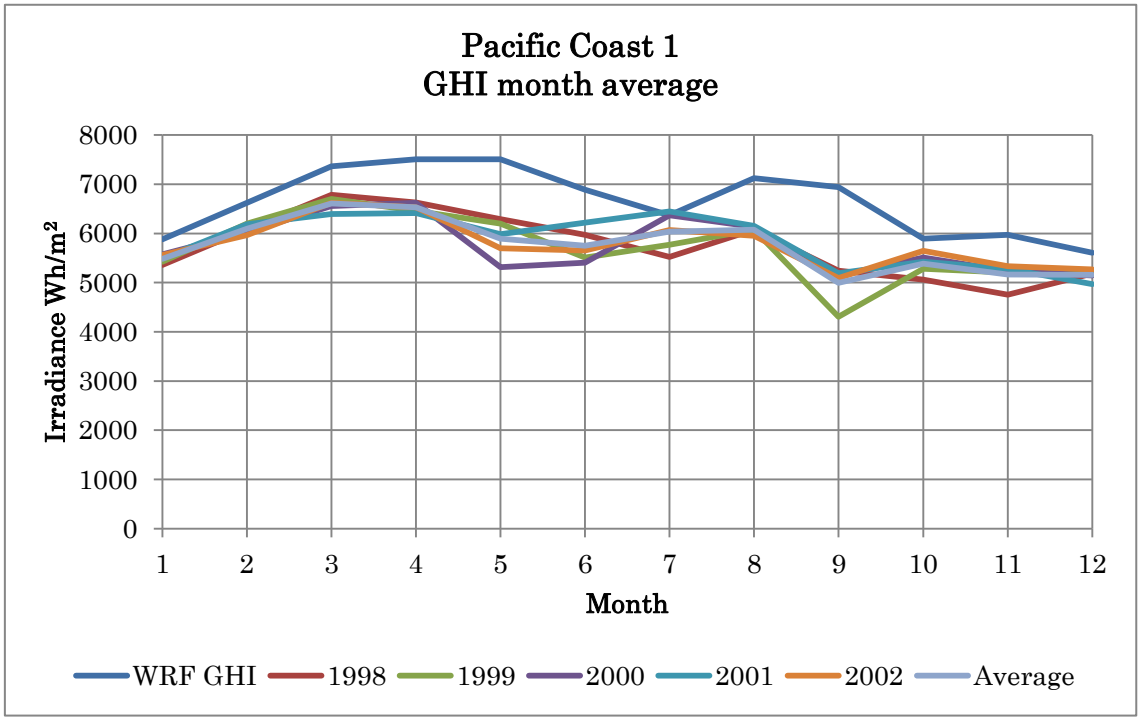

Fig. 27 (j): Pacific Coast 1 meteorological station, daily global horizontal irradiance Wh/m²

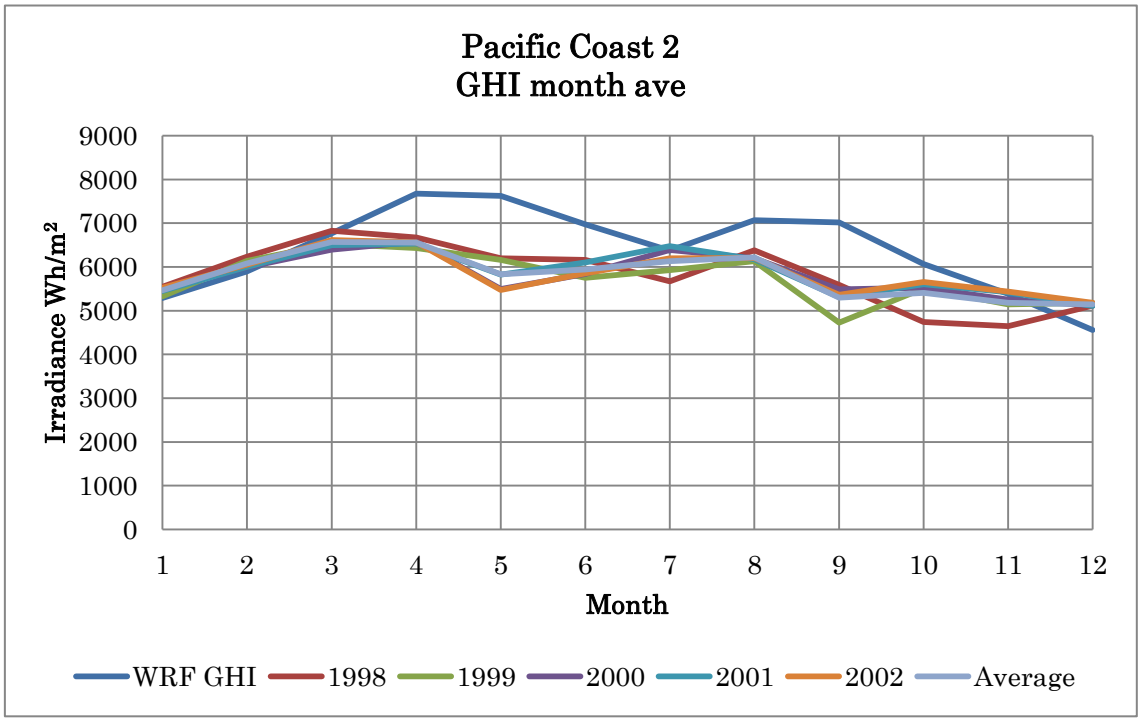

Fig. 27 (k): Pacific Coast 2 meteorological station, daily global horizontal irradiance Wh/m²

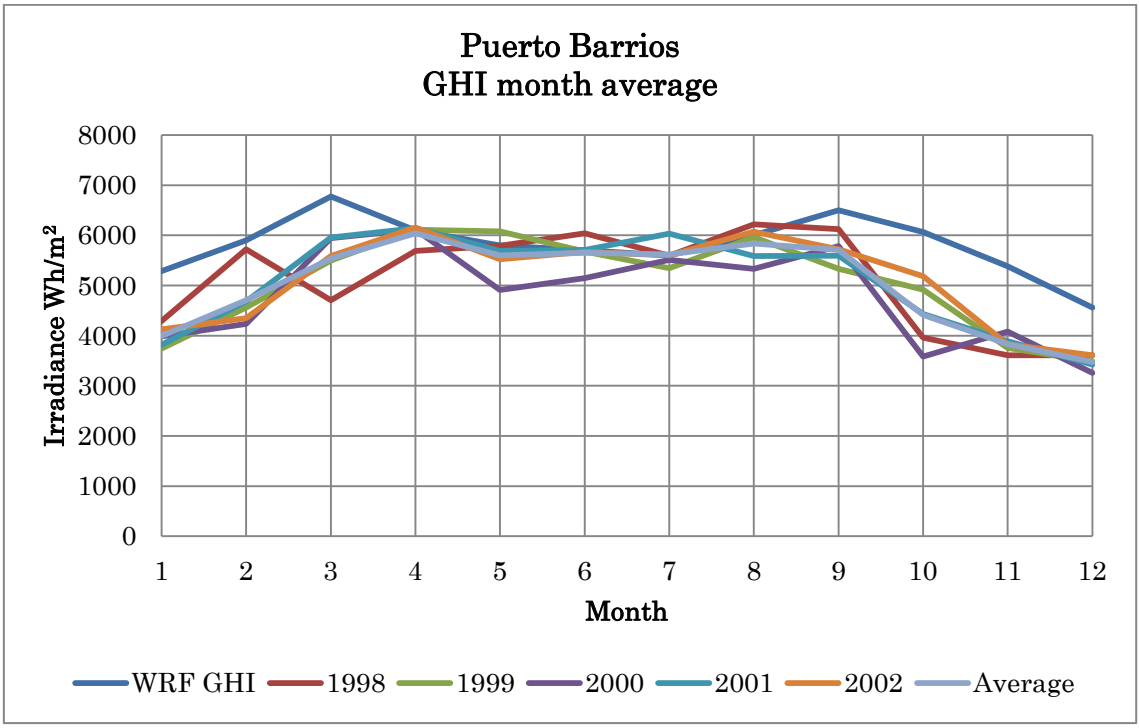

Fig. 27 (l): Puerto Barrios meteorological station, daily global horizontal irradiance Wh/m²

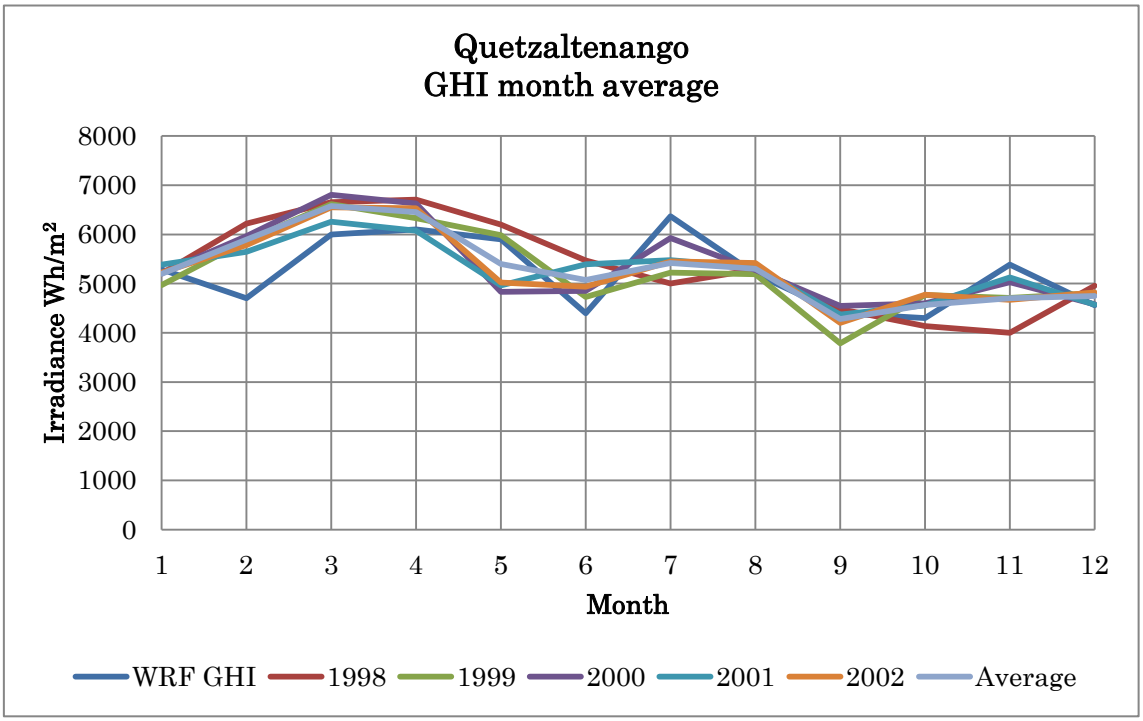

Fig.27 (m): Quetzaltenango meteorological station, daily global horizontal irradiance Wh/m²

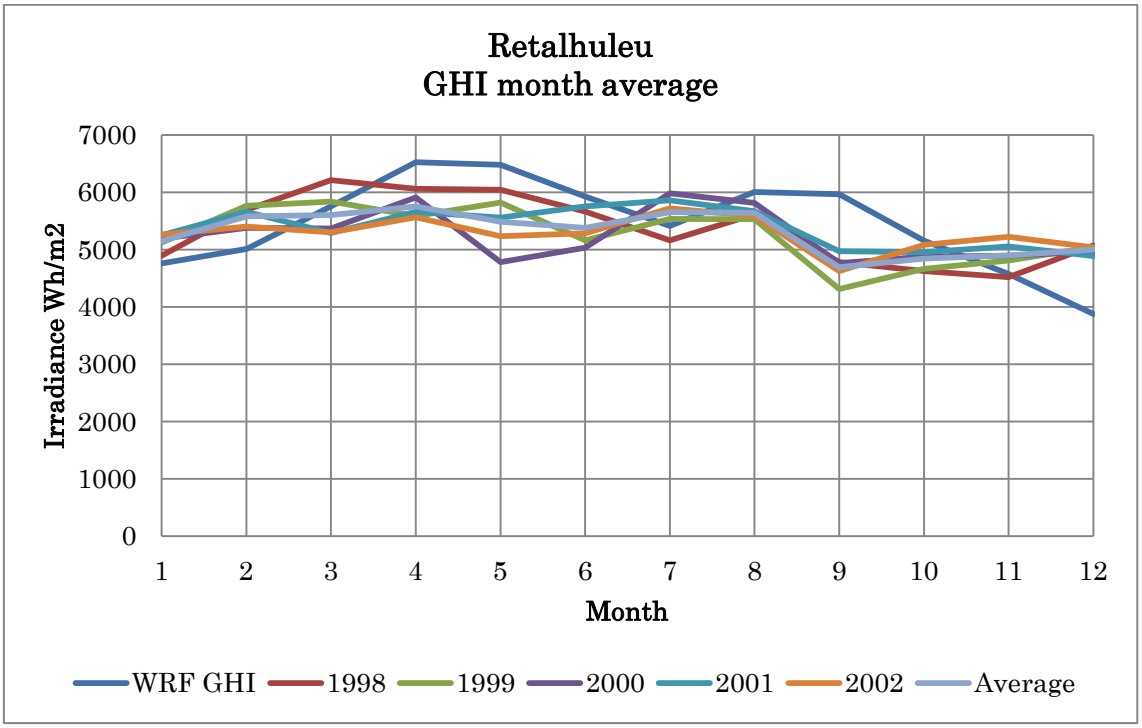

Fig. 27 (n): Retalhuleu meteorological station, daily global horizontal irradiance Wh/m^2

For each station a statistical comparison between the GHI obtained from WRF and the 5 year average is conducted. This statistical comparison consists in a 2 sample T test for comparison of the means, and an F test to compare the variances and determine if the 2 samples are statistically equal. The results are summarized in Table 6.

Table 6: Meteorological Stations, statistical tests results

2 Sample t Test and F Test with 95% Confidence Level				
Meteorological Station	2 Sample t Test		F Test	
	Test Value	Critical Value	Test Value	Critical Value
Chiquimula	0.54	2.45	2.4	2.82
Cobán	-1.19	2.45	3.42	2.82
Guatemala	0.57	2.45	2.02	2.82
Highest Guatemala	0.71	2.45	1.59	2.82

Huehuetenango	-0.14	2.45	1.37	2.82
Jalapa	0.69	2.41	1.38	2.82
Lowest Guatemala	-1.19	2.41	2.82	2.82
Motagua Valley	-0.46	2.42	2.16	2.82
North Lake Petén	-1.01	2.45	2.52	2.82
Quetzaltenango	-1.95	2.41	1.08	2.82
Pacific Coast 1	2.23	2.41	1.47	2.82
Pacific Coast 2	2.04	2.42	1.78	2.82
Puerto Barrios	0.39	2.42	1.83	2.82
Retalhuleu	0.15	2.41	2.05	2.82

The statistical tests indicate that the calculated GHI from WRF and the measurements from the different stations have equal means and variances with confidence level of 95%.The only station that does not fit is Cobán, which the F test result indicate that the variances of the WRF GHI and the observed GHI are not equal. The results indicate that the WRF data presents equal means and variances for most of the cases and therefore it can be used for the present research. In addition the distribution maps created using WRF GHI were compared with Figures 13, 14 and 15 they display similar distribution and further validate the WRF GHI. However the WRF GHI distribution has higher resolution (10km by 10km) than Fig. 13 and Fig. 14 (40km by 40km) and it also provides the time series with a one hour interval instead of the average GHI provided in Figures 13, 14 and 15.

4. PV Output in Guatemala

4.1. PV Output Estimation

In the previous sections some meteorological parameters, including global horizontal irradiance (GHI) and ambient temperature, in Guatemala are evaluated by using the meteorological model WRF. The output of a PV system is estimated in this section from the meteorological parameters.

There are many PV panel types in these days. The installation of crystalline silicon photovoltaic panels is assumed here, because they are one of the most popular panel types in these days. The crystalline silicon photovoltaic cells account for roughly 80% to 85% of the global production according to the U.S. Solar Photovoltaic Manufacturing Industry Trends, Global Competition, Federal Support report (Platzer 2012).

Huld, et al. (2011) proposes the following equation to evaluate PV output, $P(G',T')$ for the general crystalline silicon photovoltaic panels.

$$P(G',T') = G'(P_{STC,m} + k_1 \ln(G') + k_2 \ln(G')^2 + k_3 T' + k_4 T' \ln(G') + k_5 T' \ln(G')^2 + k_6 T'^2) \quad (31)$$

Where G' is the normalized in-plane irradiance, and is computed by dividing by the in-plane irradiance G by 1,000 W/m^2. T' is the temperature of the module measured on the standard test conditions. $P_{STC,m}$ is the power rating of the module; in this Part 1, 1 kW power rating is assumed for the module. The six constants k_1 to k_6 were derived empirically from the indoor experiment conducted by these authors and are displayed in Table 7.

Table 7: constants k_1 to k_6 from Huld el al. 2011.

Constants	Values and dimensions
$\boldsymbol{k_1}$	$-0.01724(dimensionless)$
$\boldsymbol{k_2}$	$-0.04047(dimensionless)$
$\boldsymbol{k_3}$	$-0.0047(°C^{-1})$
$\boldsymbol{k_4}$	$1.49 \times 10^{-4}(°C^{-1})$
$\boldsymbol{k_5}$	$1.47 \times 110^{-4}(°C^{-1})$
$\boldsymbol{k_6}$	$5.0 \times 110^{-6}(°C^{-2})$

The in-plane irradiance G, that reaches the plane with tilted angle β is estimated with the following the model proposed by Duffie and Beckman's (2006);

$$G = B_h R_b(\beta) + D_h R_d(\beta) + G_g \rho R_r \quad (32)$$

Where B_h is the direct normal irradiance on the horizontal plane. D_h and G_g are the diffused and the global horizontal irradiance, respectively. $R_b(\beta)$, $R_d(\beta)$ and R_r are the transposition factors for the direct, the diffused and the reflected irradiance, respectively. ρ is the albedo of the ground.

In this study, the ground reflected irradiance is assumed isotropic, and the following equation (Duffie and Beckman 2006) is applied:

$$R_r = (1 - \cos\beta)/2 \quad (33)$$

The albedo ρ varies depending on the surface type and its conditions. Kambezidis, Psiloglou and Gueymard (1994) found that the anisotropic albedo models do not improve the estimation for the solar irradiance on south oriented surfaces, therefore a fixed albedo is used here. A general value of 0.3 is used for the albedo according to Ahrens (2009) since the country is mostly covered in forests and grasslands.

Padovan and Del Col (2010) tested some models available for the estimation of diffused irradiance on the horizontal and tilted planes. They

reported that the models proposed by Liu and Jordan (1963), Klucher, (1979), Perez et al. (1990) and Reindl et al. (1990) estimate the diffuse irradiance with similar accuracy. The transposition factor for the diffuse irradiance on the plane $R_d(\beta)$ is estimated by using the following equation proposed by Liu and Jordan (1963) is applied:

$$R_d(\beta) = (1 + \cos\beta)/2 \quad (34)$$

Direct irradiance is estimated by Duffie and Beckman (2006) model, which describes the transposition factor for direct irradiance on the plane $R_b(\beta)$ as;

$$R_b(\beta) = \cos\theta_\beta / \cos\theta \quad (35)$$

Where θ_β and θ are the solar incidence angles on the plane with the tilted angle β and on the horizontal plane, respectively.

The direct and diffused irradiances are estimated by the GHI computed with WRF, and the above models.

Several models to evaluate the direct and diffused irradiances are proposed. And they are analyzed and compared by Khalil and Shaffie (2013). They reported that for south facing surfaces, the models proposed by Perez, et al. (1987), Skartveit, et al. (1987) and Hay (1979) have the most accurate predictions with the similar accuracy. Therefore the model proposed by Skartveit, et al. (1987) was chosen in this paper. It is indicated as follows;

For $G_g/G_0 \leq 0.22$

$$r_D = 1.0 - 0.09(G_g/G_0) \quad (36)$$

For $0.22 < G_g/G_0 \leq 0.80$

$$r_D = 0.951 - 0.1604(G_g/G_0) + 4.388(G_g/G_0)^2 - 16.638(G_g/G_0)^3 + 12.336(G_g/G_0)^4 \quad (37)$$

For $G_g/G_0 > 0.80$

$$r_D = 0.165 \quad (38)$$

$$D_h = G_g \times r_D \quad (39)$$

$$B_h = G_g \times 1/r_D \quad (40)$$

Where G_0 is the Solar Constant and r_D is an empirical parameter estimated by Skartveit and Olseth (1987) in order to calculate the diffuse and the direct components of the GHI.

Huld, et al. (2011) also proposes the empirical model to evaluate the module temperature T' under standard test conditions from the ambient temperature T_{amb} and the in-plane irradiance G as follows:

$$T' = T_{mod} - 25℃ \quad (41)$$

$$T_{mod} = T_{amb} + k_T G \quad (42)$$

Where T_{mod} is the temperature of the module, T_{amb} is the ambient temperature and k_T is a constant related to the panel type and G is the in-plane irradiance. The typical values of this constant range from 0.03 to 0.035 $°Cm^2W^{-1}$. This study uses the value 0.035 $°Cm^2W^{-1}$, which is the same one used in Huld et al (2011). Their results from the indoor experiment also showed that Eq. 31 predicts the PV output within 1% error. However, for irradiances lower than 100 W/m^2 the predictions fit within 5% to 10% error (Huld et al. 2011).

4.2. PV Generation and Tilted Angle

In order to determine the optimal tilted angle for PV panels in Guatemala, the energy productions are evaluated with different tilted angles from 0° to 30°, with a 1 kW installed PV capacity. The target site chosen for this analysis is Guatemala City (14°35'14" N, 90°31'59"W), which is located in the middle of the country as shown in Fig. 3.

Figure 28 shows the relationship between the tilted angle of the panel and

the PV energy output. It shows that the energy production increases moderately from 0° until reaching its peak at 10°. Afterwards the energy production drops, as the angle becomes larger. From this figure, the angle 10° is lead as the optimal tilted angle for the solar panels in the target point.

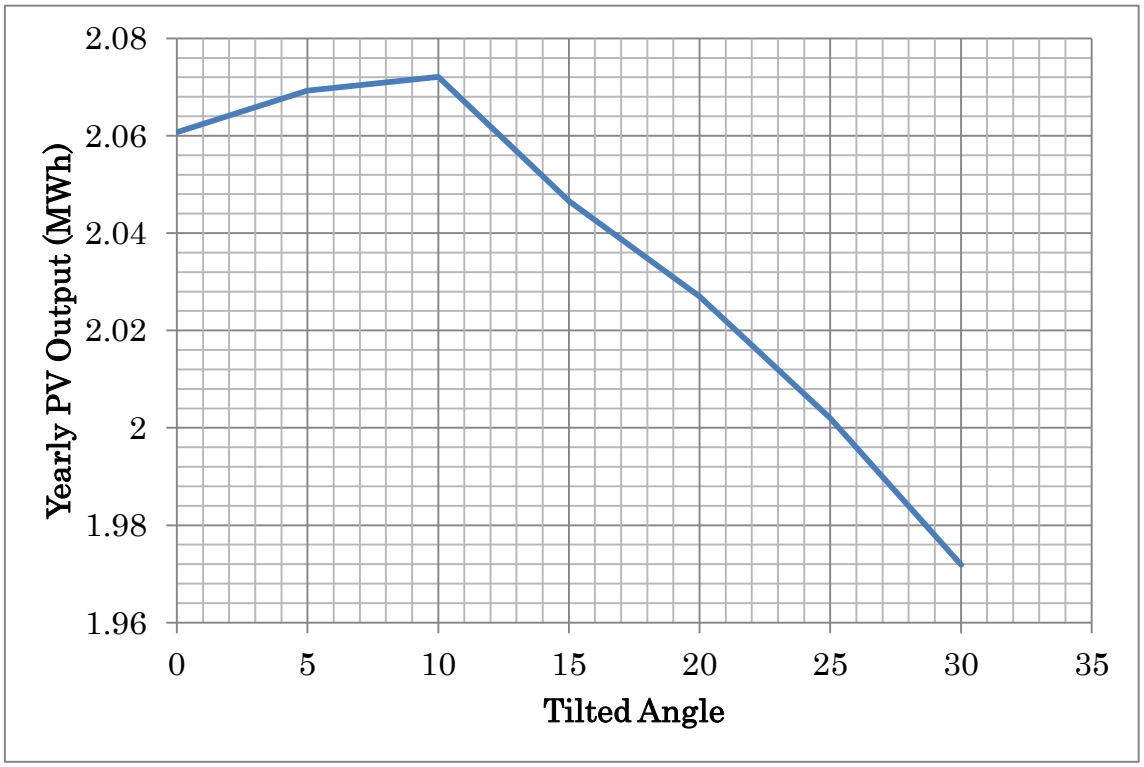

Fig. 28: PV output in relationship with tilted angle of a panel (Power rating 1 kW, facing to south)

4.3. Energy Potential Maps

The output of the PV system is evaluated in Guatemala with the methods explained above, and it is indicated as the PV potential map as shown in Fig. 29. The tilted angle of the PV panels is assumed to be 10°, which is the optimal tilted angle in Guatemala City derived in the previous section. The map shows that the estimated total PV output for one year in Guatemala generated from the PV system with a power rating 1 kW.

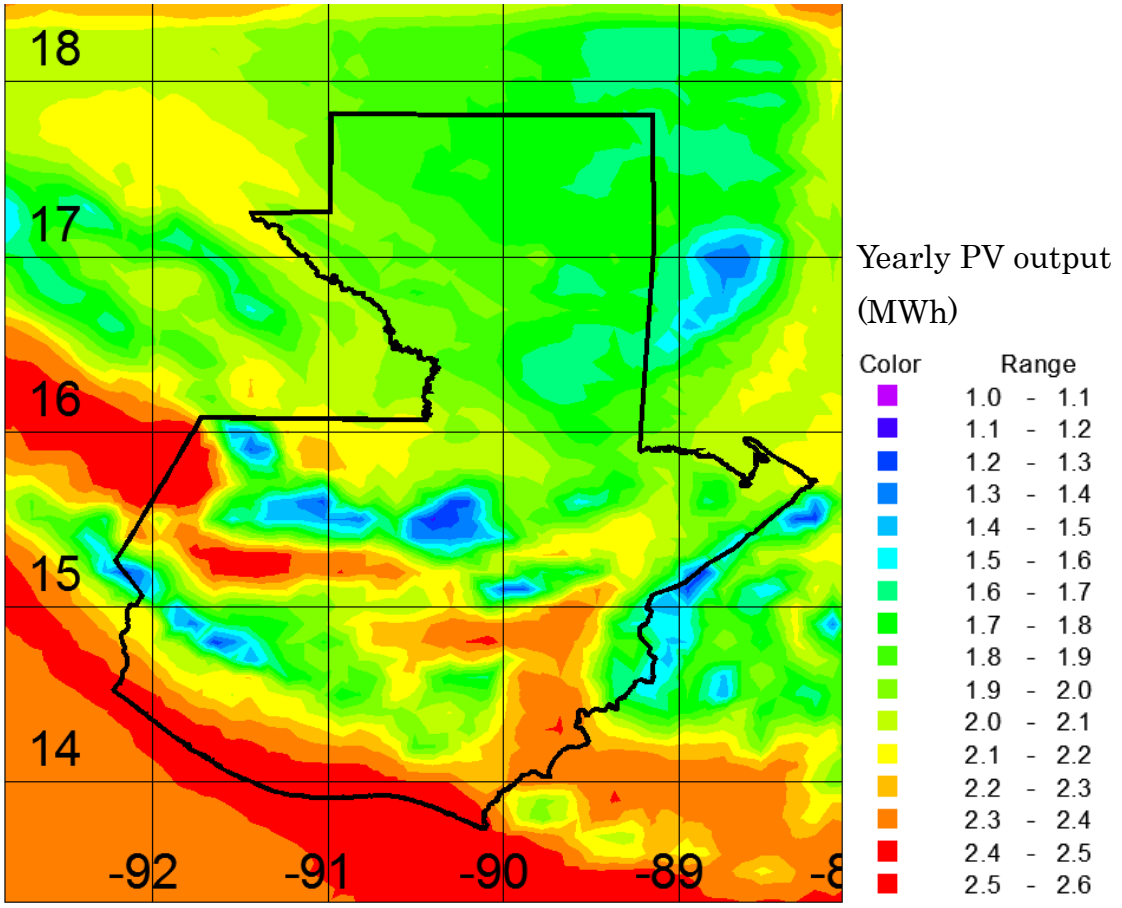

Fig. 29: Evaluated PV output in one year. (The system conditions are 1 kW installed capacity with 10° tilted panel angle)

The distribution of the PV output in Fig. 29 fits well with the irradiance maps in Figs. 23 and 24. This is because the tilted angle of the PV panels is small, the irradiance of incidence to the PV panel is similar to the GHI, and the PV output is directly correlated with the solar irradiance. The northern lowlands of Guatemala are flat and humid, which means that cloud coverage commonly occurs throughout the year, and its effects are both the low irradiance and the small amount of PV output as seen in Figures 23 and 29. The mountain area south of the 16°N grid line in West Guatemala gets high irradiance in Fig. 24 and therefore PV output in that area is also high as shown in Fig. 29. The area along the southern coast, facing the Pacific Ocean, also gets high irradiance and large PV output. The estimated power

generation in these areas is about 2.4 to 2.5 MWh per year for a PV system with 1 kW power rating.

Figure 30 shows the evaluated monthly PV output in Guatemala City (14°35'14" N, 90°31'59"W). The power rating used here is 1 kW and the tilted angle is 10°. The PV output varies due to the sun's altitude and the weather, and the maximum output reaches 7.83 kWh per day in March.

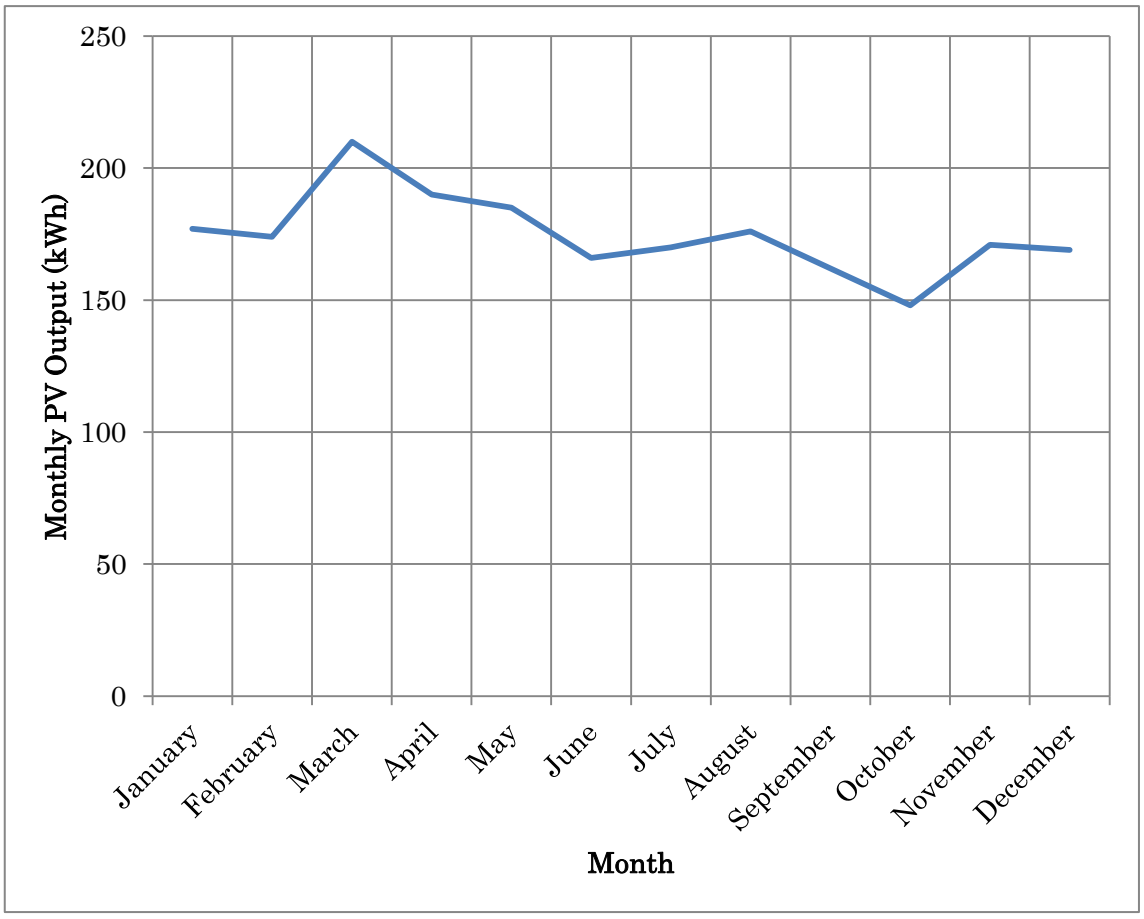

Fig. 30: Evaluated Monthly PV output in Guatemala City in 2011.

5. Appropriate Area for PV Power Plants

In the previous section, the PV energy potential is evaluated as shown in Fig. 29. Based on the result, the appropriate area for large-scale PV power plants is selected. In Fig. 29 and the geography map (Fig. 3), it is found that the areas along the southern coast facing to the Pacific Ocean and the eastern plateaus connected to Mexico have high potential for PV power generation.

In the present work, the following conditions are applied to evaluate the appropriate area for the PV power plants; high potential area of PV generation, and close to the regions of energy consumption. Figure 31 shows the population distribution in Guatemala (Instituto Nacional de Estadística, Guatemala C.A. 2014). From the conditions for the appropriate site for installing PV system and Figs. 29 and 31, the center of the southern coast is selected. The estimated PV power generation in this site is about 2.4 to 2.5 MWh/year for a PV system with 1kW in power rating, and the site is near from the populated area, Guatemala City as shown in Fig. 3.

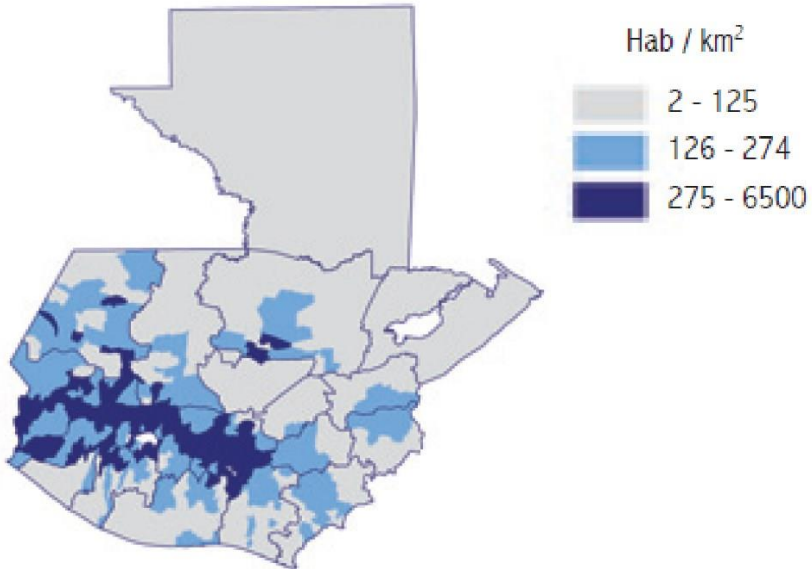

Fig. 31: Population density in Guatemala in 2013 (Instituto Nacional de Estadística, Guatemala C.A. 2014)

6. Grid Managing Analysis

There are several approaches to apply the nonlinear analysis tools to analyze the management of the photovoltaic energy. Movilla, Miguel and Blázquez (2013) use the tool named System Dynamics, in order to analyze the future profitability of photovoltaic energy in Spain. Hsu (2012), Ahmad, Mat Tahar, Muhammad-Sukki, Munir and Abdul Rahim (2015) and Silveira, Tuna and Lamas (2013) use the System Dynamics to analyze the role of policies in the development of photovoltaic energy in their respective countries. Their research is focused on the economic and political assessment of PV systems in the target countries. However, they do not discuss the integration of PV systems in to the electric power grid from the engineering point of view. Since PV output varies frequently due to the diurnal motion and weather changing, PV output varies evidently during the day, and the detailed analysis is required for the management of the electric power grid after PV installation.

Li, Zhou, Li and Zeng (2012) use the System Dynamics to analyze power grid engineering projects management. They found that System Dynamics can be used to optimize the management aspects of power grid engineering projects. Kaifel (2011) develops a model for the simulation and optimization of a power grid system including renewable energies, such as PVs and wind powers. Ramli, Hiendro, Sedraoui, and Twaha (2015) discuss the optimal sizing of grid-connected PV system in Saudi Arabia.

6.1. Analyzed Model

In order to analyze Guatemala's electric system, we employ the "System Dynamics" and construct the analysis model on it.

6.1.1. System Dynamics

The System Dynamics is a modeling tool to analyze the nonlinear behavior

of complex systems over time. It's constituted with stocks, flows, feedback loops and time delays. It was originally developed by Forrester (Forrester 1961) in order to provide a tool for managers to understand business and industrial processes and their interactions. However, its applications cover any complex system, i.e. social, managerial, economic or industry processes. Any Dynamic Systems characterized by interdependence mutual interaction, information feedback and circular causality (System Dynamics Society 2014).

This approach involves:

- Defining problems in terms of time depending variables
- Focus inward on the characteristics of a system that themselves generate or exacerbate the perceived problem
- Thinking of all concepts in the real system as continuous quantities interconnected in loops of information feedback and circular causality
- Identifying independent accumulations in the system and their inflows and outflows
- Formulating a behavioral model capable of reproducing the dynamic problem.
- Implementing changes resulting from model-based understandings

The basic structure of a formal system dynamics computer simulation model is a system of coupled, nonlinear, first-order differential equations

$$\frac{d}{dt}x(t) = f(x, p)$$

Where x is a vector of stocks, p is a set of parameters, and f is a nonlinear vector-valued function. The simulation is accomplished by partitioning simulated time in to discrete intervals of length dt at a time. Each state variable is computed from its previous value and net rate of change $x'(t): x(t) = x(t - dt) + dt * x'(t - dt)$. Forrester (1961) stressed a

continuous approach, however, increasingly modern applications of system dynamics contain a mix of discrete difference equations and continuous differential or integral equations.

The feedback concept is a key part of the system dynamics approach. A feedback loop exists when information resulting from some action travels through a system and eventually returns in some form to its point of origin, potentially influencing any future actions. When a loop reinforces the initial action it is called positive feedback, and if the loop opposed the initial action it is called negative feedback. Balancing loops can be characterized as goal-seeking, equilibrating, or stabilizing processes. In addition, they can sometimes generate oscillations.

Complex systems change over time, a requirement for a view of a dynamic system is the ability of a mental or formal model to change the strengths of influences as conditions change, in other words, the ability to shift active or dominant structure. In a system of equations, this ability to shift loop dominance comes about endogenously from nonlinearities in the system.

The concept of endogenous change is also a key part of the system dynamics approach. Exogenous disturbances are seen as triggers of system behavior the causes are contained within the structure of the system. Corrective responses are also not modeled as functions of time, but are dependent on conditions within the system. Time by itself is not seen as a cause.

Taking an endogenous view exposes the natural compensating tendencies in systems. The Feedback and circular causality are delayed, devious, and deceptive. For understanding, system dynamics practitioners strive for an endogenous point of view. The effort is to uncover the sources of system behavior that exist within the structure of the system.

Forrester (1961) proposed the following structure:

- Closed boundary
    - Feedback loops

- Levels
- Rates
  - Goal
  - Observed condition
  - Discrepancy
  - Desired action

The modeler's goal is to assemble a formal structure that can, without exogenous explanations, reproduce the essential characteristics of a dynamic problem.

The causally closed system boundary at the head of this organizing framework identifies the endogenous point of view as the feedback view pressed to an extreme. Feedback thinking can be seen as a consequence of the effort to capture dynamics within a closed causal boundary. Without causal loops, all variables must trace the sources of their variation ultimately outside a system. Assuming instead that the causes of all significant behavior in the system are contained within some closed causal boundary forces causal influences to feed back upon themselves, forming causal loops. Feedback loops enable the endogenous point of view and give it structure.

Stocks and flows are essential components of the system structure. A constant inflow yields a linearly rising stock; a linearly rising inflow yields a stock rising along a parabolic path, and so on. Stocks are the memory of a dynamic system and are the sources of its disequilibrium and dynamic behavior.

Forrester (1961) placed the operating policies of a system among its flows, many of which assume the classic structure of a balancing feedback loop striving to take action to reduce the discrepancy between the observed condition of the system and a goal.

6.2. Model Description

6.2.1. Model Structure

The model constructed here includes all electric power plants and electric grids in Guatemala. Since there are 85 plants in this model, the entire structure of the model cannot be indicated in this thesis; therefore a simplified model is indicated in Fig. 32 for the explanation of the model structure. The Timer in the figure generates the date and time continuously, and synchronizes all behavior in the model. All plants, i.e. Thermal Power, Hydro Power, Geothermal Power and Biomass Power plants, generate electric power and supply it to the demand side under the direction of the Timer. The information of the Demand is feedback to the Thermal Power plants to manage them for keeping electric balance between the generations and demand. The electric power trading is also taken into the account at the nodes Import and Export in the figure.

The flows of electric power and information are indicated by double and single arrows, respectively in the figure.

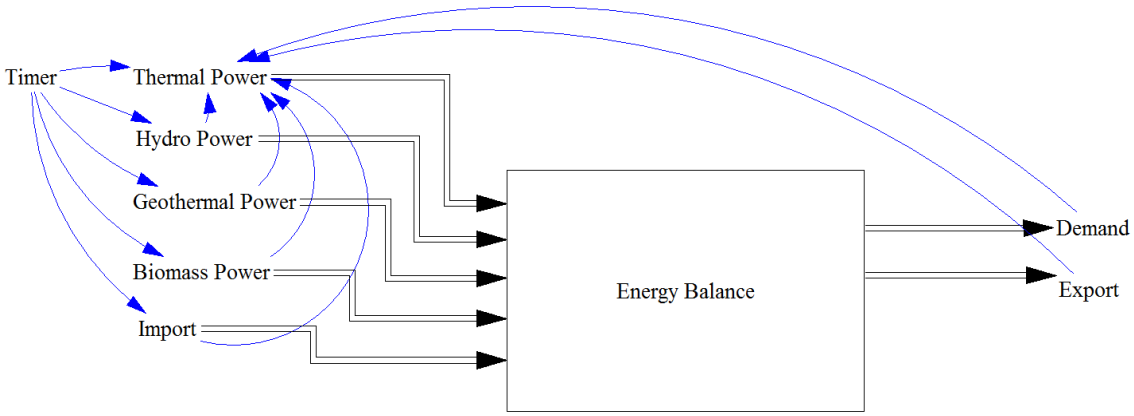

Fig. 32: Schematic view of Guatemala's electric grid model for representing current status.

6.2.2. Electric Power Plants except Thermal Power Plants

The hydro, biomass and geothermal power plants in Guatemala are

operated on the schedule planed in advance. Therefore in the model, the database for the operation schedule for each plant is prepared, and the each plant generates electric power in accordance with the database under the direction of the Timer in Fig. 32. The generation record in 2011 published from AMM (Administrador del Mercado Mayorista 2014) is used to prepare the database.

6.2.3. Electric Power Demand

The electric power demand changes due to social activity which is difficult to simulate directly. Therefore the database for the Demand in Fig. 32 is prepared from the expected electricity demand in 2011 reported by AMM (Administrador del Mercado Mayorista 2014) instead of the real one.

6.2.4. Electric Power Trading

The import/export electric power between neighbor countries is simulated with the database which is prepared from AMM (Administrador del Mercado Mayorista 2014) in the model, similar to the electric power demand.

6.2.5. Thermal Power Plants

Guatemala's law forces the electric grid administrator, AMM, to use renewable energy sources before using the non-renewable ones, and the thermal power plants will be used only to supply deficit of the electric power to the demand. It means that the thermal power plants are operated to achieve a balance between the electric power supply and the demand. The Thermal Powers are monitoring the generation of all other plants and the electric trade and the feedback from the Demand, and are controlled by the power generation in the model as shown in Fig. 32. Since there are several types of thermal power plants with different types of fuels, the plants have priority to operate in accordance to the following items:

- Fuel Price; directly linked to electricity prices, the cheaper the fuel the more priority it gets
- Efficiency; directly linked to electricity prices too, the more efficient a power plant is the better priority it has
- Reaction time; how long it takes for the power plant to warm up and start generating.

The plant with higher priority works more than the one with lower priority. In the model, the thermal power plants communicate among them, and work following to the priority for keeping the electric power balance between the generators and the demand.

6.2.6. Model Validation

In order to validate the developed model, the model is performed under the condition in the year 2011 and the simulated thermal power generations are compared with the actual one. The coefficient of determination R^2 between the simulated generation and the actual one of 11 thermal plants are listed in Table 8. In addition the Actual generation and the simulated generation for the total thermal power generation and each one of the thermal power plants in Table 8 are displayed in Fig. 33 through Fig. 44.

Table 8: Accuracy of the thermal power plants operation in 2011 represented with a model constructed with System Dynamics.

Thermal Power Plant	Actual Generation in 2011 (MWh/year)	Simulated Generation (MWh/year)	Difference in %	Coefficient of determination between simulated and actual power generations (R^2)
San José	822,155.12	845,645	(+)2.86%	0.96
Arizona	621,056.48	629,156	(+)1.30%	0.81
Poliwatt	558,486.51	598,539	(+)7.17%	0.69
Las Palmas 2	437,521.09	440,070	(+)0.58%	0.96
Genor	203,001.98	154,684	(-)23.80%	0.65
La Libertad	100,874.54	99,710	(-)1.15%	0.78
Pierto Quetzal Power	94,380.43	118,298	(+)25.34%	0.73
Las Palmas	91,428.93	102,071	(+)11.64%	0.74
Electro Generación	21,287.98	25,354	(+)19.10%	0.6
Industria Textiles del Lago (ITDL10)	19,488.70	21,233	(+)8.95%	0.81
Arizona Vapor	10,275.20	9,526	(-)7.29%	0.95
Total	2,979,956.94	3,044,286	(+)2.16%	0.92

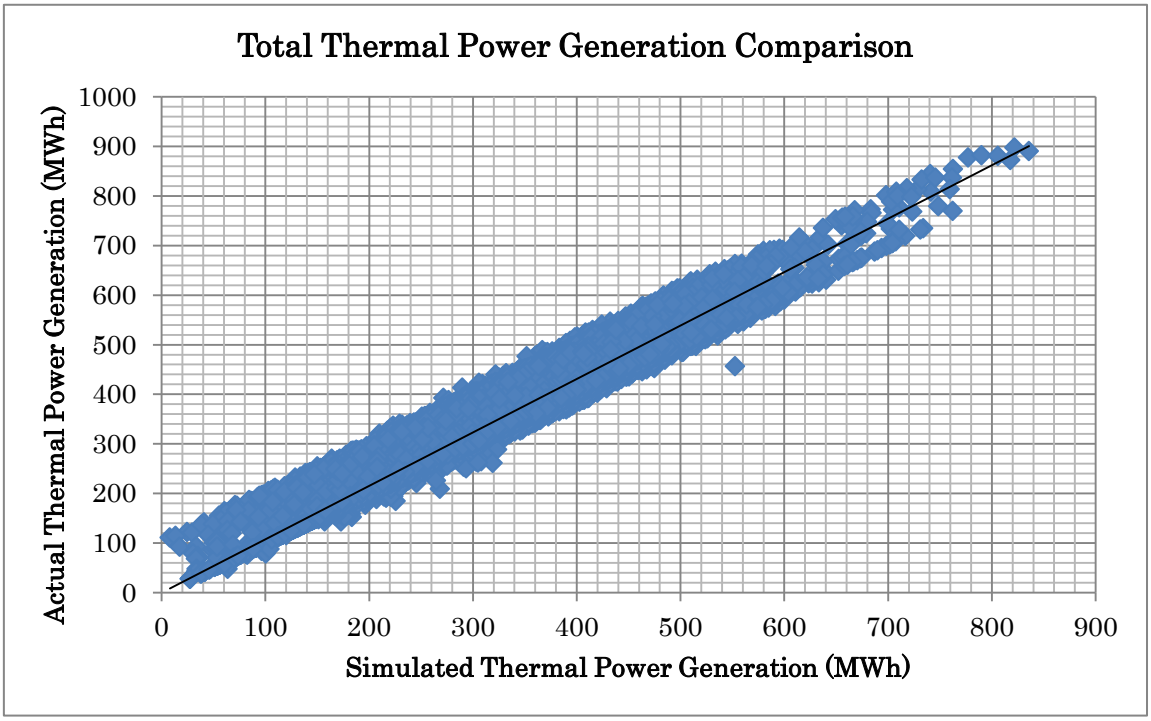

Fig. 33: Total Simulated Thermal Power Generation and Total Actual Thermal Power Generation comparison.

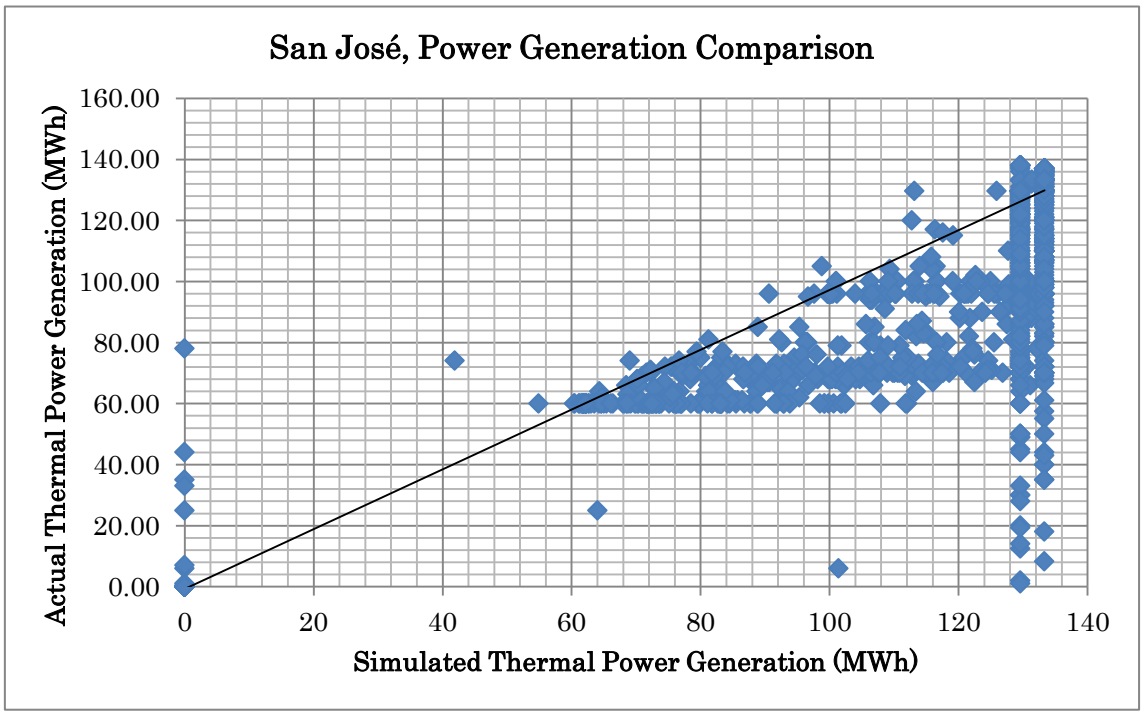

Fig. 34: San José; Simulated Power Generation and Actual Power Generation comparison.

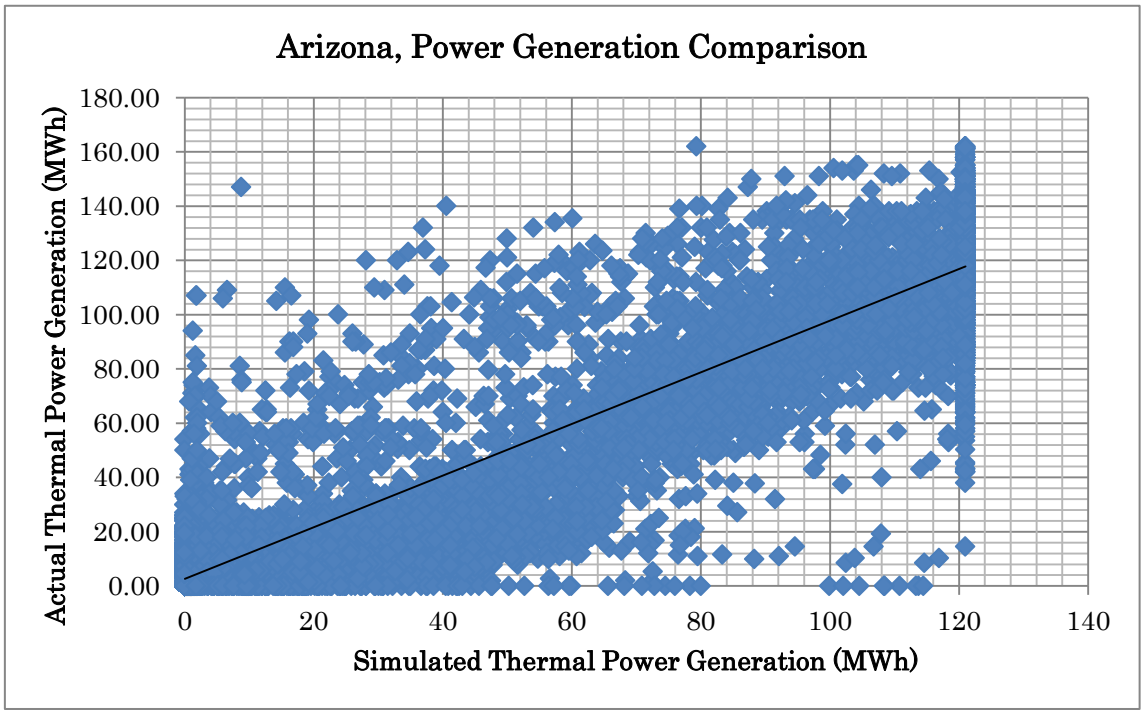

Fig. 35: Arizona; Simulated Power Generation and Actual Power Generation comparison.

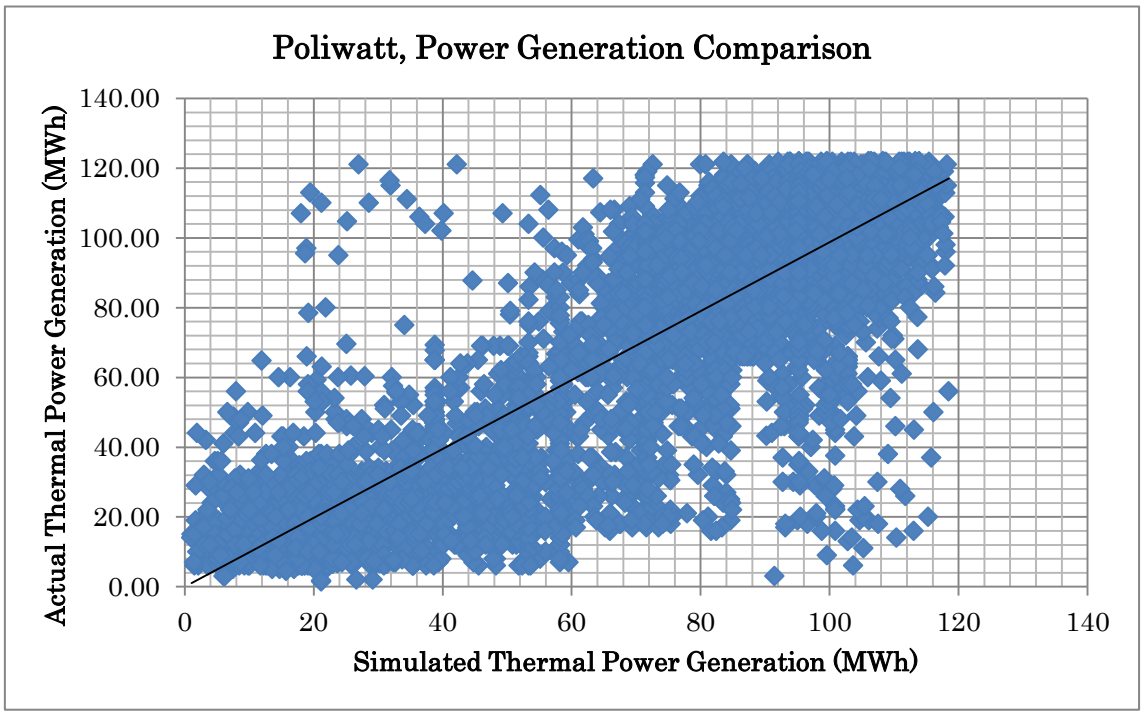

Fig. 36: Poliwatt; Simulated Power Generation and Actual Power Generation comparison.

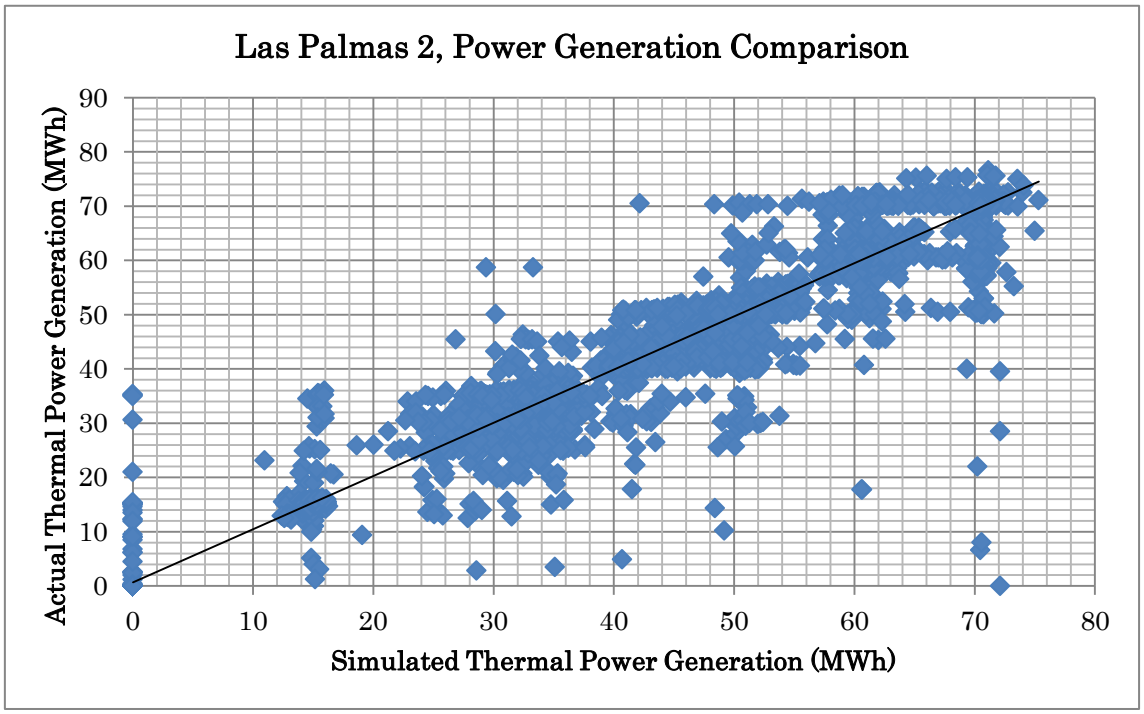

Fig. 37: Las Palmas 2; Simulated Power Generation and Actual Power Generation comparison.

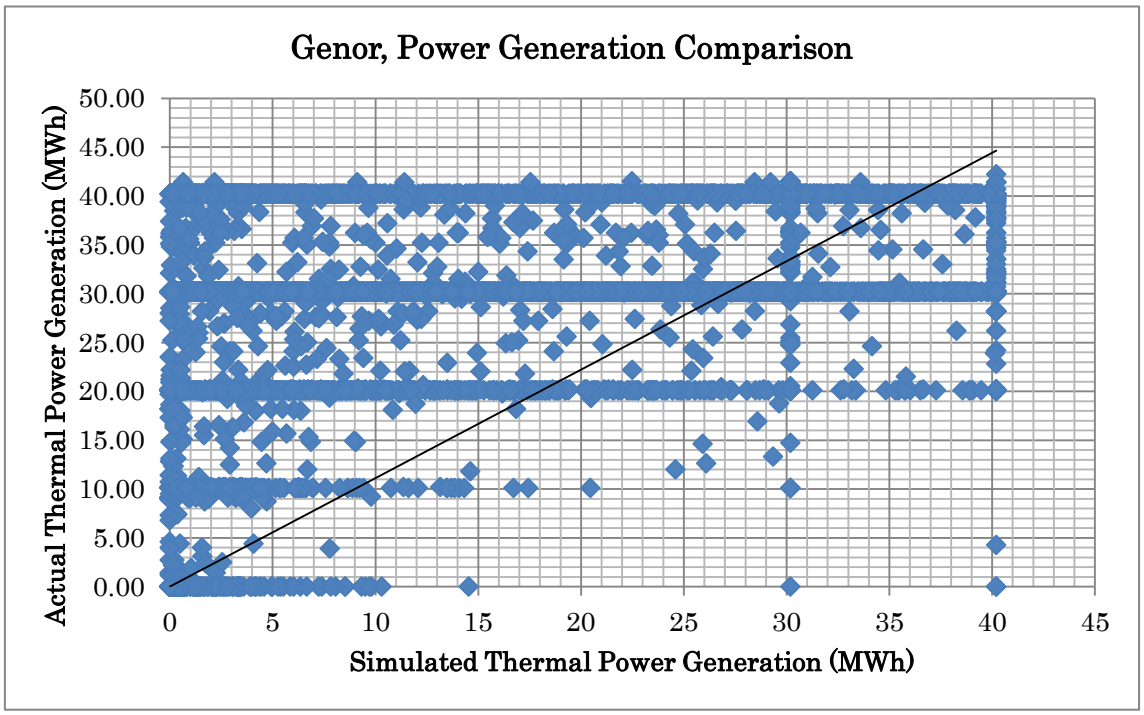

Fig. 38: Genor; Simulated Power Generation and Actual Power Generation comparison.

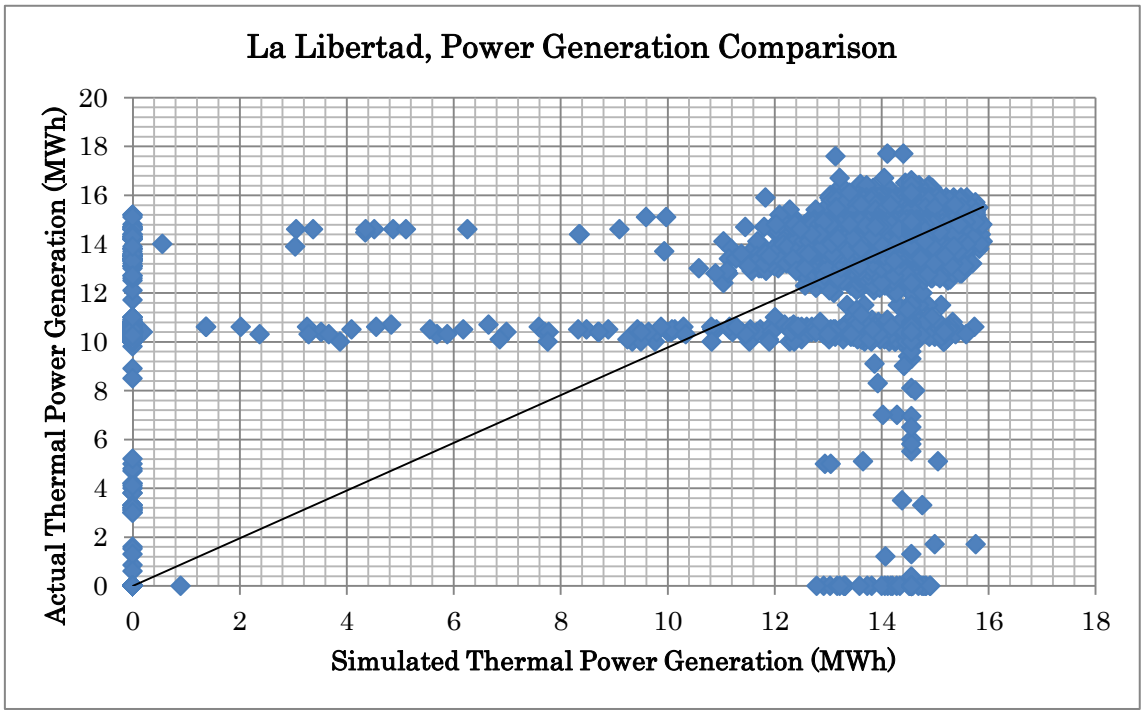

Fig. 39: La Libertad; Simulated Power Generation and Actual Power Generation comparison.

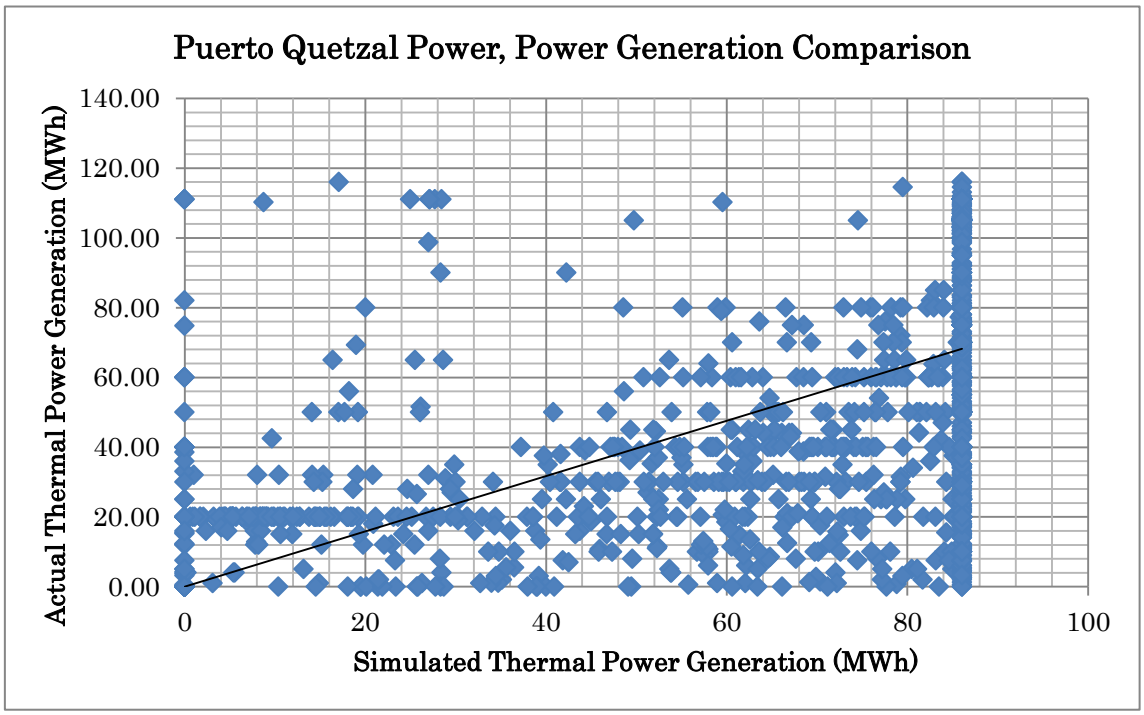

Fig. 40: Puerto Quetzal Power; Simulated Power Generation and Actual Power Generation comparison.

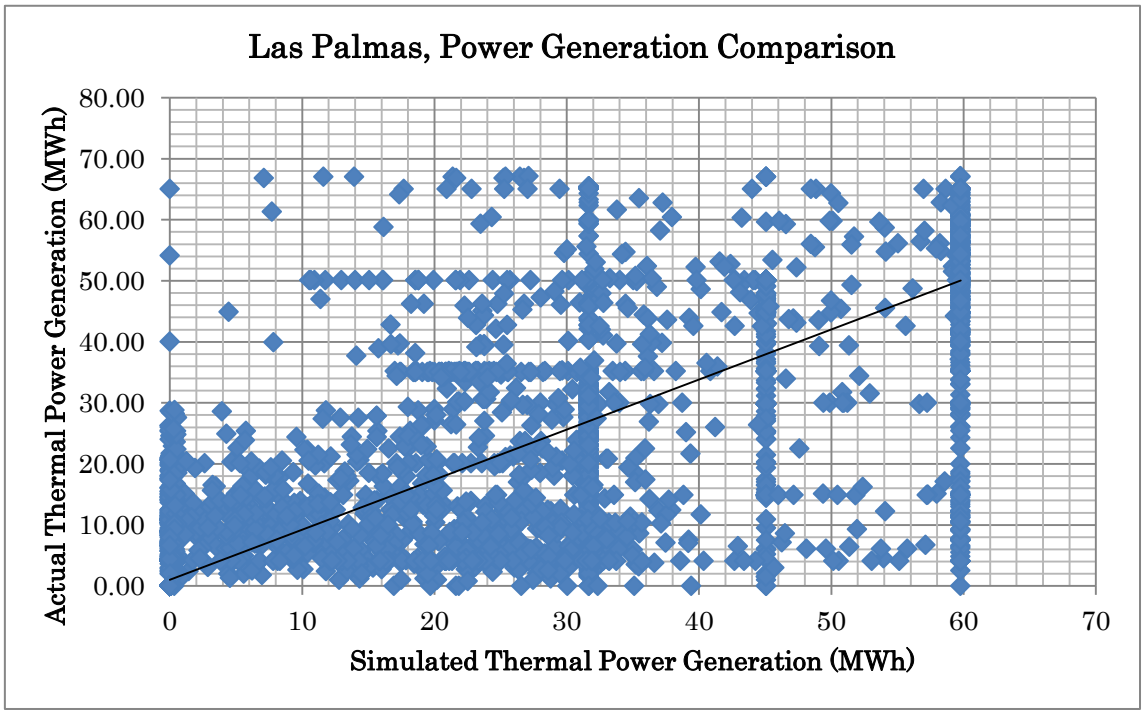

Fig. 41: Las Palmas; Simulated Power Generation and Actual Power Generation comparison.

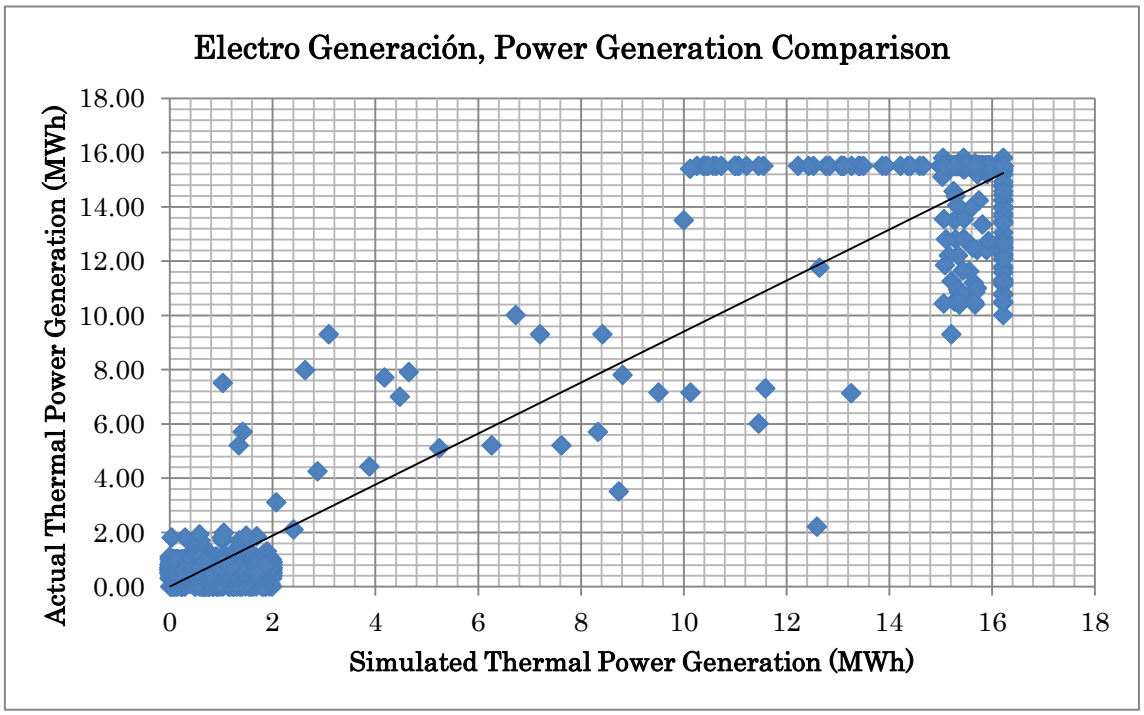

Fig. 42: Electro Generación; Simulated Power Generation and Actual Power Generation comparison.

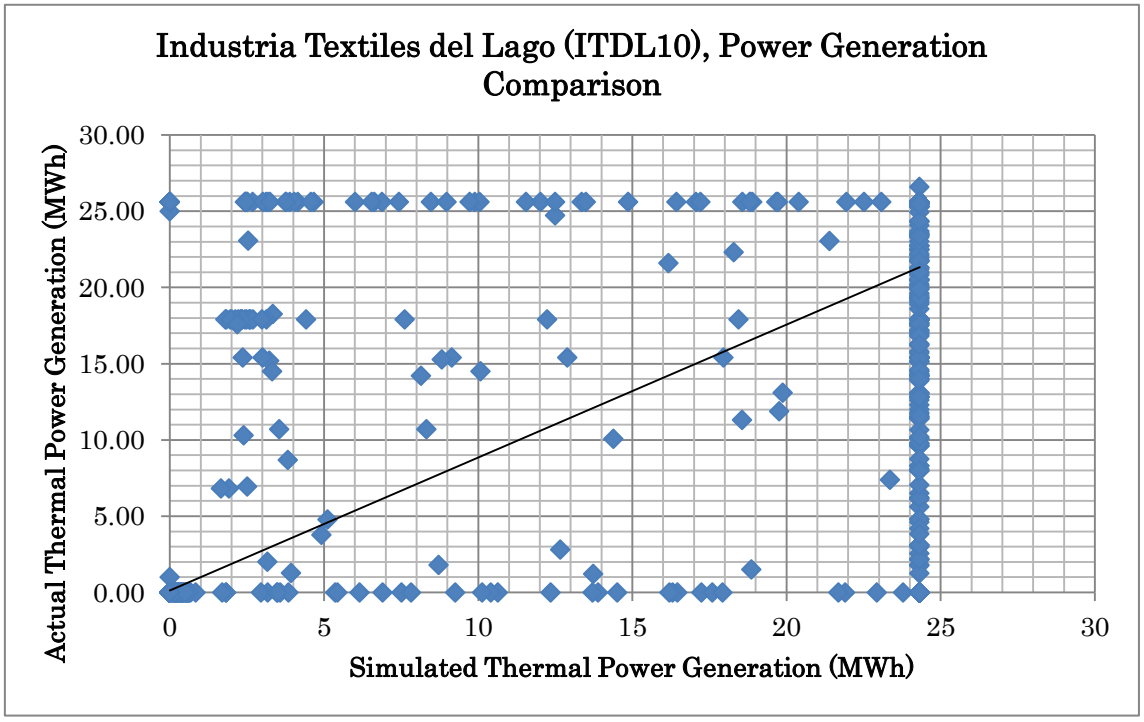

Fig. 43: Industria Textiles del Lago (ITDL10); Simulated Power Generation and Actual Power Generation comparison.

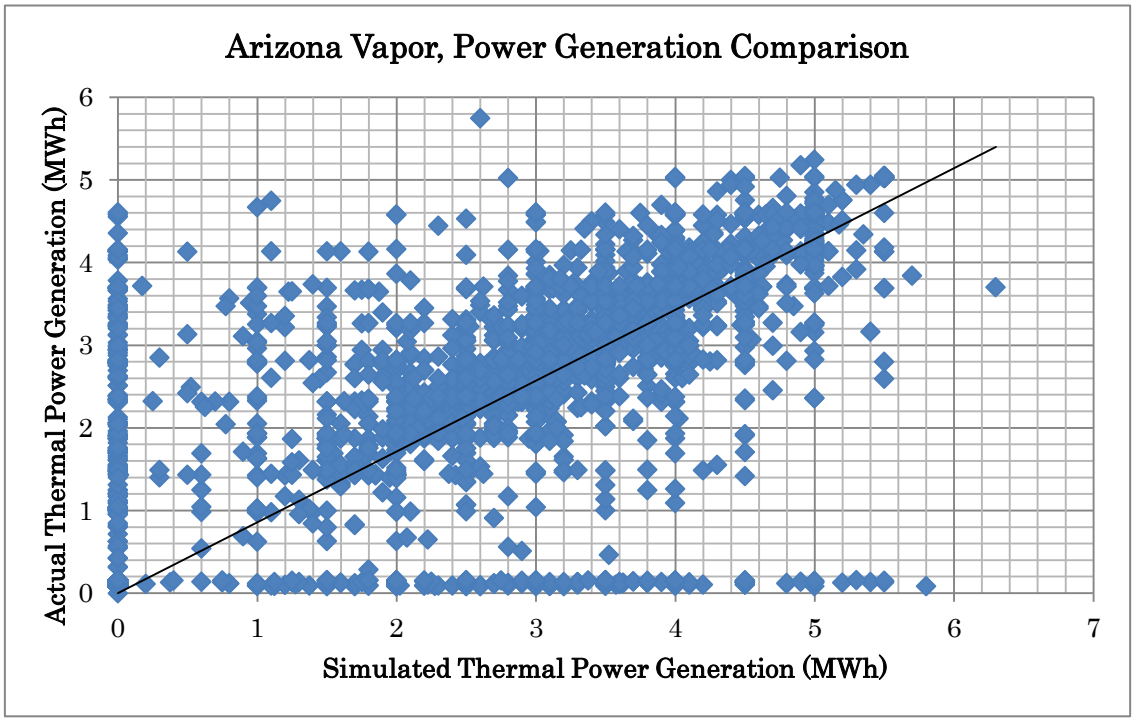

Fig. 44: Arizona Vapor; Simulated Power Generation and Actual Power Generation comparison.

The coefficient R^2 is defined as follows;

$$R^2 = 1 - (SS_{res}/SS_{tot}) \quad (43)$$

Where SS_{res} is the sum of squares of residuals and SS_{tot} is the total sum of squares and they are defined as:

$$SS_{res} = \sum_i (y_i - f_i)^2 \quad (44)$$

$$SS_{tot} = \sum_i (y_i - \bar{y})^2 \quad (45)$$

Where y_i is the actual power generation data in 2011, f_i is the simulated power generation and $\bar{y}$ is the mean of the actual generation. The other thermal plants work less than 100 hours (about 1% of a year) in a year, and the data isn't effective for this validation. The coefficient R^2 for all simulated thermal power operation is 0.92. These results show the validity of the model.

In addition to the coefficient of determination (R^2), in order to evaluate the accuracy of the simulation, for each thermal power plant displayed in Table 8 a statistical comparison was conducted. This statistical comparison consists in a 2 sample T test for comparing the means, and an F test to compare the variances and determine if the 2 samples are statistically equal. The results are shown in Table 9. They show that the simulated power generation is statistically equal to the actual generation.

Table 9: Thermal Power plants, statistical test results

2 Sample t Test and F Test with 95% Confidence Level				
Thermal Power Plant	2 Sample t Test		F Test	
	Test Value	Critical Value	Test Value	Critical Value
Arizona Vapor	1.04	1.96	0.98	1.04
Las Palmas 2	0.35	1.96	0.93	1.04
San José	0.44	1.96	0.71	1.04

La Libertad	0.13	1.96	0.85	1.04
Poliwatt	0.26	1.96	0.65	1.04
Arizona	0.29	1.96	0.77	1.04
Puerto Quetzal Power	0.68	1.96	0.60	1.04
Las Palmas	0.57	1.96	0.73	1.04
Industria Textiles del Lago (ITDL10)	0.09	1.96	0.60	1.04
Genor	0.16	1.96	0.50	1.04
Electro Generación	0.12	1.96	0.09	1.04

7. Impact Analysis of PV Installation

7.1. Model Reconstruction with PV System

A large-scale PV system is installed with the optimized conditions in the model constructed with the System Dynamics for the impact analysis of PV installation to the grid.

The large-scale PV system install conditions are as follows:

- Panels tilted angle: The optimal 10° tilted angle is used in accordance to the estimation conducted in section 4.2.
- Meteorological data time series: The meteorological data is obtained by the use of the meteorological model WRF in accordance to the simulation conditions detailed in section 3.4
- PV output estimation: The estimation is conducted using the equations detailed in section 4.1
- Appropriate area for the large-scale PV power plant: from the area selected in section 5, the meteorological data time series is extracted.
- Installed capacity: The installed capacity will vary from 0 to 200 MW in order to conduct the analysis. Further details for the installed are discussed in section 8

The calculation of the PV output is conducted within the system dynamics simulation model, by introducing the equations from section 4.1. The meteorological data time series (e.g temperature and irradiance from section 3.4) are introduced as data bases and are synchronized by the "Timer" like the power plants described in section 6.2.

The simplified model including the PV system is indicated in Fig. 45. It is found that the PV System is added similar to the ordinal electric power plants by the comparison between Figures 32 and 45. In this model, Power Rating of the PV System is fixed first. Irradiance and Temperature of the

Meteorological Model in Fig. 45 are generated from the meteorological database with the direction of Timer. The PV System evaluates its output from them with the method explained at section 3.4, and supply the output to the electric power grid together with the ordinal power plants.

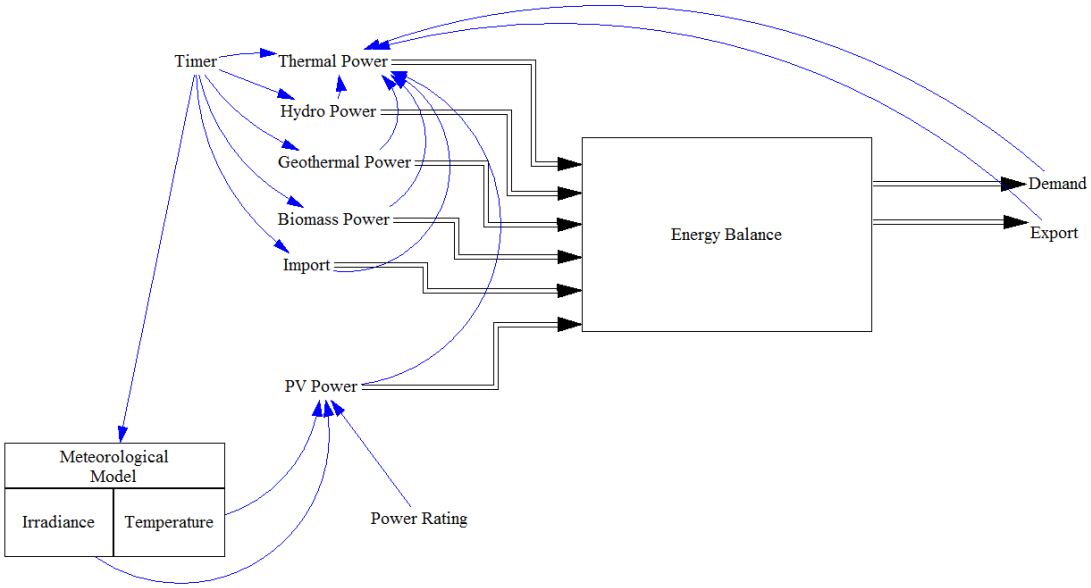

Fig. 45: Schematic view of Guatemala's electric grid model after installing large-scale PV system

8. Results and discussions

By installing the PV system, the electric generation of the thermal power plants may be reduced, because the plants get feedback from the demand and control the electric balance on the grid as shown in Fig. 45. The reduction of the power plants' generation is evaluated as the impact of the PV installation to the electric grid. The capacity of the installed PV system, which is corresponding to the Power Rating in Fig. 45, changes from 0 to 200 MW in this impact analysis.

The period of the simulation is the complete year 2011 with a one hour interval. Figure 46 shows the total thermal power generation time series month sum and the PV Power Generation time series month sum when PV panels installed capacity is 0, 100 and 200 MW.

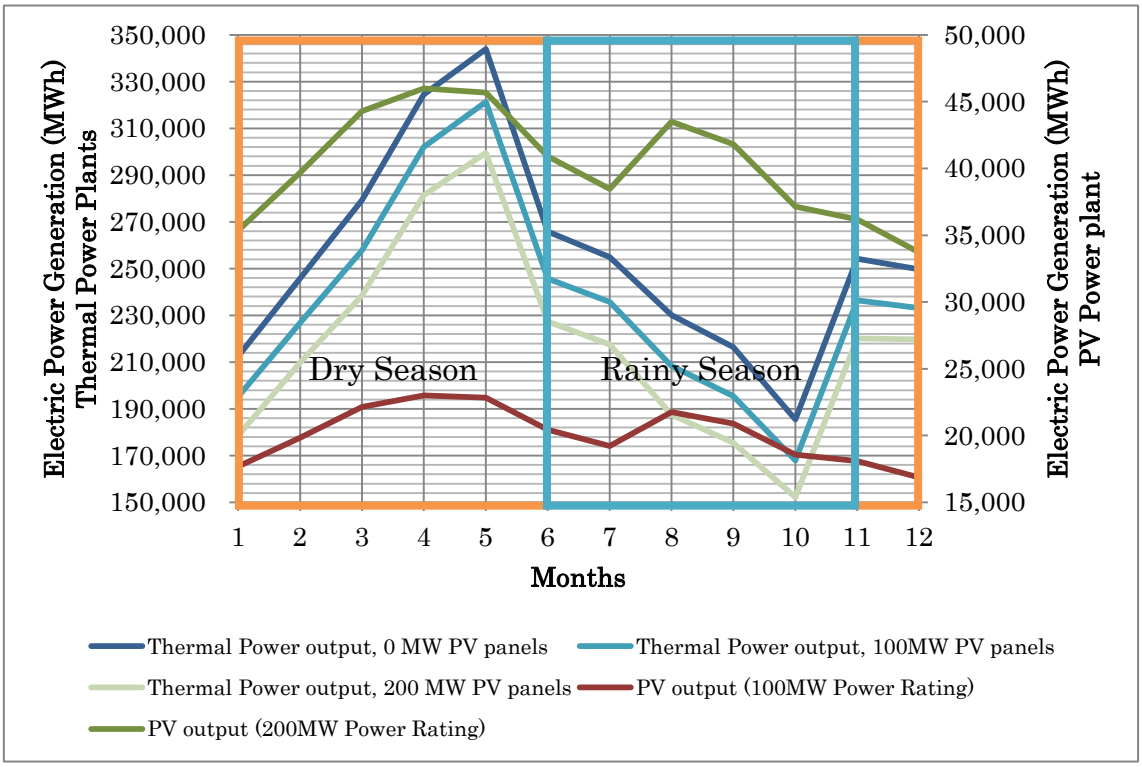

Fig. 46: Total Thermal Power Generation time series and PV Power Generation time series, month sum.

Figure 46 also displays the seasons of Guatemala. The overall trend of both the thermal power output time series reduction can be observed as well. However, this figure includes the thermal power generation per month sum, therefore the detailed day by day change in thermal power generation as PV power generation is increased is difficult to observe. In order to be able to observe the day by day trend Figures 47 and 48 were created. They are typical days of each season.

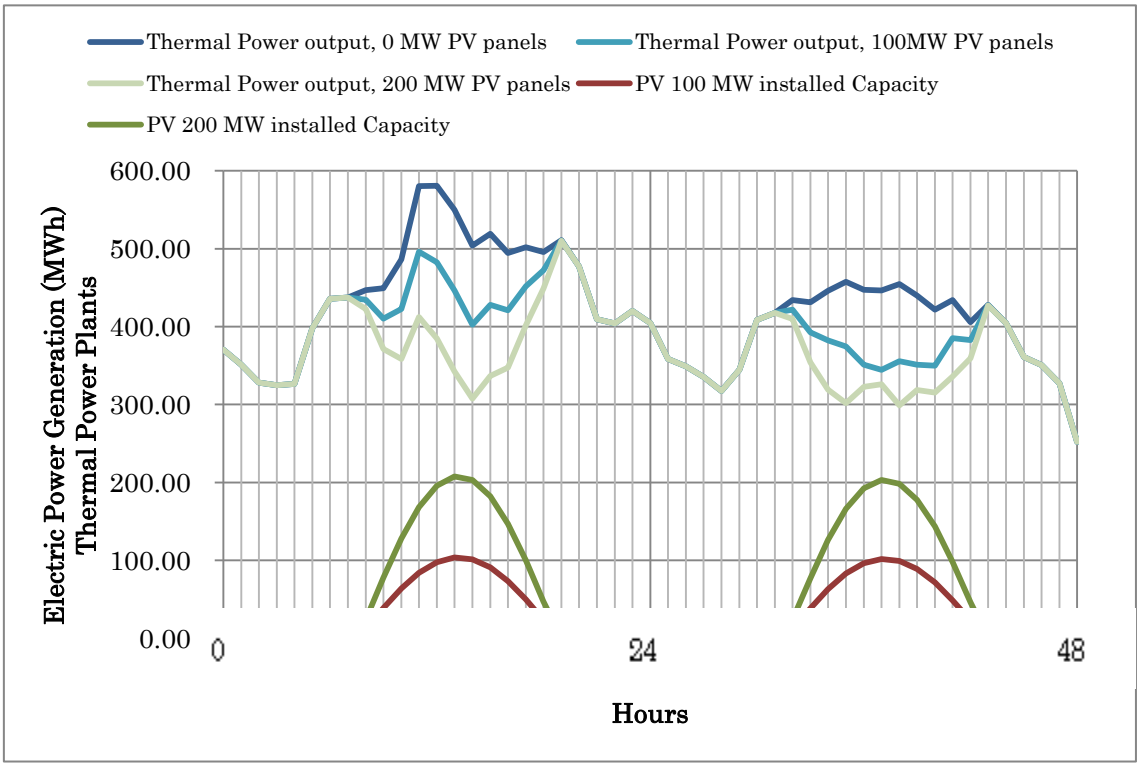

Fig. 47: Typical thermal and PV electric power generation during the dry season.

Figure 47 shows the time series of the typical thermal and PV electric power generation during the dry season. It can be seen that the gap between the thermal power output time series with 0MW and 100MW of PV panels is larger than the gap between the thermal power output time series with 100MW and 200MW of PV panels. It can also be observed that there is no change in thermal power generation at night when the PV panels cannot generate electricity

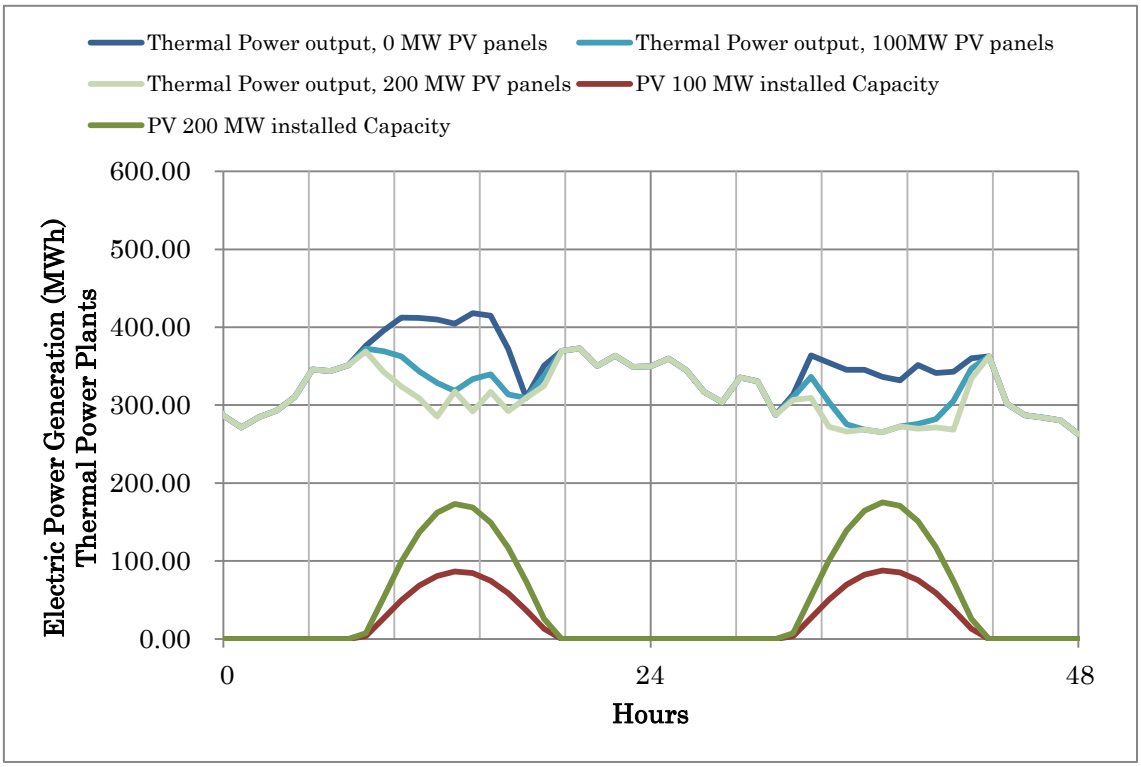

Fig. 48: Typical thermal and PV electric power generation during the rainy season.

Figure 48 shows the time series of the typical thermal and PV electric power generation during the rainy season. Similar to the trend in Fig. 47, it can be seen that the gap between the thermal power output time series with 0MW and 100MW of PV panels is larger than the gap between the thermal power output time series with 100MW and 200MW of PV panels. This gap change once again validates the change in sensitivity previously discussed. However, when compared to the typical dry season days, the gap between the thermal power output time series with 100MW and 200MW of PV panels is smaller. This trend is because in the rainy season the PV power output becomes unstable due to cloud coverage and the system has difficulties using PV panels efficiently. These two figures show the high resolution and accuracy that the system dynamics model has, and provide a clear trend when installing PV panels.

The generation of each thermal power plant is also estimated with

different install capacity of the PV system as shown in Figs. 49 to 52. The plants are categorized in these figures with their actual generation scale. Each thermal power plant is operated with their priority defined from the energy cost, efficiency and the reaction time, and discussion with the actual power generation is more realistic than with their capacity. The capacity and the actual generation of each thermal power plant is listed and sorted with the generation in Table 8. Some power plants, i.e. Tampa, Stewart & Stevenson and Escuintla Gas 5 generate small quantities when compared with their capacities as seen in the table, because of their low priority.

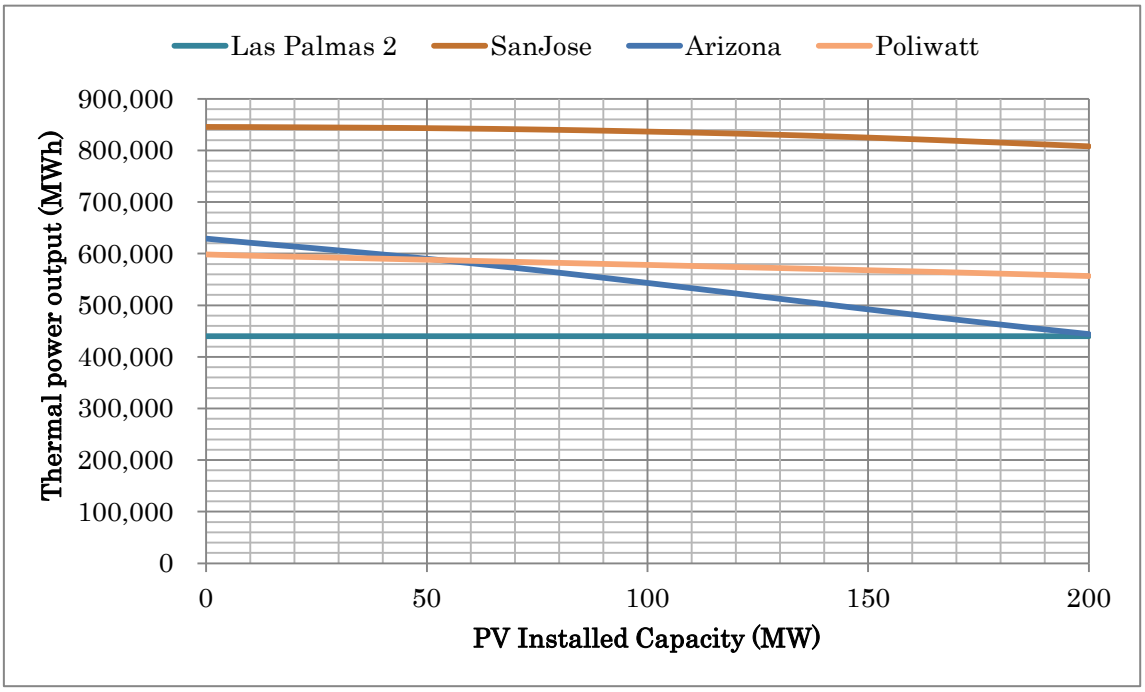

Fig. 49: Simulated yearly output of largest generation thermal power plants after installing large-scale PV system.

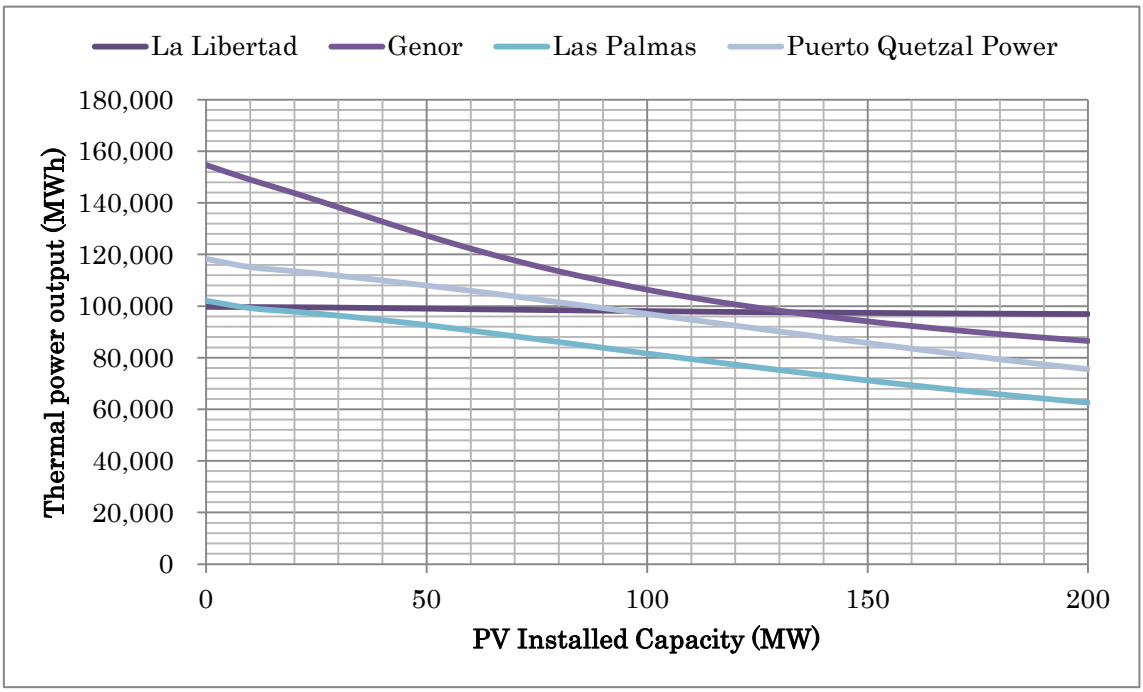

Fig. 50: Simulated yearly output of middle-large generation thermal power plants after installing large-scale PV system.

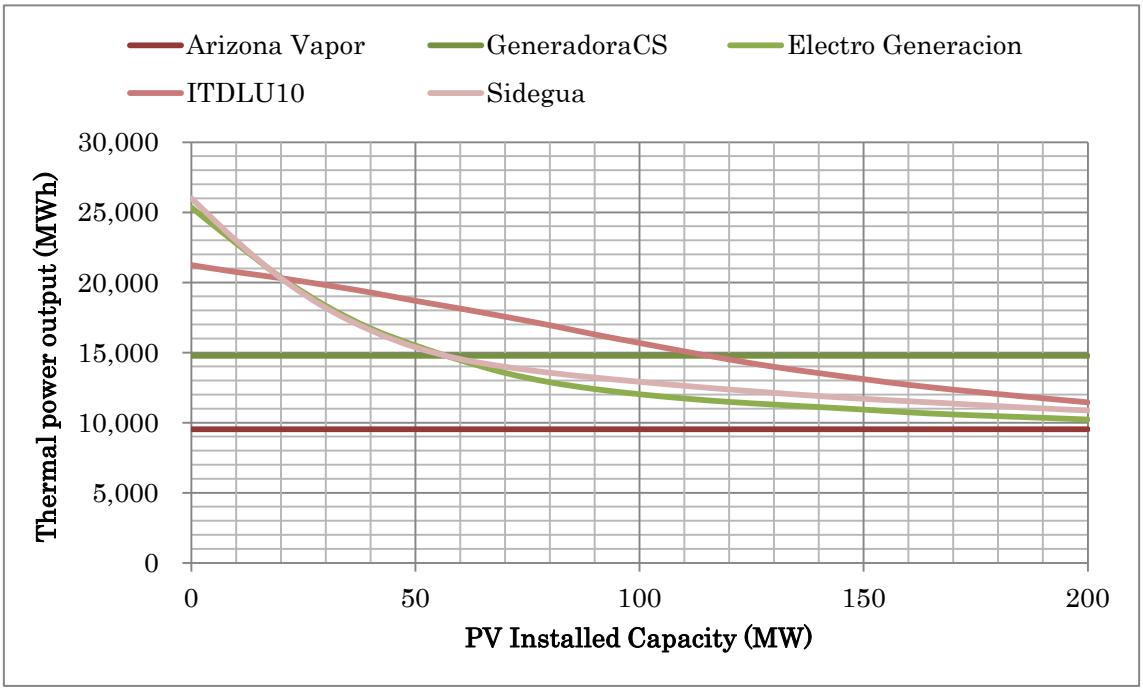

Fig. 51: Simulated yearly output of middle-small generation thermal power plants after installing large-scale PV system.

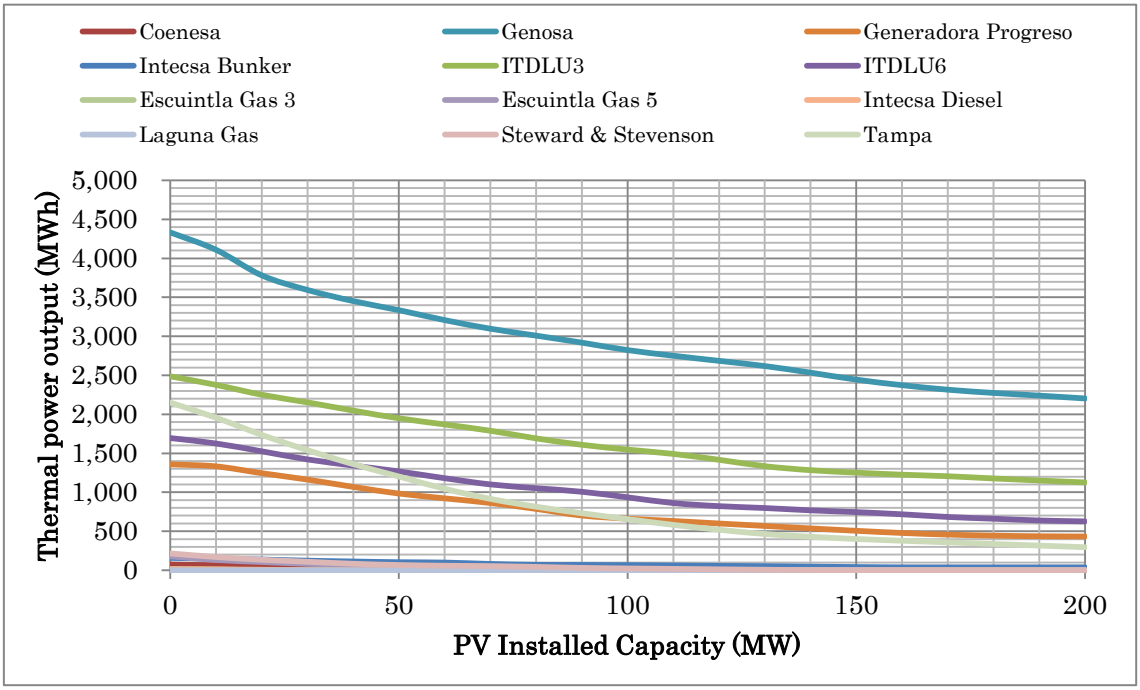

Fig. 52: Simulated yearly output of small generation thermal power plants after installing large-scale PV system.

In Fig. 49, the largest generation power plants are grouped. They are operated throughout the year in order to balance the demand with the energy generation after the use of the renewable energy sources. In this figure the Arizona power plant's generation is most evidently reduced by 29 % from 629,156 MWh before installing the PV system to 444,121 MWh with the 200 MW PV system installation. Arizona power plant generates with internal combustion engines and heavy oil, and the plant can be controlled the generation easily but the energy cost is expensive. Under its condition, the Arizona plant has the lowest priority in operation among the largest generation power plants, and it may reduce evidently the operation when the PV installed as the result of the simulation.

On the other hand, the Las Palmas 2 power plant generates 440,070 MWh, and it doesn't get any impact from the installation of the PV system. This plant uses coal as fuel and is the latest plant which was installed in May

2010, and it has the highest priority among the four largest generation power plants.

We define the parameter 'sensitivity' to the impact of the PV installation as the negative gradient of graph in Fig. 49. It's evaluated the reduction of the generation in unit MWh divided by the increase of PV installed capacity in unit MW. The sensitivity of Arizona power plant power plant is 957.19 MWh/MW at the 0 MW PV system installation, and the largest among the plants in Fig. 49. On the other hand, the sensitivity of the Las Palmas 2 power plant is 0 MWh/MW on the same situation.

The impact of the PV system installation to the mid-large generation power plants is presented in Fig. 50. The plants in this class are for supporting the increasing demand in daytime and in the early evening shown in Fig. 11, especially in the dry season when hydropower plants cannot generate enough. They usually have the lower priority in operation than the largest generation power plants in Fig. 49, their generations reduce as the install capacity of the PV system increase. Only La Libertad has a very small reaction to the installation of the PV system; the sensitivity is only 9.04 MWh/MW at the 0 MW PV system installation, and that is negligible. There are several reasons for their lower priority compare with the ones in the largest generation power plants. First, their efficiency is lower than the largest generation ones due to the scale merit of the generation. Second, they were all installed between 1993 and 1998, and use heavy oil as fuel and their operating prices are higher than those in Fig. 49. Their sensitivities at the 0 MW PV installation are from 214 to 340 MWh/MW, except the La Libertad power plant.

The impact of the PV system installation to the mid-small generation power plants is presented in Fig. 51. Their operating cost is higher, and therefore their priority is lower than the larger plants in Fig. 50. These power plants change their output throughout the day due to changing the demand, and mainly support the peak demand in the early evening in Fig. 11.

The usual operation period of the plants is after the sunset, and some plants, e.g. Arizona Vapor and Gneradora CS, don't get affected strongly from the PV installation, and their sensitivities aren't large.

Figure 54 shows the impact of the PV system installation on the smallest generation thermal power plants. The amount of the electric generation is small, but they are required, because they support the peek and emergent demands for the grid managing. These power plants are the most expensive ones, using diesel or heavy oil as fuel.

The relation between the install capacity of the thermal power plants and their sensitivity to the PV installation is plotted in Fig. 53. One of the largest generation plants, Arizona has the highest sensitivity as shown in this figure, because of its low cost operation and its short reaction time, as explained before. In this figure, the sensitivities of the middle-large generation power plants tend to be larger than the others. The plants in this class works mainly in the daytime and early in the evening to support the high demand, therefore the installed PV system supply electric power in the daytime instead of the thermal plants, and the plants may reduce their operation. On the other hand, the large thermal plants, except Arizona, operate throughout the year as the base load power plants, and their sensitivity to the PV installation is similar as shown in Fig. 53

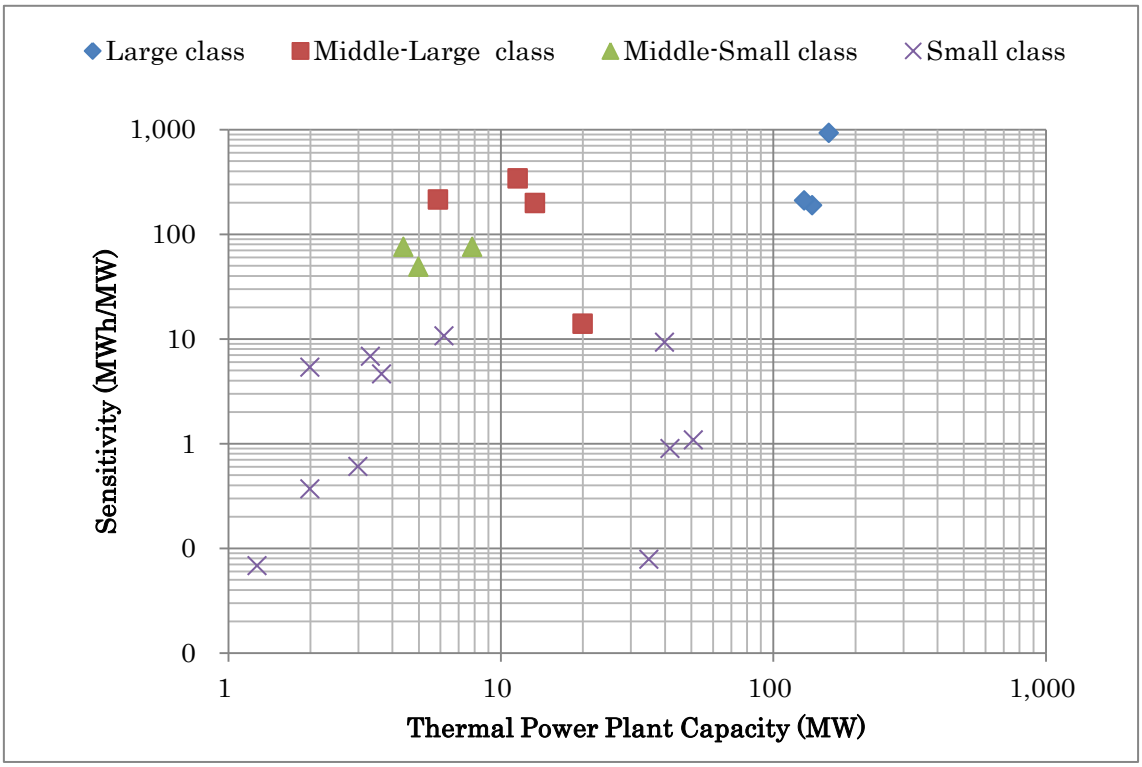

Fig. 53: Sensitivity of thermal power plants compared with their generation

Most power plants which reduce the generation due to the installed capacity of the PV system increases. And also they decrease the sensitivity, for example the sensitivity of the middle-large plant Genor in Fig. 50 decreases the sensitivity from 339 with 0 MW PV installation to 185 with 200 MW PV installation. This may be caused by the limitation of the ability of the electric power grid to the acceptance of the fluctuation of PV generation which occurs due to changes of weather and the sun altitude. The fluctuation becomes larger as the install capacity of the PV system becomes larger. When the fluctuation becomes larger, the electric power grid has to keep preliminary plants more for the absorption of the fluctuation.

9. Conclusions

The impact of the installation of a large-scale PV system to the electric power grid was analyzed in the series of our works. Guatemala was selected as the target country because the electric system in it is simple and helpful for the analysis.

The solar irradiance in the target country was computed with the meteorological model WRF and the PV energy potential was evaluated. The southern coast facing the Pacific Ocean has large irradiance and also has high PV energy potential. The maximum irradiance in this area reaches almost 2.5 MWh on the horizontal plane in the selected year. The area is also near the region of energy consumption, and it is a possible area for the large-scale PV power plants development. The optimal tilted angle of the PV panels is also proposed from the PV output simulation.

In the electric power grid system dynamics simulation, all 85 power plants operated in 2011 are represented and evaluate the reduction of the electric generation of the individual thermal power plant due to the installation of the PV system. The contribution of the PV installation to the reduction of the thermal power plants' operation is very small or nothing for the largest generation thermal plants because of their high efficiency and low cost in operation. On the other hand, the middle-large generation thermal power plants reduce their operation after installing PV system in this simulation, because these power plants work mainly in daytime to support the high demand, and the installed PV system will supply the electric power in daytime instead of the plants after the PV installation. The reduction of thermal power plants' operation becomes large as the PV installing capacity becomes large, but its reduction gradient becomes small as the PV installing capacity increases. It might be caused the acceptable limitation of the time variation of the PV power generation.

10. References

OpenEI, Open Energy Info. (2012). Retrieved December 1, 2012, from OpenEI, Open Energy Info: http://en.openei.org/wiki/SWERA/Data

Google Earth. (2015). Retrieved 12 1, 2014, from https://www.google.com/earth/

Administrador del Mercado Mayorista. (2014). *Administrador del Mercado Mayorista, Guatemala C.A.* Retrieved December 2014, from Administrador del Mercado Mayorista: http://www.amm.org.gt/

Ahmad, S., Mat Tahar, R., Muhammad-Sukki, F., Munir, A. B., & Abdul Rahim, R. (2015). Role of feed-in tariff policy in promoting solar photovoltaic investments in Malaysia: A system dynamics approach. *Energy*, DOI.

Ahrens, C. D. (2009). *Meteorology Today: An Introduction to Weather, Climate, and the Environment.* Belmont: Brooks/Cole Cengage learning.

Bazilian, M., Onyeji, I., Liebreich, M., MacGill, I., Chase, J., Shah, J., et al. (2013, May). Re-considering the economics of photovoltaic power. *Renewable Energy, 53*, 329-338.

Bracamonte Orozco, E. (1986, October 20). Guatemalan Solar Map. *Solar & Wind Technology, 4*(No 3), 381-388.

Coley, D. A. (2008). *Energy and Climate Change.* Chichester, West Sussex: John Wiley & Sons Ltd.

Cucciella, F., & D'Adamo, I. (2012). Feasibility study of developing photovoltaic power projects in Italy: An integral approach. *Renewable and sustainable Energy Reviews, 16*(3), 1562-1576.

de la Hoz, J., Boix, O., Martín, H., Martins, B., & Graells, M. (2010). Promotion of grid-connected photovoltaic sytems in Spain: Performance analysis of the perios 1998-2008. *Renewable and Sustainable Energy Reviews, 14*(9), 2547-2563.

de Martino Jannuzzi, G., & de Melo, C. A. (2013). Grid-connected photovoltaic in Brazil: Policies and potential impacts for 2030. *Energy for sustainable Development, 17*(1), 40-46.

Dincer, F. (2011). The analysis on photovoltaic electricity generation status, potential and policies of the leading countries in solar energy. *Renewable and Sustainable Energy Reviews, 15*(1), 713-720.

Duffie, J. A., & Beckman, W. A. (2006). *Solar Engineering of Thermal.* New Jersey: John Wiley & Sons, Inc.

European Small Hydropower Association. (2004). *Guide on How to Develop a Small Hydropower Plant.* Industry, European Comission, Brussels.

Forrester, J. W. (1961). *Industrial Dynamics.* Cambridge: The MIT Press.

Hay, J. E. (1979). Calculation of monthly mean solar radiation for horizontal and inclined surfaces. *Solar Energy, 23*(4), 301-307.

Hsu, C.-W. (2012). Using a system dynamics model to assess the effects of capital subsidies and feed-in tariffs on solar PV installations. *Applied Energy*, 205-217.

Huld, T., Friesen, G., Skoczek, A., Kenny, R. P., Sample, T., Field, M., et al. (2011). A power-rating model for crystalline silicon PV modules. *Solar Energy Materials and Solar Cells, 95*(12).

Instituto Geográfico Nacional, Guatemala C.A. (2014). *Instituto Geográfico Nacional, Guatemala C.A.* Retrieved October 2014, from

http://www.ign.gob.gt/

Instituto Geográfico Nacional, Guatemala C.A. (2014). *Instituto Geográfico Nacional, Guatemala C.A.* Retrieved October 2014, from http://www.ign.gob.gt/

Instituto Nacional de Estadística, Guatemala C.A. (2014). *Instituto Nacional de Estadística, Guatemala C.A.* Retrieved November 2014, from http://www.ine.gob.gt

Instituto Nacional de Sismología, Vulcanología, Meteorología e Hidrología. (2014). *Instituto Nacional de Sismología, Vulcanología, Meteorología e Hidrología, INSIVUMEH.* Retrieved December 2014, from http://www.insivumeh.gob.gt/

Jäger-Waldau, A. (2012). *PV status report 2012.* European Commisision, Joint Research Centre, Institute for Energy and Transport. Luxembourg: Publications Office of the European Union.

Kaifel, A. (2011). *P2IONEER - Virtual and Hybrid Power Plant Simulation.* Retrieved June 12, 2015, from http://www.zsw-bw.de/themen/energiewirtschaft/p2ioneer.html

Kambezidis, H. D., Psiloglou, B. E., & Gueymard, C. (1994). Measurements and models for total solar irradiance on inclined surface in Athens, Greece. *Solar Energy, 53*(2), 177-185.

Khalil, S. A., & Shaffie, A. M. (2013, November). A comparative study of total, direct and diffuse solar irradiance by using different models on horizontal and inclined surfaces from Cairo Egypt. *Renewable and Sustainable Energy Reviews, 27*, 853-863.

Klucher, T. M. (1979). Evaluation of Models to predict isolation on tilted surfaces. *Solar Energy, 23*(2), 111-114.

Li, C., Zhou, L., Li, N., & Zeng, M. (2012). Modelling and simulation of Power Grid Engineering Project baed on System Dynamics on the Background of Smart Grid. *Systems Engineering Procedia*, 92-99.

Liu, B. Y., & Jordan, R. C. (1963). The long-term average performance of flat-plate solar energy collectors. *Solar Energy, 7*(2), 249-256.

Ministry of Economy, Trade and Industry. (n.d.). *Ministry of Economy, Trade and Industry*. Retrieved 12 23, 2015, from http://www.meti.go.jp/english/index.html

Movilla, S., Miguel, L. J., & Blázquez, L. F. (2013). A system dynamics approach for the photovoltaic energy market in Spain. *Energy Policy, 60*, 142-154.

Movilla, S., Miguel, L. J., & Blázquez, L. F. (2013). A systems dynamics approach for the photovoltaic energy market in Spain. *Energy Policy*, 142-154.

National Renewable Energy Laboratory. (2014). *National Renewable Energy Laboratory*. Retrieved December 2014, from http://www.nrel.gov/

NCAR Data Support Section, Data for Atmospheric and Geociences Research. (2014). *CISL Research Data Archive*. Retrieved November 2014, from http://rda.ucar.edu/datasets/ds083.2/

Negrao Macedo, W., & Zilles, R. (2009). Influence of the power contribution of a grid-connected photovoltaic system and its operational particularities. *Energy for Sustainable Development, 13*(3), 202-211.

Nicoló, G., Escobar, E., García, G., & Ortiz, A. (2010). *Informe Especial: Missión FAO/PMA de Evaluación de Cosecha y Seguridad Alimentaria en Guaetmala.* Food and Agricultture Organization of the United Nations, World Food Program, Guatemala City.

Padovan, A., & Del Col, D. (2010). Measurement and modeling of solar irradiance components on horizontal and tilted planes. *Solar Energy, 84*(12), 2068-2084.

Pantaleon. (2015). *Pantaleon*. Retrieved 12 14, 2015, from http://www.pantaleon.com/

Perez, R. (2004, June 30). *Solar: hourly solar (direct normal (DNI), global horizontal (GHI), and diffuse) data for selected stations in Guatemala from State University of New York*. Retrieved December 2014, from OpenEI, Open Energy Information: http://en.openei.org/datasets/dataset/solar-hourly-solar-direct-normal-dni-global-horizontal-ghi-and-diffuse-data-for-selected-s7

Perez, R., Ineichen, P., Moore, K., Kmiecik, M., Chain, C., George, R., et al. (2002). A new operational model for satellite-derived irradiances: description and validation. *Solar Energy*, 307-317.

Perez, R., Ineichen, P., Seals, R., Michalsky, J., & Stewart, R. (1990). Modeling daylight availability and irradiance components from direct and global irrdiance. *Solar Energy, 44*(5), 271-289.

Perez, R., Seals, R., Ineichen, P., Stewart, R., & Menicucci, D. (1987). A new simplified version of the perez diffuse irradiance model for tilted surfaces. *Solar Energy, 39*(3), 221-231.

Platzer, M. D. (2012). *U.S. Solar Photovoltaic Manufacturing: Industry Trends, Global Competition, Federal Support.* Congressional Research Service, United States of America.

Reindl, D. T., Beckman, W. A., & Duffie, J. A. (1990). Evaluation of hourly tilted surface radiation models. *Solar Energy, 45*(1), 9-17.

Silveira, J. L., Tuna, C. E., & Lamas, W. d. (2013, April). The need of subsidy

for the implemantation of photovoltaic solar energy as supporting of decentralized electrical power generation in Brazil. *Renewable and Sustainable Energy Reviews, 20*, 133-141.

Skamarock, W. C., Klemp, J. B., Dudhia, J., Gill, D. O., Barker, D. M., Duda, M. G., et al. (2008). *A Description of the Adavanced Research WRF Version 3.* Boulder, Colorado, USA: Mesoscale and Microscale Meteorology Divisio, National Center for Atmospheric Research.

Skartveit, A., & Olseth, J. A. (1987). A model for the diffuse fraction of hourly global radiation. *Solar Energy, 38*(4), 271-274.

System Dynamics Society. (2014). *System Dynamics Society*. Retrieved 12 2014, from www.systemdynamics.org

The World Bank. (2014). *The World Bank*. Retrieved 10 2015, from http://www.worldbank.org/

Thornthwaite, C. W. (1931). The Climates of NorthAmerica: According to a New Classification. *Geographical Review*, 633-655.

U. S. Department of Energy. (n.d.). *Energy.gov*. Retrieved 12 14, 2015, from http://energy.gov/

List of Paper Publications

1. Evaluation of the Photovoltaic System Installation Impact to an Electric Power Grid. Part 1: Simulation of photovoltaic generation by applying a meteorological model.
   Authors: Wyss Porras Juan Ernesto, Shimada Susumo, Yoshino Jun, Kobayashi Tomonao.
   Published in Labor & Engenho 2015, Volume 9, Issue 4 pp. 90-102, http://periodicos.bc.unicamp.br/ojs/index.php/labore/index

2. Evaluation of the Photovoltaic System Installation Impact to an Electric Power Grid Part 2: Impact analysis of photovoltaic installation to an electric power grid by applying a nonlinear analysis model.
   Authors: Wyss Porras Juan Ernesto, Shimada Susumo, Yoshino Jun, Kobayashi Tomonao.
   To be published in Labor & Engenho 2016, Volume 10, Issue 1, http://periodicos.bc.unicamp.br/ojs/index.php/labore/index